POLITECNICO DI TORINO

Department of Mechanical and Aerospace Engineering

MSc Thesis
in Biomedical Engineering

Passive Safety of Vehicles: FE simulation of different side impact crashes, analysis of biomechanical results and study of injuries with Human Body Models.

Tutors:
Prof. Eng. Alessandro Scattina
Prof. Eng. Giovanni Belingardi

Candidate:
Elisa Peroglio

October 2022

Abstract

In this thesis, six different side impact crash tests, between a Moving Deformable Barrier (MDB) and a mid-size sedan were reproduced in a FE environment, to evaluate and compare the possible injuries that the car occupant at driver seat may suffer in those type of impacts, using Human Body Models (HBMs). The injuries were evaluated by using HBM based injury criteria and not using the traditional ones: the differences between the two are discussed in this work.

The MDB, the HBM and the vehicle models were included in a main file that permit the simulation of the side impact crashes. The simulations were performed with LS-Dyna as solver software. The biomechanical injuries were analyzed with the THUMS Injury Visualization tool, made available by JSOL Corporation.

The trolley has been translated and rotated to simulate all the different configurations. Two side impact crashes simulated that the trolley was driven into the vehicle at right angle, in correspondence of the R-point of the car occupant at driver or passenger seat. The other four impact crashes simulated the trolley colliding the vehicle in the side front parts left and right and in the side rear parts left and right, tilted of 45 degrees.

The injuries resulting from the six crash configurations were analyzed and compared. The left side impact crash at right angle, in correspondence of the R-point of the car occupant at driver seat, resulted to be the most critical for the car occupant, especially for the head and pelvis. The other five configurations were not resulting in severe injuries, the THUMS was only performing a translational movement in direction of the incoming carriage and, apart from the left orthogonal impact, only the left rear tilted configuration resulted in the head colliding the front door, but the resulting injuries were not as severe as the ones consequent to the left orthogonal impact.

Index

List of Figures

List of Tables

Preface

The studies about vehicle collisions and traumas related to them are important because of the high number of car accidents.

According to the 16th Road Safety Performance Index Report (Carson, Jost and Meiner 2022), the number of road deaths in Europe decreased by 31% between 2011 and 2021: there where 19'823 road deaths on Europe roads in 2021, as shown in figure 1. Despite the decreasing trend, the number of deaths due to car accident is still not acceptable.

In addition, worldwide, the number of road accidents is increasing alarmingly. According to World Health Organization (WHO), around 1.3 million people die each year as a result of road traffic crashes, 93% of world's fatalities on the roads occurs in least developed countries, even though these countries have approximately 60% of the world's vehicles. This is mainly due to the growing motorization of least developed countries and the presence of less advanced safety conditions than those of the European context. Indeed, in figure 2, the proportion of road deaths worldwide is presented. In Appendix A more data about road deaths are presented, to highlight the severity of the safety conditions on worldwide roads.

There is therefore a clear need to improve safety conditions on road vehicles.

In particular, concerning vehicle safety, the following three types of safety tests are performed nowadays.

- Preventive safety tests. Those tests are performed out of emergency situations, in order to reduce the risks and severity of car accidents that can occur. For example, they can be the evaluation of wellness and focus while driving the car, or the evaluation of the best view of streets and environments.

- Primary safety tests. The goal of those tests is to reduce, in emergency situations, the risks and the severity of the car accidents. For example, they can be related to the improvement of the ABS system, the Vehicle Dynamic Control (VDC), the speed limiter, the lane keeping assist system, the lane departure warning, and the Advanced Emergency Braking (AEB).

- Secondary safety tests. At least, those types of tests are carried out to reduce the negative consequences of the accident, once this has occurred. For example they lead the development of: restraint systems, structural behavior passenger compartment, airbag, and superficial aggression.

In particular, speaking of secondary safety tests, the evaluation of injuries that can occur to the car occupants is needed. For that goal, usually rigid dummies are used to simulate the behaviour of the car occupants during the impacts. Traditional crash tests with physical dummies are however very expensive and so companies have begun to use another approach: the Finite Element Method (FEM).

In this context the Human Body Models (HBMs) have been developed to investigate injuries occurring to persons involved in road accidents such as car occupants, pedestrians or cyclists.

The rate of accuracy and data related to the human response to any kind of stress of HBMs has increased so much that currently they are able to provide a more realistic response than the normal dummy used in a real crash test (Golman et al. 2014).

In this thesis, six side impact collisions were simulated and the injuries resulting from them were investigated though an HBM. The HBM used in this work is the Total Human Body Model (THUMS) developed by Toyota. The injury risks were evaluated and compared by using the THUMS Injury Visualization tool provided by JSOL company.

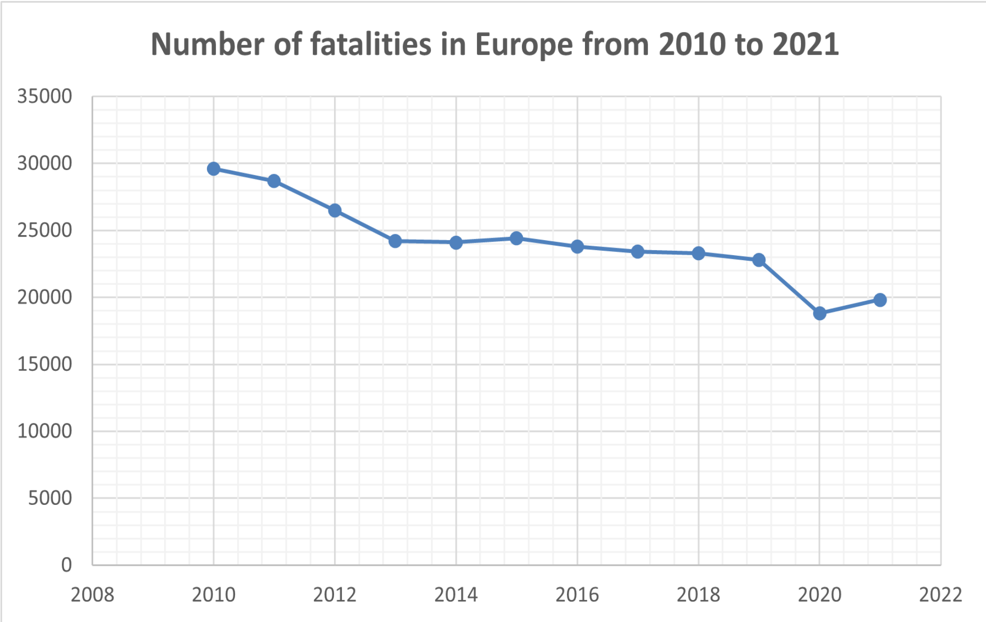

Figure 1: Number of fatalities in Europe from 2010 to 2021. Data are from: *ec.europa.eu.*

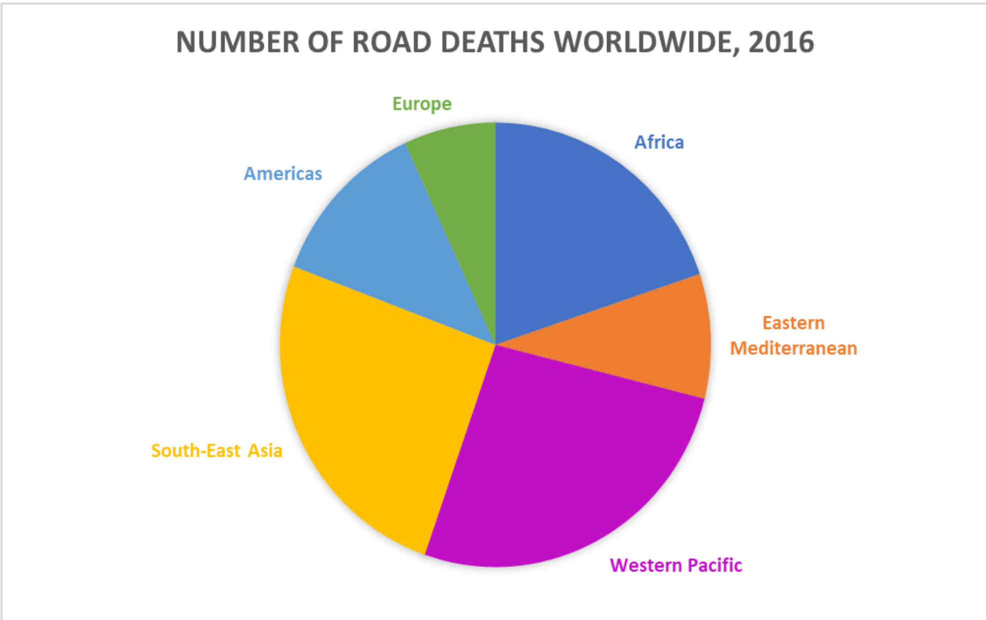

Figure 2: Proportion of number of road accidents worldwide, in 2016. Data are from: *World Health Organization (WHO).*

Roadmap

First of all, in chapter one, the thesis begins with a description about the biomechanics of impact trauma, and in particular about the side impact crashes. Then follows a literature review of the injury criteria, with a comparison between the traditional injury criteria and the HBM based ones. In this section is presented also the description of the MPS and CSDM criteria, which are going to be used to the analysis of results. The first chapter ends with the definition of the Euro NCAP side impact protocol.

In chapter two there is a description of the finite element method, which is the method adopted in this work to simulate the impacts. In that chapter are also presented the main three FE models employed in the simulations: the car model, the car occupant model and the MDB model.

Chapter three contains the pre-simulation processes, in particular the trolley placement in the six different configurations and the description of few settings, such as the velocity of the trolley, the positioning of THUMS and the termination times of the simulations.

Finally, in chapter four there is the analysis of the results. The chapter begins with some energy considerations and then it goes on by describing and comparing the injuries resulting from the six types of impacts, regarding both bones and internal organs. The chapter ends with the conclusions of the work.

The roadmap of the work is graphically presented in figure 3.

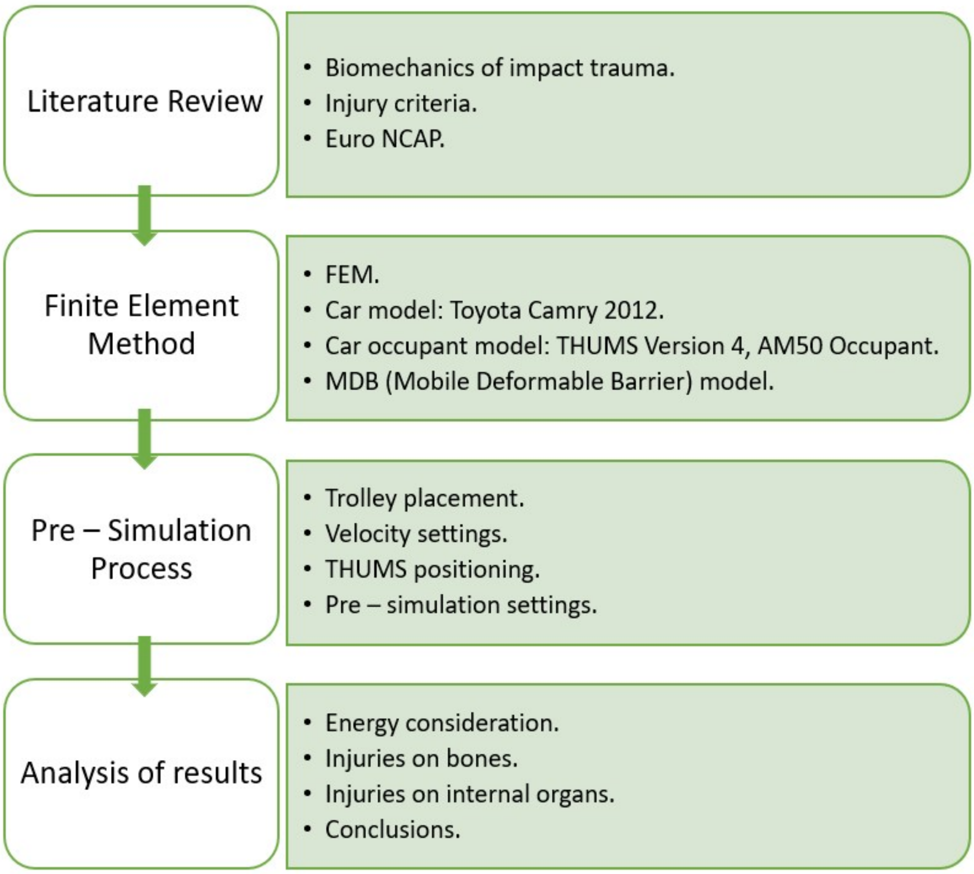

Figure 3: Roadmap of this thesis.

Chapter 1

Literature Review

1.1 Biomechanics of Impact Trauma

Biomechanics of impact trauma uses the mechanics principle to understand the response of human body in load conditions that can happen in different situations: during everyday life, sport activity or during a car accident. Moreover, it is important to notice that the difference between the generic biomechanics studies and the biomechanics studies of impact trauma is the duration of the event: the collision is an extremely fast event. This type of events is dynamic and so the inertia of the car occupant and its anatomical structures plays a crucial role in producing injuries.

Traumas related to car accidents can be various and can involve people in the car or people outside the car, such as pedestrians or cyclists. However, generically, the traumas related to road accidents depend on the velocity of the vehicles involved in the collision and on the amount of energy transferred to the anatomical structures of the person involved in the accident.

Considering that the anatomical structures have different composition and density, i.e. the bone has higher density than the muscles or the internal organs, the blast wave moves in the human body with different speeds while its velocity is reduced in various ways from the anatomical structures. However, the blast wave carries with itself a certain amount of energy that the anatomical structures dissipate in different ways based on their physical properties.

Regarding the injuries related to car occupants, it is important to analyze the type of the impact, which can be frontal, lateral, angular, rear-end collision or overturning, and the movement of the occupants inside the car, to understand which anatomical structures are the most stressed.

Injuries to car occupants are due to the impact of the bodies with the internal parts of the vehicle and to the use and operation of the restraint systems, such as seat belts and airbags. The current containment systems, while on one hand reduce potentially fatal injuries, on the other one can be responsible for minor injuries. For example, in the event of an accident at high speed, the seat belt can be responsible of bruises, bone fractures and even serious visceral damage. The mobility of the head with respect to the chest, held back by the seat belt, favors the occurrence of distractions of the cervical spine with possible vertebral involvement; the immobilized left clavicle promotes the torsion of the counter-lateral shoulder with the possibility of lesions of the same. The airbag system can also cause injuries to the face and head, in the form of abrasions, bruises and eye injuries. Those injuries are due the violent impact of the exploded airbag against the structures of the face.

1.1.1 AIS Scale

The AIS is a standardized injury scale that categorizes the level of injury by assigning a score. The AIS score is assigned to a specific anatomic part and a specific type of damage, by corresponding to a four-digit code, as clearly visible in figure 1.1.

The Association for the Advancement of Automotive Medicine developed the Abbreviated Injury Scale (AIS), together with a group of seventy-five specialists from around the world, in

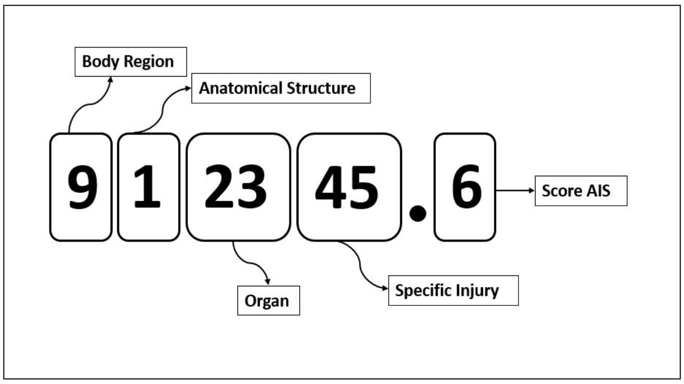

Figure 1.1: AIS scale.

AIS Level	Severity of Injury
AIS 1	Minor - Bruise, Hematoma
AIS 2	Moderate
AIS 3	Serious
AIS 4	Severe
AIS 5	Critical - 50% chance of death
AIS 6	Maximum - Death

Table 1.1: AIS score values.

the 1960s, while the AIS was officially introduced only in 1971. Then it was revised in 1980, 1985, 1990, 1998, 2005 and 2008 (Gennarelli and Wodzin 2006). In 2015, the Association for the Advancement of Automotive Medicine released the latest version, by improving brain injury coding, spinal cord impairment coding and enhancing many code definitions by incorporating current and appropriate medical terminology.

The AIS score can be a number in a range from 1 (least severe) to 6 (most severe). Table 1.1 shows simple descriptions of the severity of injuries, corresponding to the AIS score.

However, the AIS does not consider the combining effect of two or more traumas, but it only considers the risk related to one single lesion. To evaluate the severity of multiple traumas, the Injury Severity Score (IIS) must be adopted.

The IIS is obtained by summing the square of AIS level of the three most injured anatomical parts:

$$IIS = (AIS_1)^2 + (AIS_2)^2 + (AIS_3)^2$$

Where AIS_1, AIS_2, AIS_3 are the three higher AIS scores of the injured anatomical parts.

Despite this, in safety tests, the Maximum AIS is the the common system used to evaluate the injuries. Hence the injury risk resulting from the impact is the one corresponding to the maximum value of AIS. For example, if in a road accident, the car occupant presents: AIS=1 for the neck, AIS=2 for brain and AIS=3 for femur, the gravity of accidents is the one corresponding to the higher AIS score, therefore AIS=3.

1.1.2 Side Impact Trauma

Side impact crashes are one of the most severe motor vehicle accidents resulting in serious and fatal injuries. (Kumaresan et al. 2006)(Gierczycka, Watson and Cronin 2015)(Yoganandan et al. 2007). Injuries tend to be more severe in side impacts compared with front and rear impacts, mainly because of the limited side-crush space and the thinness of the side parts of the car, where the door must absorb a high amount of kinetic energy remaining in restricted constrains of deformation (Farmer, Braver and Mitter 1997).

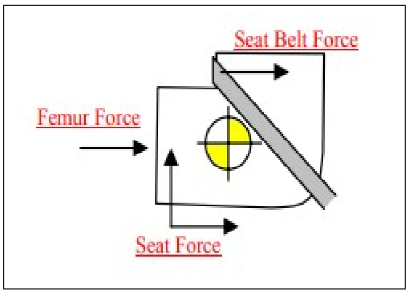

Figure 1.2: Submarining phenomenon (Couturier et al. 2007).

In side crashes, the most injured parts are the head and neck. These anatomical parts often present critical AIS level ($AIS > 3$). This can be attributed to the head passing through the side window and contacting either the window, the internal parts of vehicle or parts of the oncoming vehicle. Instead, the neck injuries can be attributed to seat belt, as previously discussed in paragraph 1.1. In fact, the mobility of head with respect to the shoulders and chest, held back by the seat belt, favors the occurrence of distractions on the cervical spine with possible vertebral involvement.

The second more injured anatomical parts are chest and abdomen.

Finally, pelvis and lower legs are the third most injured anatomical parts in side crashes (Yoganandan et al. 2007). The pelvis is often subjected to the submarining phenomenon, even if current used seat belts are designed to avoid this phenomenon as much as possible.

The submarining phenomenon consists in the sliding of the lap belt above iliac spine and loading the soft abdominal tissues (Couturier et al. 2007). Submarining phenomenon happens when the restraining forces acting on the pelvis are not in equilibrium during the deceleration of the vehicle and induce its rotation. The three forces acting are presented in figure 1.2. The phenomenon is well described in the study of Couturier et al. in 2007.

1.2 Injury Criteria

1.2.1 Traditional Injury Criteria

Injury criteria have been developed to analyze the mechanical responses of dummies used in crash tests, by evaluating the injuries resulting from the impact and the risk to life.

The traditional evaluation criteria are deterministic methods. There is a threshold value, and the evaluation criterion is design to predict an exact occurrence of injuries based on a single model, so it is based on individual characteristics of the injured person. Two examples of traditional injury criteria used in side impact crashes are presented below, for further information please refer to the numerous literature articles. (Lau and Viano 1986, Viano and Lau 1988.).

- Viscous Criteria is defined as:
$$VC = \frac{x(t)}{K}\frac{dx(t)}{dt}$$
where K depends on the dummy percentile, and it is equal to 0.140m for 50%ile male; x(t) is the ribs deflection. The human tolerance (AIS < 3) corresponds to $VC \leq 1m/s$.

- The maximum hemithorax deflection for human tolerance (AIS $<$3) must be $\leq$ 30%, that is equal to 42 mm for the 50%ile male.

From these two examples it is clear that, in traditional injury criteria, there are threshold values, and the occurrence of the lesion follows a binary fashion that can be yes, if the threshold is exceeded, or no if it is not.

Moreover, the ability to predict the lesion is only based on specific occupant, hence the measurements are made on the dummy in exam. That is a limit in predict injury occurrences in a population with varying physical characteristics.

1.2.2 HBM Based Injury Criteria

To overcome the limits of traditional injury criteria, casual probabilistic methods were developed, to predict injury risk based on stress and strain outputs from HBMs.

The probabilistic methods predict the probability of injury in each scenario that can be affected by various conditions in the dummy characteristics. Analysis of multiple variables of interest are possible, without high computational investment, by using distribution of stress and strain values coming from HBM, without needing to perform substantial number of simulations. It is possible to simulate a range of different conditions across the population with several characteristics. The output is a parametric risk curve or surface, with no binary fashion.

It is therefore possible to scale the dummy with different age, in fact the same stress and strain conditions can produce several severity of injuries in people with different age. In fact, through studies with rib segments, Carter and Spengler in 1978, found that the strain at fracture decreased with increasing age and that the bone's strength and stiffness are greatest between 20 and 39 years of age, while children's bone exhibits more deformation to failure than bone from adults, instead aging further than 39 years old is associated with a decrease in strength, stiffness, deformation to failure, and energy absorption capacity, and an increase in plastic modulus (Carter and Spengler 1978).

In following sections, the main HBM based injury criteria will be introduced.

1.2.3 MPS

The Main Principal Strain (MPS) is the evaluation criterion much used to predict the injury risks, above all for bones fractures. The criterion uses the ultimate strain distribution to predict the risk of injury. The ultimate strain is the strain threshold at which the material failure is expected (Forman et al. 2012).

The injury risk is plotted using risks curves such as sigmoid function, Weibull distribution or normal distribution. Those ones are mathematical functions used in probability theory and statistics.

The Weibull distribution is a continuous probability distribution, described in detail by Waloddi Weibull in 1951. A mathematical description of the Weibull distribution is presented in the study of Arthur J. 1993.

The sigmoid function is a mathematical function which have the characteristic sigmoid curve. Sigmoid curves can be various, but in statistics the more common used are the cumulative distribution functions, such as the integrals of the logistic density, the normal density, and Student's t probability density functions. A mathematical description of the cumulative distribution functions is presented at: `https://mathworld.wolfram.com/DistributionFunction.html`.

Finally, the normal distribution is the Gaussian distribution, which is a continuous probability distribution characterized by a mean value μ and a standard deviation σ. A detailed mathematical description is provided at: `https://mathworld.wolfram.com/NormalDistribution.html`.

In the study of Forman et al. in 2012, is presented the flow to follow to get the curve risk representing the probability of risks, starting from the FE models outputs. This flow is summarized in figure 1.3.

At first, failure strain data, coming from literature, can be scaled with age. In fact, as previously said, Carter and Spengler in 1978 found that the ultimate strain of rib cortical bone decrease with increasing age. Extending this concept to all the bones, and to all the anatomical structures, it is possible to predict a modified ultimate strain at an arbitrary target age, from an original ultimate strain value and a corresponding age, by using the following formula:

$$\varepsilon_{ult,mod} = \varepsilon_{ult,original} \frac{(1 - (age_{mod} - 25)\frac{0.051}{10})}{(1 - (age_{original} - 25)\frac{0.051}{10})}$$

where:

- $\varepsilon_{ult,mod}$ is the modified ultimate strain;
- age_{mod} is an arbitrary target age;

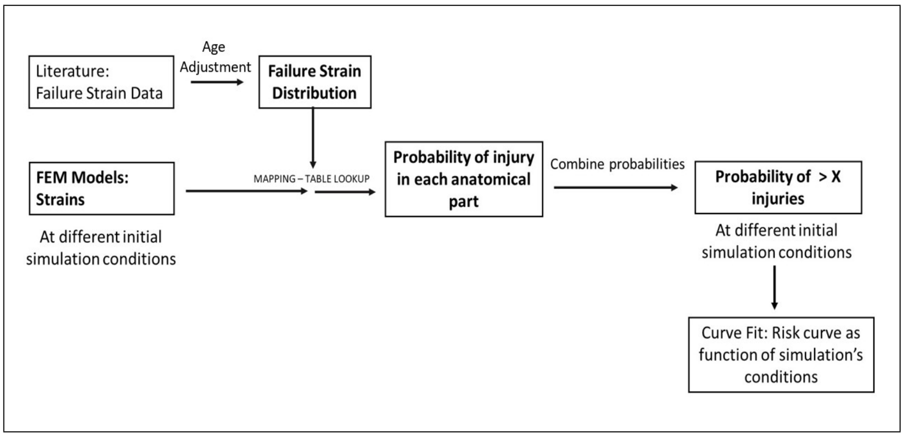

Figure 1.3: Flow to follow in order to get the MPS curve risk representing the probability of risks, starting from the FEM models outputs.

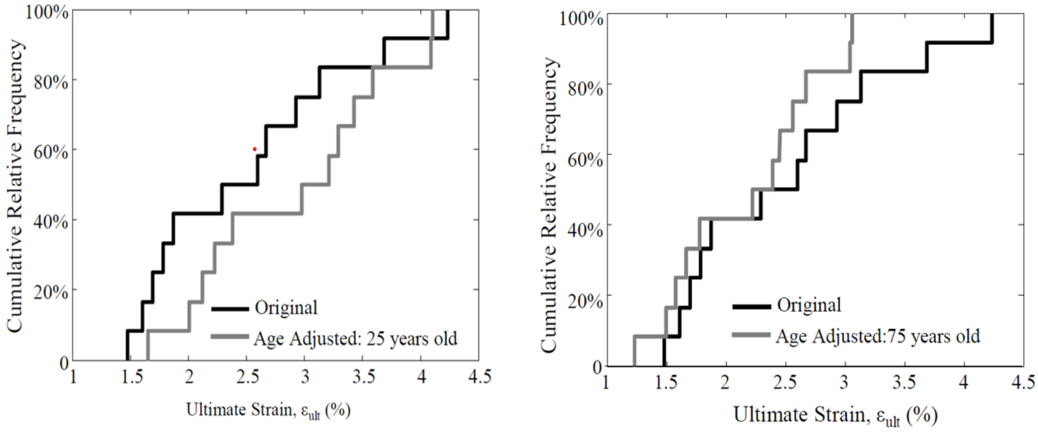

(a) Scaling with age at 25 years old.

(b) Scaling with age at 75 years old.

Figure 1.4: Original cumulative relative frequency distributions of rib cortical bone ultimate strains and the distributions scaled with two different age (Forman et al. 2012).

- $\varepsilon_{ult,original}$ is the original ultimate strain value;
- $age_{original}$ is the original age (Forman et al. 2012).

The adjustment with age can produce significant differences in output. Indeed, in figure 1.4 are represented the cumulative frequency distributions of rib cortical bone ultimate strains original and scaled with age at 25 years old (a) and scaled with age at 75 years old (b) (Forman et al. 2012).

Once predicted the failure strain distribution, scaled with particular age, the strain failure relationships must be defined, based on the probability that local strains observed from FEM models exceed the ultimate strain of bone coming from literature, using a cumulative non-parametric distribution of mean ultimate strains, adjusted to a particular age.

For example, in Table 1.2 there is the tabulation of strain observed in a trivial simulation. For each of N location, called *site*, there is the associated strain coming from FE models (ε_N) and, in the last column, the probability that each strain (S) is higher than the ultimate strain derived from literature (US): that means the probability of injury at each location (p_N).

Once obtained the probability of injury in each potential site, those probabilities are aggregated to determine the probability of a chosen number of injuries occurring in the entire anatomical structure.

Site	Strain	P(S > US)
1	0,5	0,00
2	2,5	0,41
3	1,5	0,09
4	3,0	0,59
5	3,0	0,59
...	...	...
N	ε_N	p_N

Table 1.2: Probability of injury at each location, for a trivial simulation.

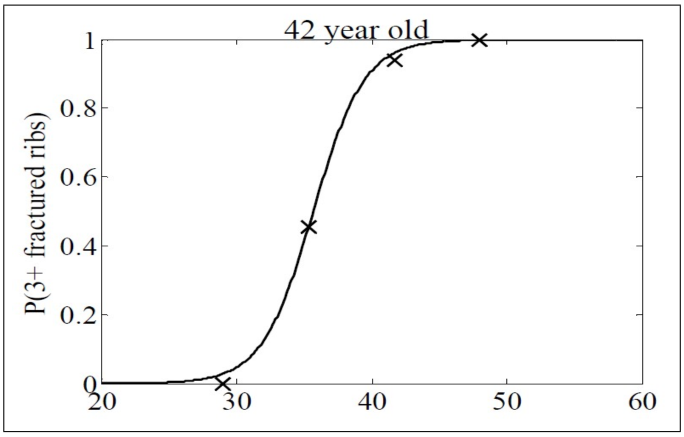

Figure 1.5: Probability of ribs bone fractures, depending on the velocity of the collision (Forman et al. 2012).

Finally, instead of simulating for different values of initial condition (e.g., different values of collision's velocity), it is possible to describe the relationship between injury and initial conditions, by using parametric function. The risk curve obtained shows the probability of the injury to happens, depending on the simulation's features. For example, in figure 1.5 there is the graphical representation of the probability of ribs bone to fracture, depending on the velocity of the collision. (Forman et al. 2012)

In conclusion the MPS is the most used injury criterion, predicting the probability of injury as function of simulation's conditions. The MPS is the only injury criterion discussed in this work that can be used to predict injury risks for all the anatomical parts: both internal organs and bones.

The most important limitation of MPS criterion is that it does not have a direct correlation with the AIS. The MPS returns only the injury risk curve with reference to the particular injury risk value for the body region analyzed. Although the MPS criterion does not have a correlation with the AIS scale, there are thresholds values currently used by scientific community when using Human Body Models. For example, for brain contusion, occurring in gray matter of brain, when reaching 26% of MPS critical injury output level, the AIS 3 level is reached, while for diffuse axonal injury , occurring in white matter of brain, the AIS 4 level is reached when 21% of MPS critical injury output level is reached.

1.2.4 CSDM

Temporary or permanent cessation of axonal functions has been shown to occur when axons were subjected to extensional deformations. This can happen during collisions and brain traumas. The functional failure of axonal structures does not correspond always with mechanical failure: sometimes the stretch can be in a reverse range mechanically but not functionally. This axonal damage has been termed DAI (Diffuse Axonal Injury).

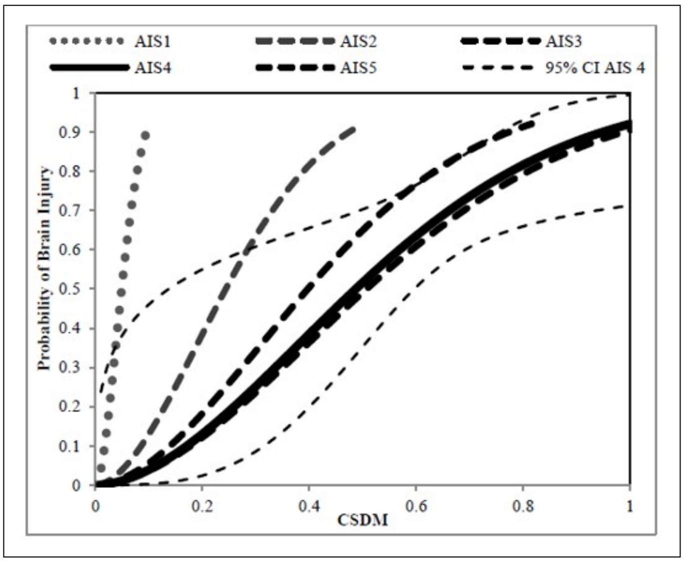

Figure 1.6: CSDM brain injury risks for variuos AIS levels. (Forman et al. 2012)

However, the axonal damage in one single axon does not reflect the severity of DAI, that is why the Cumulative Strain Damage Measure (CSDM) was introduced by Bandak and Eppiger in 1994, as a measure to evaluate the extent and severity of strain related damage within the brain. The CSDM is a cumulative measure which represents the percentage of brain volume that exceeds a certain strain threshold (Bandak and Eppinger 1994).

The steps to follow to obtain the injury risks through the CSDM criterion are the following.

1. At each time increment, the volume of all the elements that have experienced a strain above prescribed threshold is calculated. The strain level is calculated from a strain tensor that is obtained by integration of the rate of deformation tensor (Bandak and Eppinger 1994). A major detailed explanation is provided in the study of Bandak and Eppiger. The threshold values are instead coming from animal experiments.

2. The affected volume monotonically increases in time during the stretch deformation. The cumulative sum means that the end state corresponds to the total consequence of the event. In fact, CSDM metrics predict injuries by monitoring the accumulation of strain damage.

3. CSDM risk curve is then constructed using Weibull distribution:

$$InjuryRisk = 1 - e^{-(\frac{CSDM}{\lambda})k}$$

   where λ is the scale and k the shape parameter for Weibull distribution.

4. The injury risks curves obtained through this procedure provide the injury risks values corresponding at least to AIS 4 brain injury (Takhounts, Hasija et al. 2011). It is possible to scale to other levels of AIS, by using the risk curve for HIC as explained in the study of Takhounts, Hasija et al. In figure 1.6 are presented the brain injury risks curves for various AIS severity, based on CSDM criterion.

1.2.5 HIC

In 1972, the National Highway Traffic Safety Administration (NHTSA) proposed the Head Injury Criterion (HIC), which is an injury criterion that gives the measure of head injury severity, arising from an impact. It includes the effect of linear accelerations on the head and the duration of them, during the collision. The HIC is defined as:

$$HIC = (t_2 - t_1)\frac{[\int_{t1}^{t2} a(t)dt]^{2.5}}{t_2 - t_1}$$

Where

- a(t) is the resultant acceleration evaluated in the center of the head, measured in g's (where g is the gravity acceleration $g = 9.81m/s^2$). Hence the real acceleration of the head is $a' = a/g$.
- $t_2 - t_1$ is the time interval and normally can be 36 ms, for the HIC_{36}, or can be 15 ms for the HIC_{15}.

The HIC takes into consideration only linear accelerations, and so this criterion may underestimate the injury risks, because it is not taking into consideration the effect of rotational accelerations. (Zhang, Yang and King 2004)

1.2.6 BrIC

Since 1940s, several scientific studies have shown the importance of head rotational kinematic in head related injuries.

Takhounts, Craig et al., in 2013, developed the Kinematic Brain Injury Criterion (BrIC). The BrIC takes into accounts both CSDM and MPS, and also the rotational velocity, but not the rotational acceleration, by considering that the values of angular velocity are directional dependent. In fact, it has been shown that the most convenient quantity to describe the relationships between brain and skull kinematics is the angular velocity (Takhounts, Craig et al. 2013).

To obtain the BrIC, Takhounts et al. correlate the physical injury metrics (CSDM and MPS) and the kinematic parameters (linear and angular velocity) by using pendulum tests (Takhounts, Craig et al. 2013). The result is the definition of BrIC as:

$$BrIC = \sqrt{\left(\frac{\omega_x}{\omega_{xc}}\right)^2 + \left(\frac{\omega_y}{\omega_{yc}}\right)^2 + \left(\frac{\omega_z}{\omega_{zc}}\right)^2}$$

Where ω_x, ω_y, ω_z are the maximum angular velocities about X, Y and Z axes while ω_{xc}, ω_{yc}, ω_{zc} are the critical angular velocities in their respective directions.

In conclusion, BrIC is a rotational injury criterion while HIC is a translational injury criterion and the combining of the two can give a better evaluation of the head injury, because the motion of the head cannot be all rotational or all translational, but usually the head is experiencing both.

1.2.7 PVP

There is no correspondence between the above injury criteria and all the AIS levels: they all do not provide the extraction of injury severity.

Bastien, Neal-Strugess et al., in 2020, proposed a new injury criterion to predict injury severity after head traumas: the Peak Virtual Power (PVP). Differently from the previous criteria, the PVP returns the severity of the traumas, in terms of AIS level. The PVP is a criterion based on second principle of thermodynamics which states that the entropy increases after every mechanical process. While the power during a process goes up and down, the entropy never goes down: it is always increasing, as we can see in figure 1.7. PVP is proportional to the entropy and represent the trauma severity (Bastien, Neal-Sturgess et al. 2020).

The construction of PVP, derived using the Clausius - Duhem inequality, is presented in the study of Bastien, Neal-Strugess et al.

In conclusion, the PVP is proportional to stress and strain and to AIS level:

$$PVP \propto max(\sigma \cdot \dot{\varepsilon}) \propto AIS$$

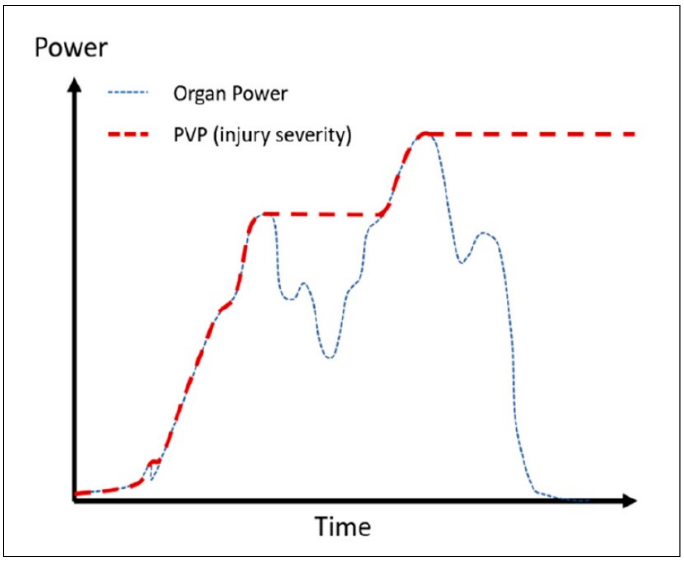

Figure 1.7: Trends of PVP (injury severity) and Organ Power, during time. (Bastien, Neal-Sturgess et al. 2020)

The PVP criterion can be used to estimate the DAI in white tissues of brain, or to estimate the crain Contusion in gray tissues of brain.

As previously explained, one of the main innovative features of PVP is that it can also returns the information regarding all the AIS level. As it is constructed, the PVP returns the AIS 4 severity, but can be scaled to know how much PVP the organ can withstand to reach AIS 1, 2, 3 and 5, with cubic functions (Bastien, Neal-Sturgess et al. 2020). The result is a plot in which five curves are presented and they represent all the 5 AIS levels; one dot is representing the actual value of PVP in mW. The AIS level correspondent to the PVP value is the one of the AIS curve above the dot. An example is provided in figure 1.8.

As all the above criteria, the PVP can be scaled with age: in the study of Bastien, Neal-Strugess et al., is also described how to scale 39 years old THUMS 4.01 model to a 63 years old THUMS 4.01 model, to replicate its frailty due to ageing.

1.3 Euro NCAP

1.3.1 Introduction to EuroNCAP

The European New Car Assessment Program (Euro NCAP) is an European car safety performance assessment program, founded in 1996 and based in Leuven (Belgium). Starting from 1970s a number of European governments had been working, through the European Experimental Vehicles Committee (EEVC), on assessing various aspects of car secondary safety. In following years, this research had resulted in the development of full-scale crash test procedures, for protection of car occupants in frontal and side impacts, and a component test procedure for assessing the protection of pedestrians, hit by the fronts of cars. In June 1994, the UK Department of Transport proposed the creation and diffusion of NCAP in the UK, that later could be expanded across all european countries. The program would be more comprehensive and based on the test procedures developed by the EEVC. Finally, in 1996, the Swedish National Road Administration (SNRA), the Federation Internationale de l'Automobile (FIA) and International Testing were the first organizations to join the car safety test program. This resulted in Euro NCAP being formed.

Euro NCAP has created the five-star safety rating system to help consumers to compare vehicles more easily and to help them identify the safest choice for their needs (NCAP 2022). The stars safety rating is determined by testing vehicles. The tests are designed and conducted

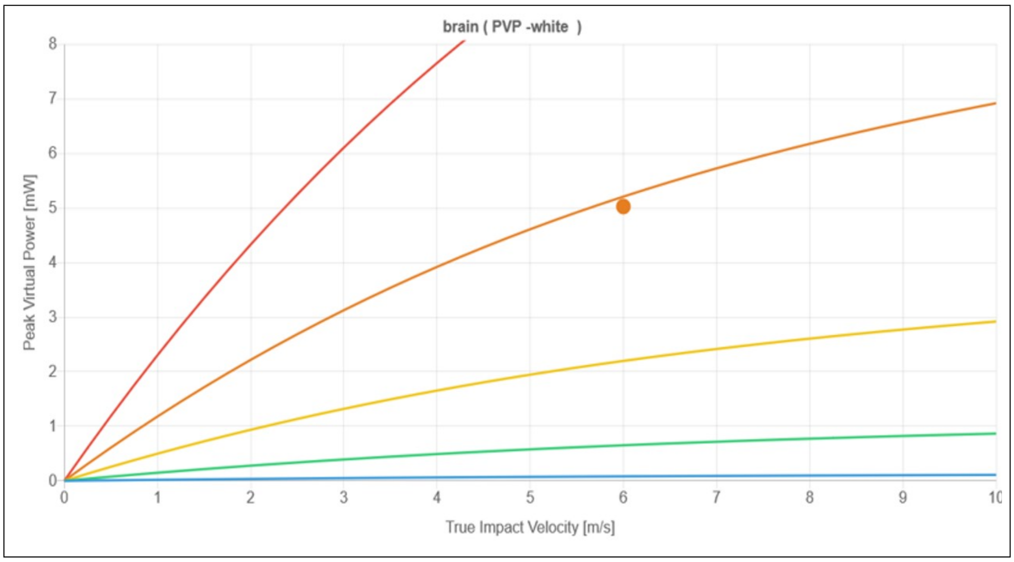

Figure 1.8: Trauma prediction through PVP criterion, for $PVP{=}8.68mW$. The red curve corresponds to AIS=5, the orange one to AIS=4, the yellow one to AIS=3, the green one to AIS=2, and the blue one to AIS=1. In this case, the corresponding AIS level is AIS=4. (Bastien, Sturgess et al. 2021)

in a standard procedure by Euro NCAP, simulating critical real-life accident scenarios.

A high number of stars shows not only that the test result was good, but also that safety equipment on the tested model is readily available to all consumers in Europe. The star rating goes beyond the legal requirements and not all new vehicles need to undergo Euro NCAP tests. A car which is rated poorly is not necessarily unsafe, but it is not as safe as its competitors that were rated better. This increases the competitiveness of the market in the security field and raises the safety standards. The five-star safety rating is evolving during years, as well as the technology is evolving (NCAP 2022). It is here presented an overview of the Euro NCAP stars system scores for vehicles.

- 5 stars safety. Overall excellent performance in crash protection and well equipped with comprehensive and robust crash avoidance technology.
- 4 stars safety. Overall good performance in crash protection; additional crash avoidance technology may be present.
- 3 stars safety. At least average occupant protection but not always equipped with the latest crash avoidance features.
- 2 stars safety. Nominal crash protection but lacking crash avoidance technology.
- 1 star safety. Marginal crash protection and little in the way of crash avoidance technology.
- 0 stars safety. Meeting type-approval standards so can legally be sold but lacking critical modern safety technology.

The number of test protocols are increasing over the years, nowadays there are many of them. In this work, the version 8.1.3 of side AE-MDB test protocol for adult occupant protection was used (NCAP 2021). This testing protocol is used as reference in only one of the six configurations, the others five impacts were not referenced to any standards.

1.3.2 Side impact testing protocol

The Euro NCAP standard for side impact was firstly created in 1997 and was updated many times: the latest version is the 8.1.3, available from 2020. The protocol includes a dummy

Figure 1.9: Euro NCAP side impact standard (NCAP 2022).

with several sensor and a mobile deformable barrier (MDB) driven at speed of 60±1 km/h into the side of the stationary vehicle at right angle. The direction of impact is pointed on the R-point, with a tolerance of ±25 mm. The R point is the point of the vehicle, provided by the constructor of vehicle, corresponding to the junction point between the body segmet leg and the body segment trunk of the dummy, when the seat is considered to be in its lowest and most rearward position. Instead, the H point, corresponds to the actual point occupied by the joint between the body segment leg and the body segment trunk of the dummy. Theoretically these two points should coincide.

An instant view of the Euro NCAP side impact test is shown in figure 1.9.

A male dummy is placed on the driver's seat. The test aims to ensure that the most vulnerable parts of the body are adequately protected.

A lot of requirements must be taken into consideration, the complete list is available in documentation of NCAP 2021. Some of those requirements can concern the vehicle, such as the measure of the total mass of vehicle, the heights of vehicle at all four wheels, and the checks about the car's tank, which must be filled on 90% of its capability, and about all the others liquid containers, which have to be filled with their full capacity.

The following requirements are instead concerning the dummy.

- The dummy placed in driver's position must be 50%ile dummy.
- The dummy shall be instrumented with sensors to record a series of measurements.
- The torso of the dummy must be arranged as close as possible to the driver seat and to the H-point.
- The hands of the dummy must be in contact with the steering wheel at a position quarter to three.
- The left foot must be positioned parallel to the floor in a rest position.
- The right foot is positioned on the acceleration pedal not pressed, with the heel as far forwards as possible and in contact with the floor. The right foot should overlap the accelerator pedal with at least 20mm.

Not only the dummy must be instrumented with sensors: also the vehicle and the trolley. An acceleration sensor in placed on the car to measure the lateral acceleration on the unstruck B-pillar. The accelerometer must be horizontal with a tolerance of ±5 degrees.

Regarding the trolley, is has to be fitted with an accelerometer at its Center of Gravity. The accelerometer is to be fitted in the fore/aft direction.

Chapter 2

Finite Elements Method

2.1 Introduction to Finite Elements Method

Reality is made up of extraordinarily complex phenomena, in which the acting forces are inertial and variable over time. This inertial nature gets particular importance when the forces are strong and acting in a brief time interval, such as in collisions between vehicles. The equations of motion governing such systems are generally nonlinear partial differential equations which are difficult to solve mathematically. In order allow the resolution of these mathematical models, the Finite Element Method (FEM) is usually used.

This method considers the system as composed of many domains of elementary forms, each of them will be characterized by a certain number of nodal points in which, through approximation functions called shape functions, it is possible to define the kinematic and dynamic conditions which, added together, will characterize the entire system. The differential equations remain unmodified but are solved on the discrete domains in a simpler way and then summed together to provide the final solution.

In summary, the FEM method consists in representing a continuous system in a set of discrete elements corresponding locally to the same portions of the continuum.

In figure 2.1 there is an example of a system modeled with FEM. The system is a part of a foot, which is modeled in all its parts and materials a set of discrete elements.

Two distinct phases are needed to generate the FE model:

- Modeling phase. The real system is simplified with a model, which contain the main aspects of the real system. This is done through the introduction of simplifying hypotheses and eliminating the irrelevant components for the required solution. The simplifying hypotheses can be made on the material, the geometry, load, and constraints.

- Discretization. After the modeling phase of the real system, there is the transition from the infinite model to the finite one: the system is no longer described by infinite points but by finite nodal ones. The discrete domain is called mesh. Those finite nodal point are named nodes and they are going to define the vertexes of the figures in which the model is divided: the elements.

2.1.1 Types of finite elements

The types of elements that can be used to create the mesh can be one-dimensional elements, two-dimensional line elements, two-dimensional planar elements, and three-dimensional solid elements.

- One-dimensional elements are defined in one direction of the space.

  The Truss element required two nodes to be defined. Each node has only transnational degree of freedom and not rotational ones, hence each node has three degrees of freedom. It can transmit only axial forces. Also, the beam element is defined in one dimension

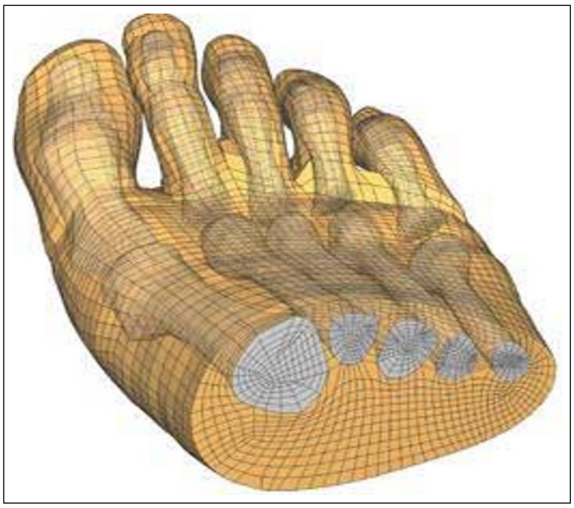

Figure 2.1: Part of a foot modeled with FEM. Source:*www.truegrid.com*

and required two nodes to be defined, but differently from the truss element, the beam can deform outside this reference system. Therefore, the beam has two nodes, each one with six degrees of freedom. Others one-dimensional elements are the ones used to apply boundary conditions to elements. The spring element is used to apply a specific spring constant at a specified node or set of nodes. It requires two nodes to be defined and it has axial and rotational stiffness. Also, the rigid element requires two nodes to be defined and is used to create a rigid connection between two elements. Finally, the gap elements specify a gap between two pieces of geometry.

- Two-dimensional elements are defined in two directions of the space.

  The membrane element required three or four nodes to be defined. It has three degrees of freedom for each node and can transmit only stress perpendicular to its plane and momentum around the axes in its plane. In conclusion the membrane element can transmit only shear stresses and bending moments.

  The stress plane required three or four nodes to be defined. It has three degrees of freedom for each node and can transmit only stress along its plane.

  The shell elements required three or four nodes to be defined. They are composed of the overlapping between the two previous discussed elements: the membrane element and the stress plane one. It can transmit shear stresses, axial stresses and bending moments.

- Three-dimensional elements are defined in three directions of the space. The most common one is the brick element. The brick element, or tetrahedra, may have 4,5,6,7,8,15 or 20 nodes which support three degree of freedom each. It is usually used to model solid objects.

2.1.2 Steps of FEM process

The phases of FEM process can be summarized in three steps, as shown in figure 2.2.

1. Pre-processing. In this phase the geometric model is generated: the mesh is created, the materials are characterized, and the boundary conditions are defined, such as the loads and the kinematic conditions.

2. Solving. This phase is consisting of numerical process in which the system of equations is solved.

3. Post-processing. The last phase consist in the analysis and visualization of results (displacements, stresses and strains) by means of animations and plots. The data available for

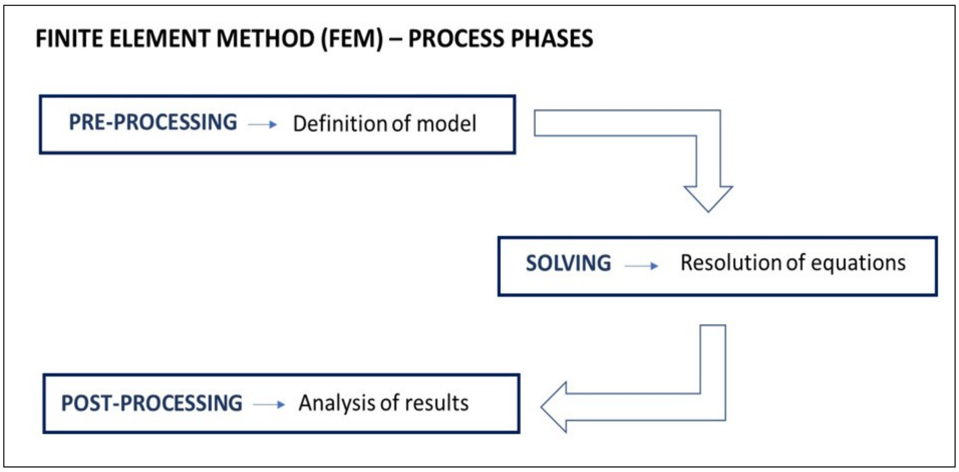

Figure 2.2: Steps of FEM process.

the analysis in the post-processing phase must have been requested in the pre-processing phase.

2.1.3 Hourglass

The phenomenon of hourglass takes particular importance in FEM simulations. When applying a moment to an element, ideally it is not generating any shear stress, but in cases of FE models, a shear stress in point of Gauss is observed, but actually it is not existing. This phenomenon is known as Shear Locking. The deeper the mesh, the more negligible this problem will be, but deeper mesh means higher computational costs. So, it was decided to reduce the integration points, to reduce the computational cost, calculating only the central point: in this point, in fact, the shear stress is not observed. This method is known as Reduced Integration method. However, this method leads to the observation of zero deformation energies on the integration points of the element. This phenomenon is known as hourglass. Basically, there is a sort of numerical dispersion of energy, since the nodes can present ways of deforming to which corresponds a zero-deformation energy. For this reason, the energy of hourglass should be as low as possible, because that energy is computationally dispersed due to the phenomenon of hourglass. In general, energy contributions of hourglass less than 5% of the maximum value of the total energy are considered acceptable.

2.2 FE Model

In this work, the side impacts were simulated with the use of the following three FE models.

- The car model, 2012 Toyota Camry, that hosted the Human Body Model (HBM) during the crash. The model will be discussed in detail in section 2.4.
- The Human Body Model (HBM), positioned in the driver's seat of the vehicle. The model will be discussed in detail in section 2.3.
- The mobile deformable barrier (MDB) model, on trolley driven into the side of the stationary vehicle. The model will be discussed in detail section 2.5.

2.3 Human Body Models

The dynamical analyses of the human body in various situation requires a set of governing equations applicable to a wide variety of situations.

(a) Hybrid III dummy for front impac.

(b) Eurosid2 dummy for side impact.

(c) Biorid dummy for rear impact.

Figure 2.3: Dummies for different impact crashes. Source: www.humaneticsgroup.com

For example, regarding automotive field, the type of trauma can be various and can involve car occupants, pedestrians, or cyclists, each of them can collide with the vehicle is many different configurations, with several boundary conditions such as the velocity and angulation of impact, the position of the dummy, the presence of wet floor, and so on.

Over last century, concerning the automotive field, human surrogates or dummies have been used to perform security tests. Even if dummies and human surrogates are accurate test devices, they can be used only in specific conditions, and so the characteristics of the dummy and the boundary conditions of the impact test, make the simulations not generalizing. In fact, there are different types of dummies that can be used to perform different types of crash simulations: the Hybrid III is used for frontal impact, Eurosid2 for side impact and the Biorid for rear impact collision. These types of dummies are presented in figure 2.3.

For the reasons just mentioned, it is clear the needing of a models that can easily simulate several characteristics of the car occupant or pedestrian involved in crash impact. The creation of such a model is critical because of the difficult in developing impact governing equations, due to complex geometry of the human body shape that can change, even if a little, from one situation to another (Huston and Passerello 1971). Moreover, the abundance of possible motions that the person involved in the impact can do, makes results obtained from traditional dummy simulations even less generalizing, and make more difficult to develop the correct human body model.

For these reasons, new human modeling tools, designed based on Finite Element Method (FEM), were introduced and they are named Human Body Models (HBMs).

The HBMs are virtual geometric and mechanical representations of the human body. The geometry of the model must be in agreement with standard databases, resulting in masses, dimension and moments of inertia for each body parts. It must consider the complex human anatomy and consist of a full skeleton composed of all bones and soft tissue. All the bones should be articulated in a realistic manner enabling a bio-accurate range of motion.

The use of HBMs make possible to simulate various initial conditions, indeed a large amount of population is represented with HBMs: male, female, and children. HBMs make also possible to analyze the overall injuries of whole human body, at the same time and reducing the economic impact that is required in order to perform the same analyses, with traditional dummies.

However, the HBMs are still not used for homologation tests but the number of studies concerning this promising tool is increasing.

Despite, during years, several types of HBMs were developed, the following section will deal with Total Human Body Model, since this is the HBM used in this thesis work.

2.4 Total HUman Body Model for Safety (THUMS)

The Total Human Model for Safety (THUMS) is a virtual human body model software program for computer analysis of human body injuries caused in vehicle collisions. It was designed and developed in cooperation with Toyota Motor Corporation and Toyota Central R&D Laboratories Inc. and presented in 2000. That was the world's first virtual human body model software, enabling the simulation and analysis of injuries caused in vehicle collisions. Over one hundred clients nowadays use THUMS to research and develop many different safety technologies, such as seatbelts, airbags, and vehicle structures. The original THUMS base model reproduces a mid-size adult male occupant, including all the deformable human body parts with respect to anatomical geometry and biomechanical properties. From 2000 to the latest version of 2019, it has been evolved to add a range of model with different genders, ages and physiques that include skeletal structures, internal organs, and muscles. Compared to the physical crash dummies commonly used in vehicle collision tests, THUMS can analyze impact related injuries in more detail, because it precisely models the shapes and durability of human bodies. It also provides the analysis of injuries at joints level.

Simulations conducted on computers also enables repeated analysis in a range of different collision patterns, in fact the traffic accidents can occur in a nearly infinite number of configurations, while THUMS can dramatically reduce development lead times and costs associated with collision testing.

The THUMS was developed to evaluate injuries not only in car occupants, but also in pedestrians and other non-car-occupant causalities.

2.4.1 Evolution of THUMS

The evolution of THUMS is presented in figure 2.4.

The first version of THUMS (Version 1) was completed in 2000. It is based on a physique of 175cm height, 77kg weight, 30-40 years old male. It models the body's shape, bone strength and dermal tenacity. It is also recreating detailed anatomical components such as vertebrae, hand and foot joints, ligaments, and tendons, while the motions around body joint are simulated without implementing any kinematic joint element, only simulating the relative motion between bones. The brain and internal organs are simplified as solid part, with homogeneous material properties. It is composed up on more than 80'000 finite elements, with an average size of 15mm. (*Toyota Unveils Virtual Human Body for Simulated Crashes.* 2000)

In 2004 some new features about THUMS were presented and then validated in 2005, when the second version (Version 2) was launched. The female occupant model was added, considering the differences between male and female anatomy, in terms of material and geometry. Moreover, were added also the models of internal organs and brain and was introduced also a detailed face mapping.

In 2008 third version (Version 3) was released adding an improved brain model. The brain is composed by hexagonal solid elements and there is the distinction between gray matter, white matter, and cerebral spinal fluid (CSF). The number of elements was around 130'000.

In 2010 was introduced the fourth version (Version 4) that includes the detailed models of internal organs, still not present in previous versions. Those detailed models can simulate internal organs injuries at tissue level. To reach this level of precision the Toyota Motor Corporation and

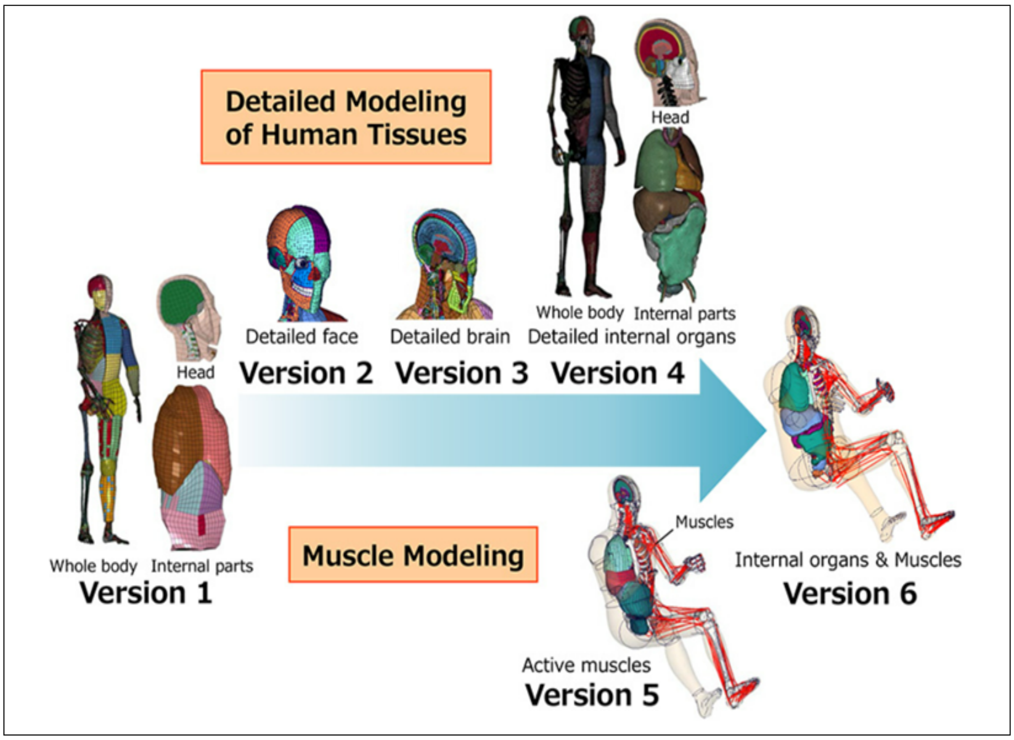

Figure 2.4: Evolution of THUMS. *Toyota Offers Free Access to THUMS Virtual Human Body Model Software.* 2020

the Toyota Central R&D Laboratories Inc utilize high precision computed tomography (CT) scanner to make detailed measurements of internal organs. As result, the version 4.0 of THUMS contains approximately fourteen times more information than the previous versions, the total number of elements was around 2'000'000.

In Version 4 also a variety of different physiques was added, including small female (AF05), representing a 5^{th} percentile American female person 152cm tall and weighs 52kg weight, and large male model (AM95), representing a 95^{th} American male person 188cm tall and weighs 101kg. In 2016 was also included children's models. As shown in figure 2.5 the models can represent both car occupants and pedestrians.

While version 4 of THUMS was the one used in this work, it will be analyzed in more detail in following section.

In 2015 the fifth version (Version 5) was released considering that drivers and passengers take defensive action to soften the impact, by activating their muscles in order to hold their driving or sitting postures just before and after impacts. The drivers that brace themselves in the collision have significant different body movements, comparing to the drivers that are in a relaxed state. This behavior cannot be simulated with the dummies used in traditional crash testes. To address this, Toyota has added in Version 5 of THUMS a muscle detailed model that can simulate human postural states right before and during the collision. Both the braced and relaxed postures can be simulated, as shown in figure 2.6.

This update makes possible the evaluating of safety not only for those system that came into action during the effective collision such as seatbelts, airbags, and other safety equipment, but also the pre-collision systems.

The last version of THUMS, Version 6, was released in 2019. It includes detailed models of human body structures and activable muscles. Both Version 5 and Version 6 has only the sitting occupant model: at the moment there is no implementation regarding the pedestrian model.

In addition to those models, some other were developed for research purpose, such as Elderly AF50 and AM50, Obese BMI35, PregnantAF05, Whiplash AF50 and AM50.

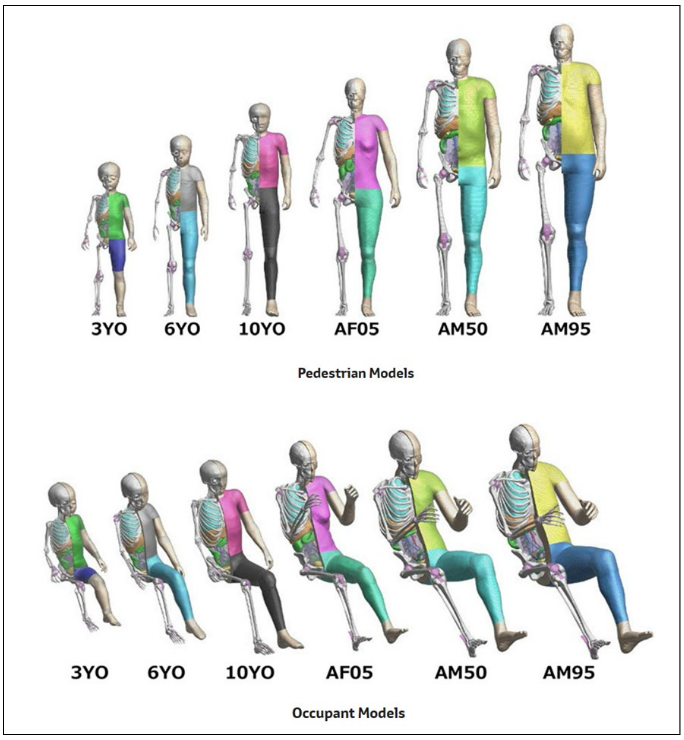

Figure 2.5: THUMS Version 4, types of physiques. *Toyota Offers Free Access to THUMS Virtual Human Body Model Software.* 2020

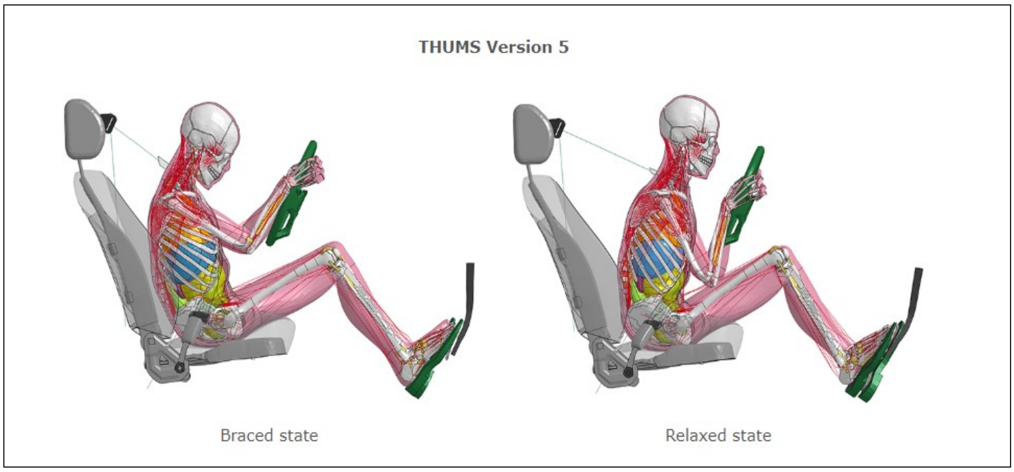

Figure 2.6: THUMS Version 5, comparison between braced and relaxed posture. `https://global.toyota/en/detail/8487899`

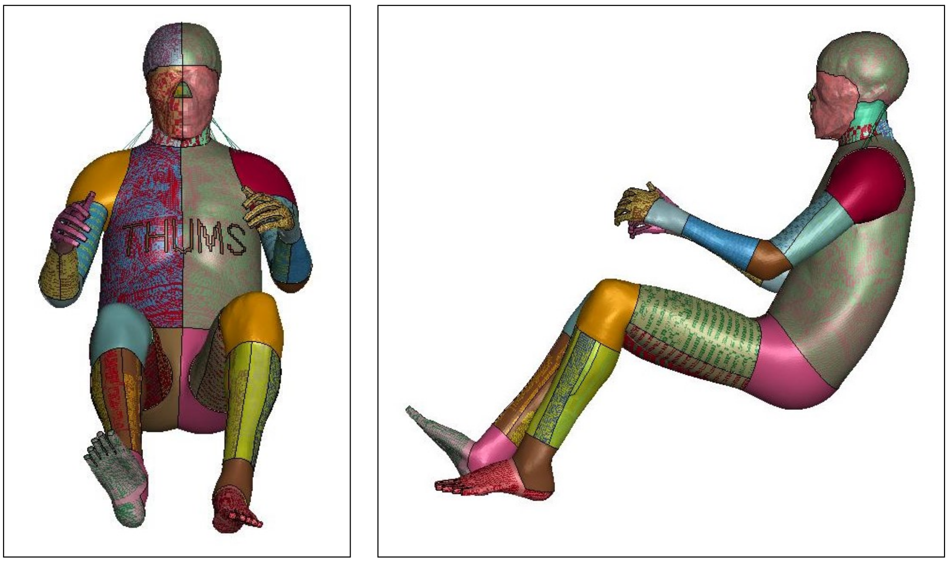

(a) Front view. (b) Side view.

Figure 2.7: THUMS Version 4 for AM50 Occupants Model, academic version.

2.4.2 THUMS Version 4.1

The THUMS model used in this work is the Version 4.1, AM50 Occupant, which has a height of 175cm and a weight of 77kg. The version is an academical one, recognizable by the logotype "THUMS" on the chest, as visible in figure 2.7.

As previously said, the Version 4 includes the detailed model of whole body, including internal parts and organs. The version 4.1 includes some improvement from 4.0, the updates included are briefly presented here.

- Pelvis geometry was modified to average size of AM50 (American Male mid-size).
- Cortical bone thickness of ribs and vertebrae were modified.
- The soft tissue thickness of the anterior abdominal was modified to have the average value.
- Model parameters for compatibility were adjusted to minimize the difference in results between different number of CPUs in parallel computing.

Detailed information about the improvement from Version 4.0 and more technical information about the models composing the THUMS, are available in the documentation of AM50 Occupant Model, Version 4.1, downloadable from `https://www.toyota.co.jp/thums/download/list`.

Model Description

The torso model was developed in cooperation with the University of Michigan, based on high quantities of data coming from high-resolution CT scans, originally performed for medical purpose. The geometries of head and extremities were, instead, defined based on Version 3, by define a deeper mesh.

For the most, the model is composed of solid elements; shell elements were used only for modeling thin tissue parts such as cortical bones with a thickness of less than 1 mm, thin ligaments, and membrane tissues. A few parts were modeled with beam elements, such as neck muscles.

The materials chosen are the following.

- Elasto-plastic material for skeletal parts.

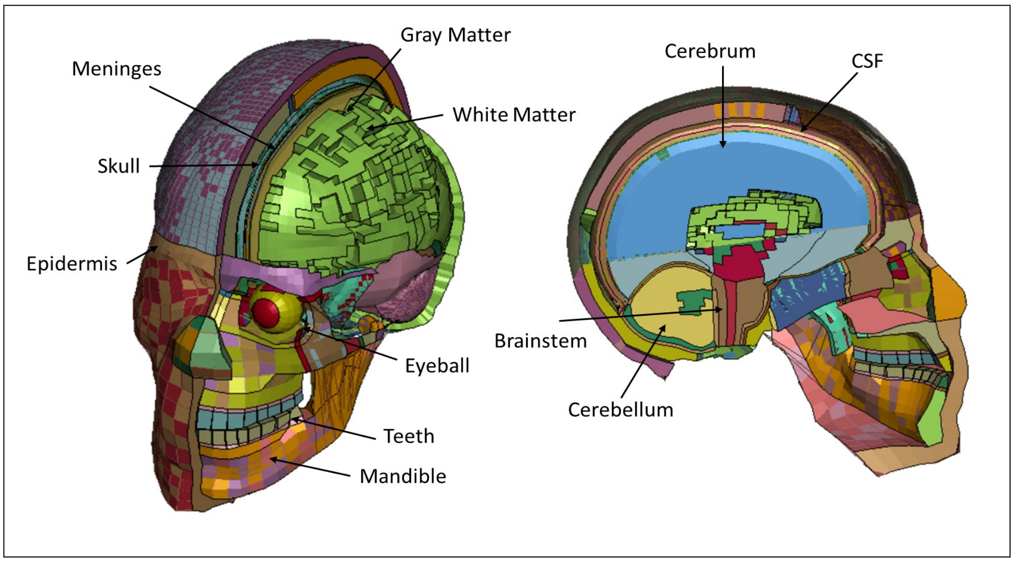

Figure 2.8: Head Model.

- Hyperelastic material for soft tissue.
- Material with low stiffness for small elongation and high stiffness for large elongation for ligaments and tendons.
- Material with incompressive mechanical properties for solid organs such as liver and kidney. While the heart is a hollow organ, it has thick muscular walls and blood inside, so the mechanical property is very incompressive.
- Material with compressive mechanical properties for hollow organs such as lungs and intestine.

The head model is presented in figure 2.8. It includes anatomical parts such as the epidermis, skull, mandible, eyeballs, teeth, meninges, cerebrum, cerebellum, brainstem, CSF etc. The head muscles are modeled with beam elements. The inferior part of the head is connected to the torso through the neck.

The torso model includes the skeletal anatomical parts, the connective tissues, the internal organs, and the muscles. The skeletal parts of the model and the connective tissues, such as cartilages, intervertebral disks, pubic symphysis and ligaments, are presented in figure 2.9 (a), while internal organs and muscles are presented in figure 2.9 (b).

Extremity models include the skeletal parts and soft tissues of legs and arms. The major components are presented in 2.10. The skin which covers all the extremities is modeled with shell elements.

The joints are modeled as bone-to-bone connections with ligaments. In figure 2.11 the knee joint and ankle joint are presented, but the other anatomical joints models are constructed in an analogous way. For instance, ACL, PCL, MCL, LCL are knee ligaments.

The whole-body model was then generated by integrating all those three components (head, torso, and extremities). The boundaries between the parts above described were constructed to not determine geometrical instability.

The total model includes approximately 760'000 nodes and 1.9 million elements.

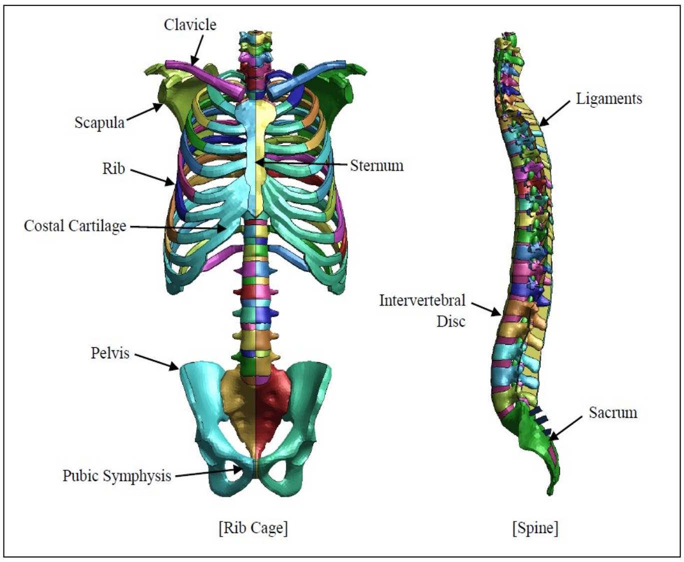

(a) Skeletal parts in Torso Model. Source: AM50 Occupant Model, Version 4.1 documentation. `https://www.toyota.co.jp/thums/`.

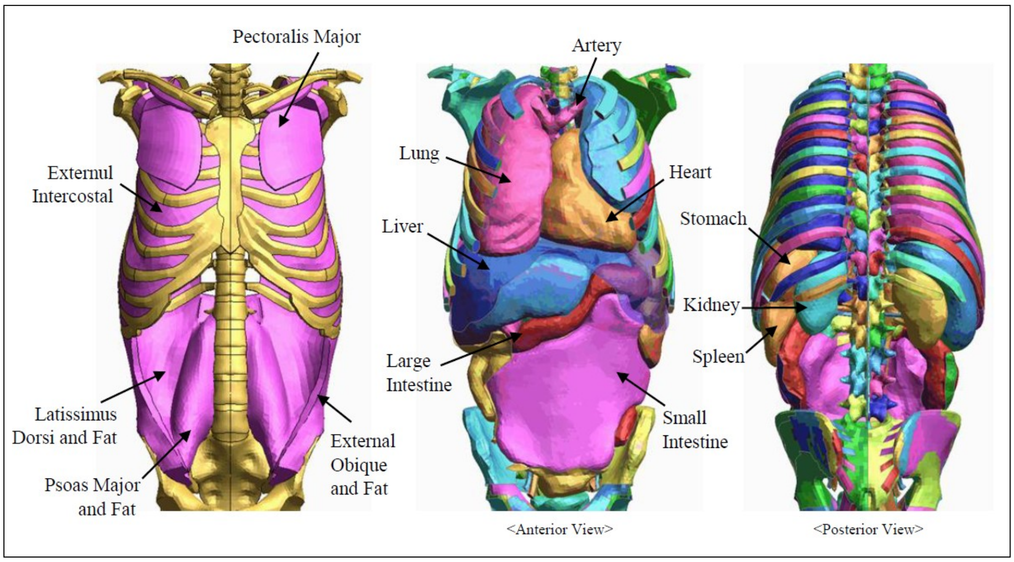

(b) Soft tissue parts in Torso Model. Source: AM50 Occupant Model, Version 4.1 documentation. `https://www.toyota.co.jp/thums/`.

Figure 2.9: Torso Model.

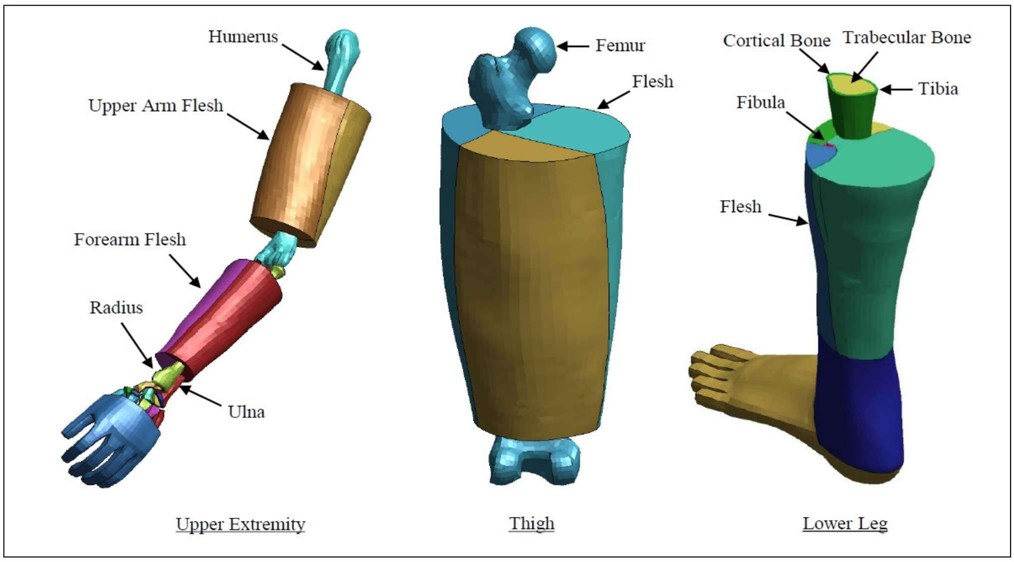

Figure 2.10: Extremity Models. Source: AM50 Occupant Model, Version 4.1 documentation. `https://www.toyota.co.jp/thums/`.

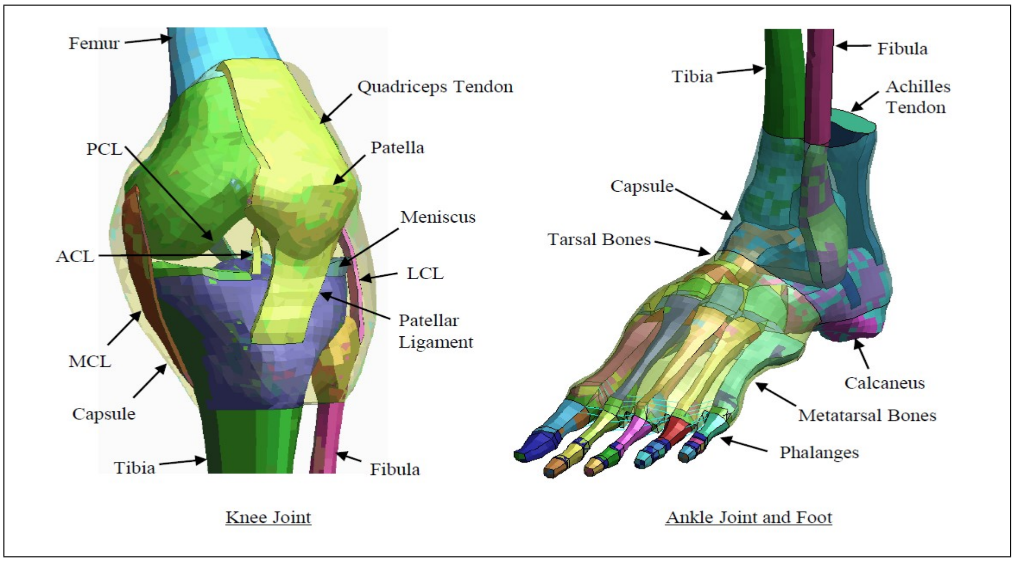

Figure 2.11: Joints Models. Source: AM50 Occupant Model, Version 4.1 documentation. `https://www.toyota.co.jp/thums/`.

(a) Real vehicle.

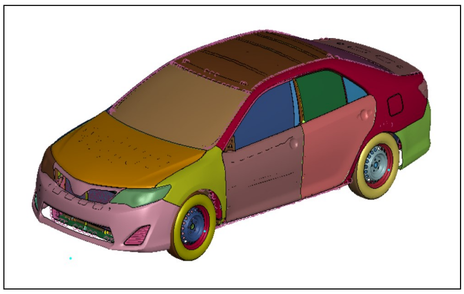

(b) FE model.

Figure 2.12: 2012 Toyota Camry Sedan.

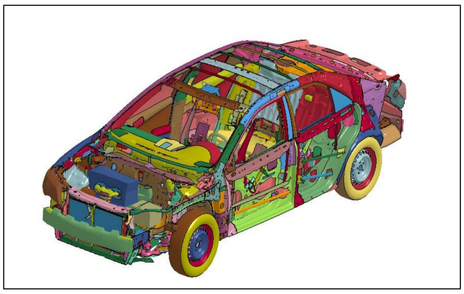

Figure 2.13: 2012 Toyota Camry Sedan, details of the modeled vehicle structure (Collision Safety and (CCSA) 2016.)

2.5 Toyota Camry Model

The vehicle model used in this work is the 2012 Toyota Camry four-door, mid-size passenger sedan for crash simulations use. It was developed through a reverse engineering process by Center for Collision Safety and Analysis (CCSA) researchers under a contract with the Federal Highway Administration (Collision Safety and (CCSA) 2016). The reverse engineering process, named also back engineering process, consists in a disassembling of each vehicle part. Each part was then catalogued and scanned to define its geometry, measured for thicknesses, and classified by material type. All data was entered into a computer file and then each part was meshed to create a computer representation for finite element modelling which reflects all of the structural and mechanical features in digital form. Material data for the major structural components was obtained from manufacturer specifications or determined through coupon testing from samples. The material information provided appropriate stress and strain values for the analysis of crush behavior or failures in crash simulation (Collision Safety and (CCSA) 2016).

The comparison between Toyota Camry Sedan 2012 real vehicle and FE model is presented in figure 2.12. While in figure 2.13 are shown the details of the modeled vehicle structure.

The resulting FE vehicle model has 2'257'280 elements, in which 2'032'594 are shell elements, 5'901 beam elements and 218'785 solid elements. The model is composed of 2'255'361 nodes.

The FE model was verified and validated in several ways to assure that it was an accurate representation of the actual vehicle, more information are presented in the documentation of the FE model of the vehicle: Collision Safety and (CCSA) 2016.

2.6 Mobile Deformable Barrier Model

The third model involved in the simulations is the Advanced European Mobile Deformable Barrier (AE-MDB) model, on trolley.

Livermore Software Technology Corporation (LSTC) have developed the mobile deformable barrier. The model is based on the Advanced European Movable Deformable Barrier Version

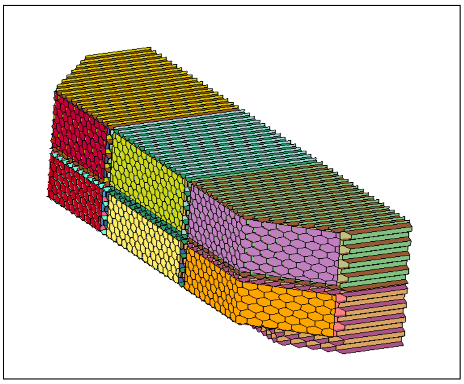

(a) Aluminium honeycomb blocks composing the barrier model.

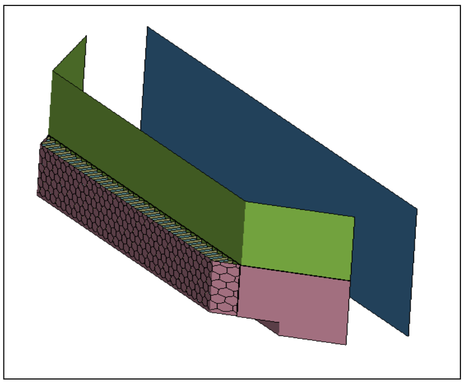

(b) Front and rear plates, together with the bumber.

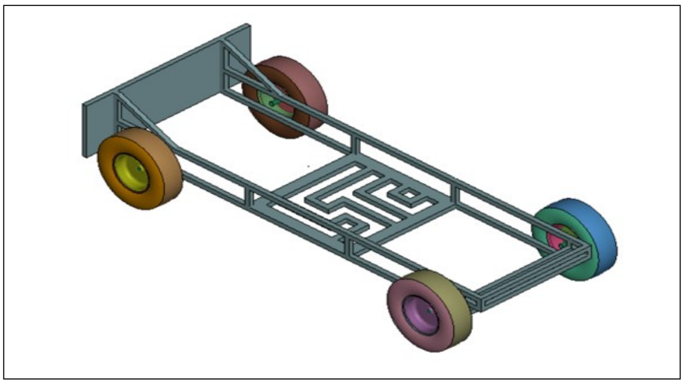

(c) Trolley.

Figure 2.14: Mobile Deformable Barrier Model.

1.0 specification, released on 26th February 2013. The MDB is made mainly by shell elements and recreate the real behavior. All the MDB specifications and test validation are presented in the documenattion of the model: (NCAP 2013).

The mobile deformable barrier consists of two parts: a trolley and an impactor. The impactor consists of six single blocks (Block A_shell.k, Block B_shell.k, Block C_shell.k, Block D_shell.k, Block E_shell.k, Block F_shell.k) of aluminum honeycomb, which have been processed in order to give a progressively increasing level of force with increasing deflection (NCAP 2013).The Yung modulus (E) is set to 70GPa, the Poisson coefficient to 0.3 and the density to $2.7\frac{kg}{mm^3}$. An additional single element is attached of 60mm depth to the front of the lower row of blocks, representing the bumper of vehicle that is colliding the Camry in exam. Front and rear aluminum plates are attached to the aluminum honeycomb blocks. The models of the aluminum honeycomb blocks and the front and rear plates, together with the model of the bumper, are shown in figure 2.14 (a) and (b). While in figure 2.15 is presented the exploded isometric view of AE-MDB.

The bumper is composed of a material with higher Yung modulus than the one of the aluminum used for the honeycomb blocks (79 GPa), and so less deformable. In fact, the material chosen with LS-Prepost for the bumper is the number 081 (PLASTICITY_WITH_DAMAGE) which, differently from the 024 (PIECEWISE_LINEAR_PLASTICITY) presents damage even before the break occurs.

The barrier is placed at the end of the trolley which is instead composed of four wheels and a rigid structure. The trolley is presented in figure 2.14 (c). The rigid structure has an elastic modulus of 206.8GPa and a density of $2.82\frac{kg}{mm^3}$ which correspond to the Corten Steel. The four tires are composed each of a rigid part (tire belt, E=200GPa) and a deformable part with an Elastic modulus of 0.05GPa.

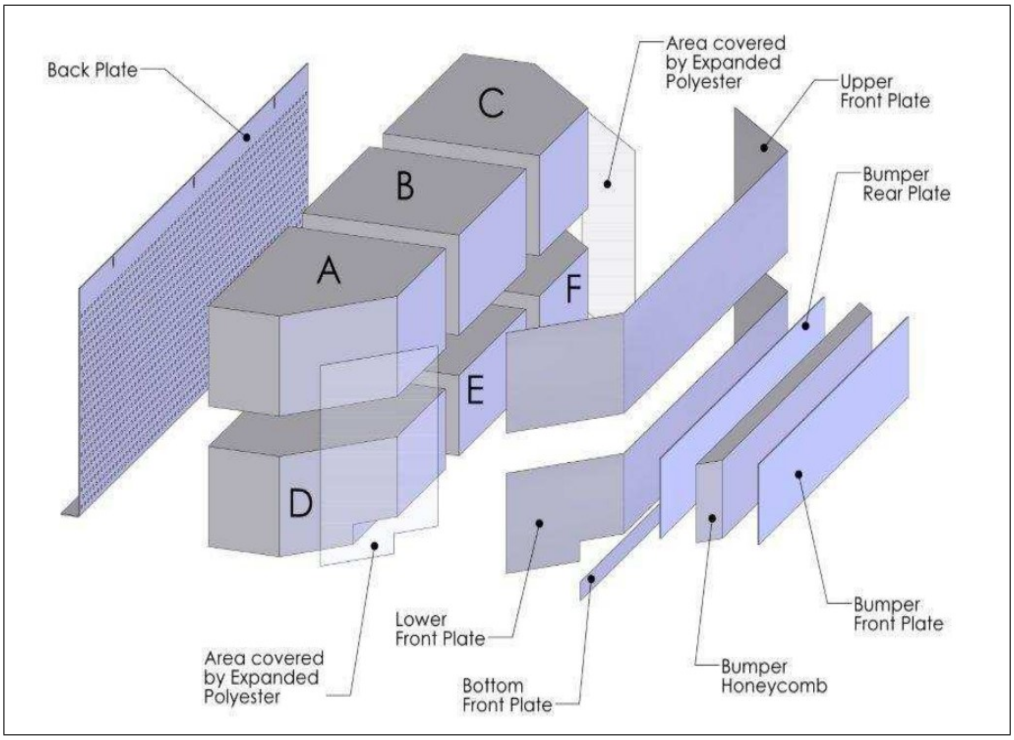

Figure 2.15: Exploded isometric view of AE-MDB. Source: NCAP 2013.

Chapter 3

Pre-Simulation Process

3.1 Simulation settings

The aims of those FE simulations were to recreate the reality of six side impact crashes. Indeed, six different arrangement were taken into analysis: starting from the side impact with reference to the Euro NCAP standard, and then by analyzing five others different configurations, which will be described in following sections.

The THUMS used in this work was already instrumented with all the sensors, as will be described in section 3.4, compliant with the Euro NCAP protocol. Also, the vehicle and the trolley model were already instrumented, compliant with Euro NCAP protocol.

The pre-simulation processes were done with LS-Prepost (LS-PP).

The critical settings to be done for each simulations were the following:

- definition of contacts;
- definition of controls;
- definition of the ground;
- definition of trolley's position and velocity.

To analyze the results with the THUMS Injury Visualization Tool, which will be presented in section 4.3.1, the strain information were needed in the output files of the simulations, and so in keyword *DATABASE_EXTENT_BINARY the SRNFLG must be set to 1.

Contacts In the simulations, the contacts definitions are needed to define how the parts composing the model are in contact with each other. Many contacts definitions were present in the models of this work: some of them were already defined inside the FE models of the vehicle, MDB and THUMS, while the contact between those three subsystem have to be defined. The contacts between the mobile deformable barrier and the vehicle were defined through the keyword *CONTACT_AUTOMATIC_SURFACE_TO_SURFACE: the part set of the car was defined as slave and that of the barrier as master. Other contacts were defined, such as the ones between the THUMS and the driver seat of the vehicle, defined at the same way as the one between the carriage and the vehicle, by defining the part set of the driver seat as master and the one of the THUMS as slave. Also the contacts between seatbelt and THUMS were performed by setting the segment set of seatbelt as master and the THUMS as slave.

Controls The control cards are an important aspect that needs to be set to optimize the simulations. The following control cards were added to fully run and improve the simulations.

- *CONTROL_ACCURACY. The card was used with the purpose of defining controls parameters that can improve the accuracy of calculation.

- *CONTROL_BULK_VISCOSITY. The bulk viscosity is used to treat shock waves. The default quadratic viscosity coefficient was set to 1.5 and the default linear viscosity coefficient to 0.6.
- *CONTROL_CONTACT. It was used to change defaults for computation with contact surface.
- *CONTROL_CPU. It was used to control CPU time, without setting any limit time.
- *CONTROL_ENERGY. The purpose was to provide controls for energy dissipation options. The Stonewall energy, the sliding interface energy, the Rayleigh energy, the initial reference geometry energy, and the hourglass energy dissipation were computed and included in the energy balance.
- *CONTROL_HOURGLASS. The purpose was to set the values of the hourglass control. The hourglass coefficient was set to 0.1.
- *CONTROL_OUTPUT. The card was used to set miscellaneous output parameters.
- *CONTROL_SHELL. The purpose of the card was to provide controls for computing shell response.
- *CONTROL_SOLID. The card was used to provide controls for solid elements response.
- *CONTROL_SOLUTION. Through this cards the solution was set to structural only.
- *CONTROL_TERMINATION. Through this card the duration of the simulation was set to 100ms.
- *CONTROL_TIMESTEP. The card was used to set structural time step size control to 4.440e-07, accordingly to the value given with THUMS Version 4.1.

Definition of the ground It was also necessary to define a floor that recreates the interaction between the wheels and the ground. To accomplish this, the keyword *RIGIDWALL_PLANAR_FINITE was used. The friction coefficient was set to 0.9, in order to simulate the friction between the rubber and the asphalt. The rigid wall created is shown in figure 3.1.

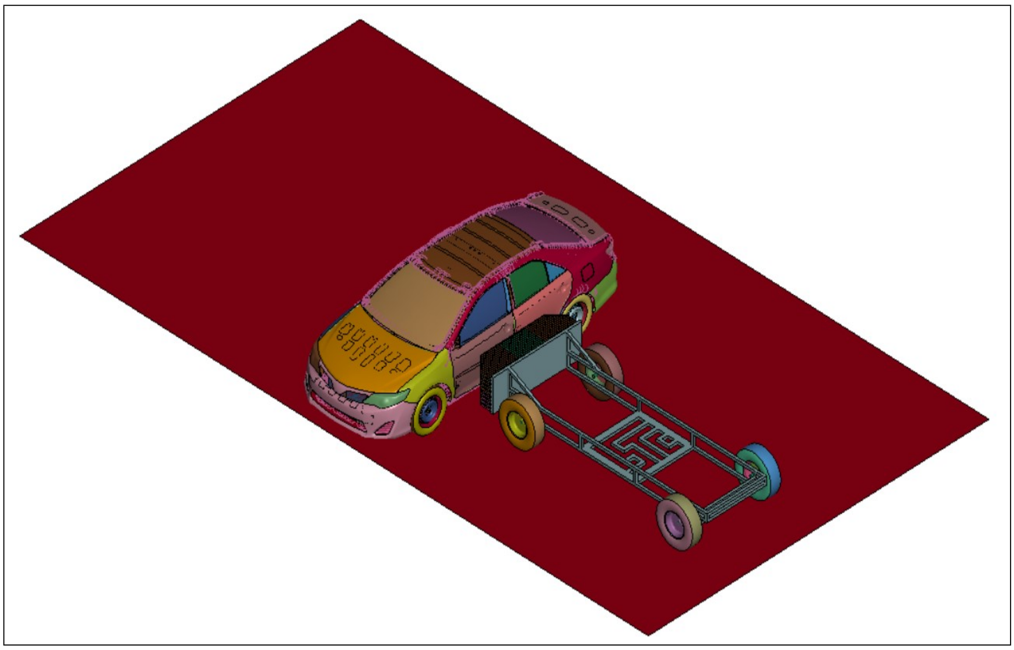

Figure 3.1: Isometric view of the vehicle and trolley on the planar finite.

3.2 Trolley position

The trolley's positions are schematically shown in figure 3.2 and will be described in details in the following sections. The trolley's positions were set in LS-Prespot, by using the transformation tool.

The velocities of the impacts were set considering the Euro NCAP standard for the side impact crash. Indeed, the car was stationary while the MDB impacted the vehicle with an initial speed of 60 km/h.

The velocities were set with the *INITIAL_VELOCITY keyword, considering the trolley's movement direction, in all the six crashes. To set the correct initial velocity to the trolley, a *NODE_SET was created, which included all the nodes composing the MDB and the carriage.

3.2.1 Left Orthogonal Side Impact

The first arrangement was complying with the Euro NCAP standard for side impact. The trolley was aligned to the R-point of the HBM and impact at right angle to the left side of the vehicle, as can be seen in figure 3.3. The trolley's velocity was set equal to -60km/h in Y direction.

3.2.2 Left Front Tilted 45 Degrees Side Impact

In this arrangement the trolley was translated to the front of the vehicle of 1600mm on X axis, to collide the vehicle in its front part but keeping the impact as side impact, and not as a front one. Then the trolley was translated of 400mm on Y axis, to start the simulation of the collision with the MDB not yet contacting the vehicle. Finally, the trolley was tilted of 45 degrees on Z axis, to impact the left front side of the car as shown in figure 3.4. There is no standard defining this type of side impact, anyway the initial velocity was set to be 60km/h on the direction of impact, indeed the X and Y components of velocity were set both to $-60 * \frac{\sqrt{2}}{2} km/h$, while the tilted angle was 45 degrees.

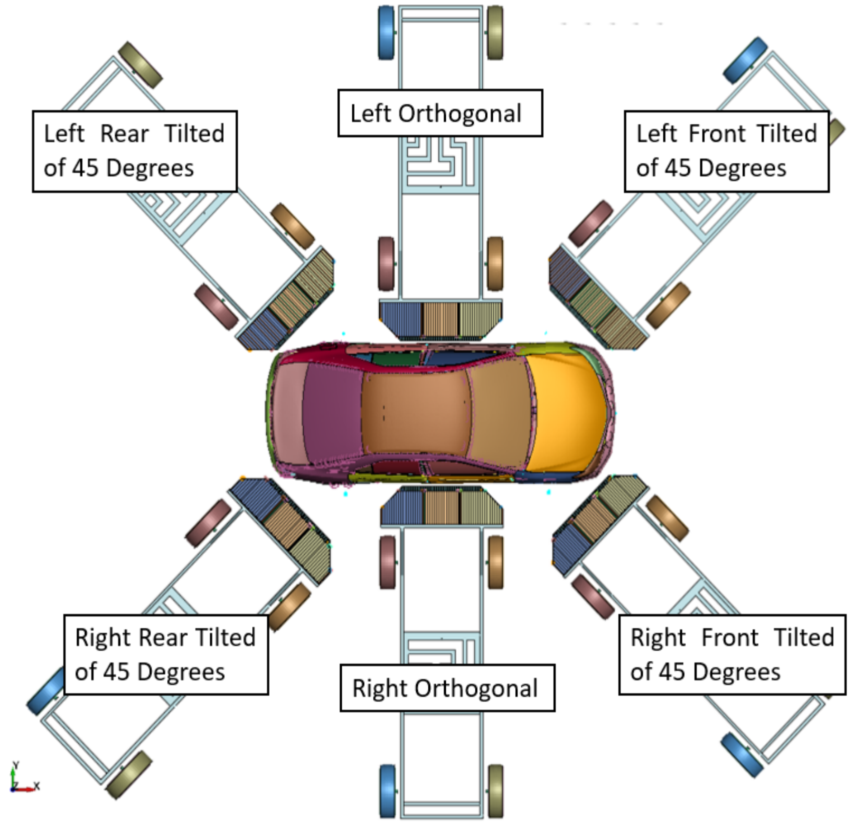

Figure 3.2: Schematically representation of the six configurations of impact.

3.2.3 Left Rear Tilted 45 Degrees Side Impact

In this arrangement the trolley was translated to the rear part of the vehicle of -1600mm on X axis, to collide the vehicle in its rear part but keeping the impact as side impact, and not as a rear one. Then the trolley was translated of 400 mm on Y axis, also in this case, to start the simulation of the collision with the MDB not yet contacting the vehicle. Then it was tilted of 45 degrees to impact the left rear side of the vehicle, as can be seen in figure 3.5. Also in this case there is no standard defining this type of side impact, and the initial velocity was set to be 60km/h on the direction of impact: the X component was set to $+60 * \frac{\sqrt{2}}{2} km/h$, while the Y component was set to $-60 * \frac{\sqrt{2}}{2} km/h$.

3.2.4 Right Orthogonal Side Impact

In this arrangement the trolley was translated from the left orthogonal configuration, on the right side on the vehicle. The trolley was reflected on the right side of vehicle, by choosing as origin of reflection a point in the middle of the segment which goes from the element corresponding to the R-point on left side of vehicle, the one at driver seat, to the element corresponding to R-point ar right side of vehicle, which is the one at passenger seat. The reflection was done on the plan normal to X axis. In the end, the MDB was impacting the right side of the vehicle at right angle, as can be seen in figure 3.6. The velocity was set to + 60km/h on Y axis.

3.2.5 Right Front Tilted 45 Degrees Side Impact

In this arrangement the trolley was translated from the Right Orthogonal Side Impact configuration to the front of the vehicle, by translating at the same way as was done for the left impact: 1600 mm on X axis and -400 mm on Y axis, to start the simulation with the MDB not yet in

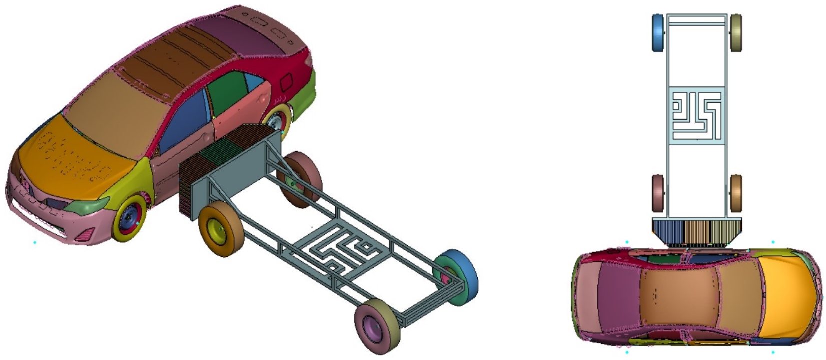

(a) Isometric view. (b) Top view.

Figure 3.3: Left Orthogonal Side Impact in LS-Prepost.

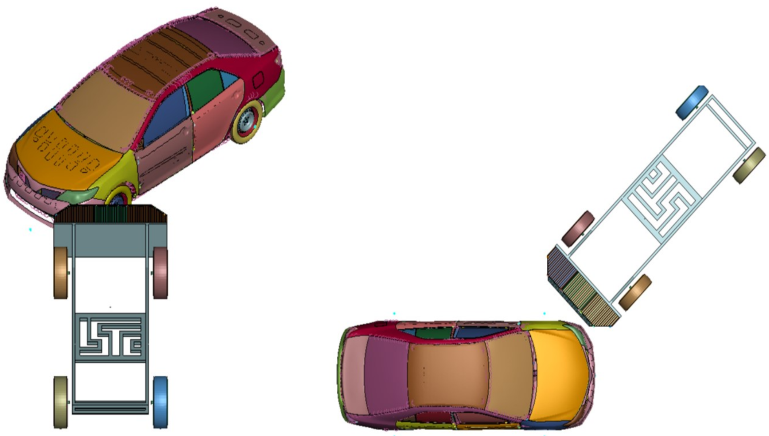

(a) Isometric view. (b) Top view.

Figure 3.4: Left Front Tilted 45 Degrees Side Impact.

contact with the vehicle and colliding the vehicle in its front part. Then the carriage was tilted of 45 degrees to impact the right front side of the vehicle, as shown in figure 3.7.

Also in this case there is no standard defining this type of side impact, and the initial velocity was set to be 60km/h on the direction of impact: the X component was set to $-60 * \frac{\sqrt{2}}{2} km/h$, while the Y component was set to $+60 * \frac{\sqrt{2}}{2} km/h$.

3.2.6 Right Rear Tilted 45 Degrees Side Impact

Finally, in this arrangement, the trolley was translated from the Right Orthogonal Side Impact configuration to the rear part of the vehicle, by translating of -1600 mm on X axis and -400mm on Y axis, and then tilted of 45 degrees to impact the right rear side of the vehicle, as can be seen in figure 3.8. Also in this case there is no standard defining this type of side impact, and the initial velocity was set to be 60km/h on the direction of impact: the X component was set to $+60 * \frac{\sqrt{2}}{2} km/h$, while the Y component was set to $+60 * \frac{\sqrt{2}}{2} km/h$.

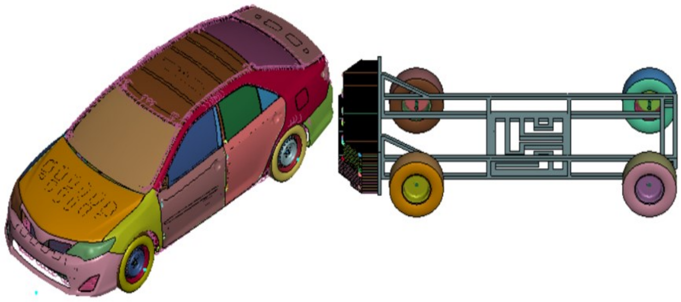

(a) Isometric view.

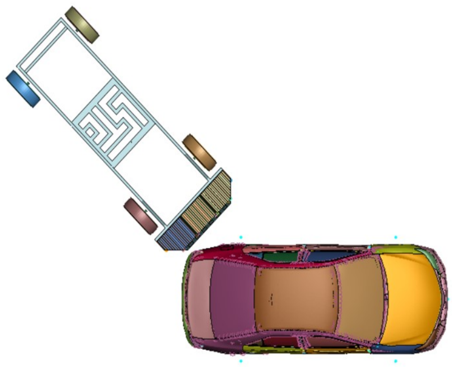

(b) Top view.

Figure 3.5: Left Rear Tilted 45 Degrees Side Impact in LS-Prepost.

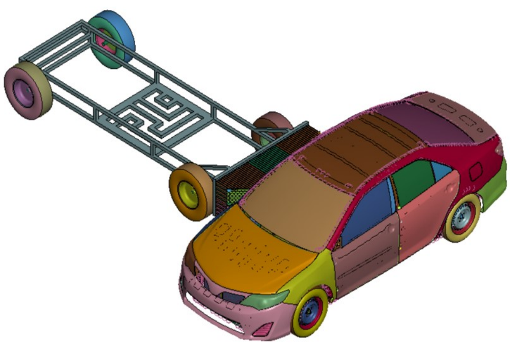

(a) Isometric view.

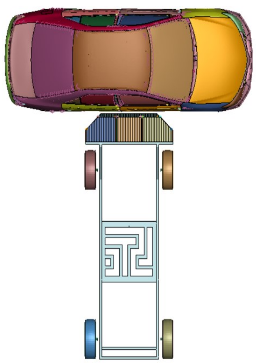

(b) Top view.

Figure 3.6: Right Orthogonal Side Impact in LS-Prepost.

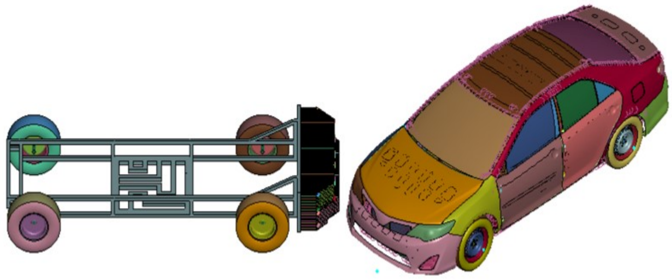

(a) Isometric view.

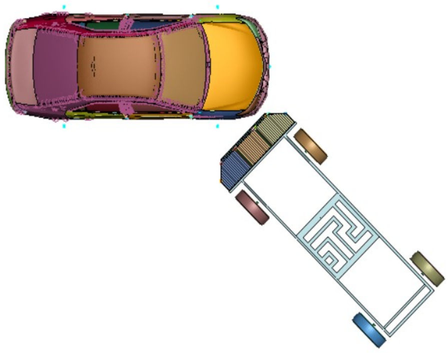

(b) Top view.

Figure 3.7: Right Front Tilted 45 Degrees Side Impact in LS-Prepost.

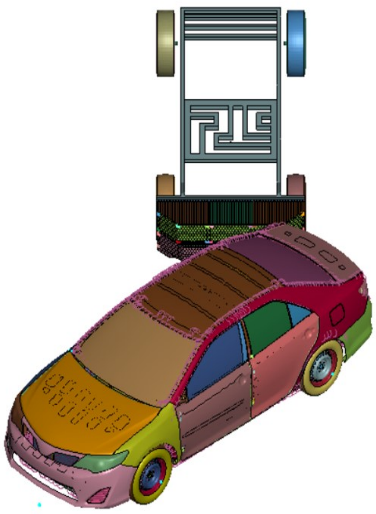

(a) Isometric view.

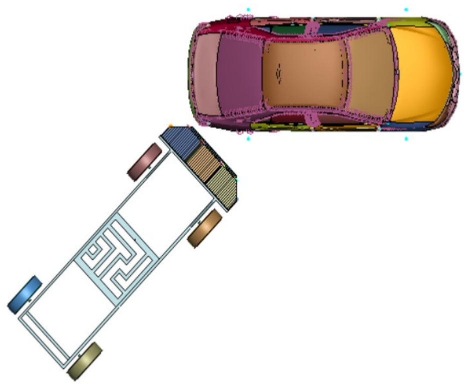

(b) Top view.

Figure 3.8: Right Rear Tilted 45 Degrees Side Impact in LS-Prepost.

(a) Isometric view of THUMS and seat belt.

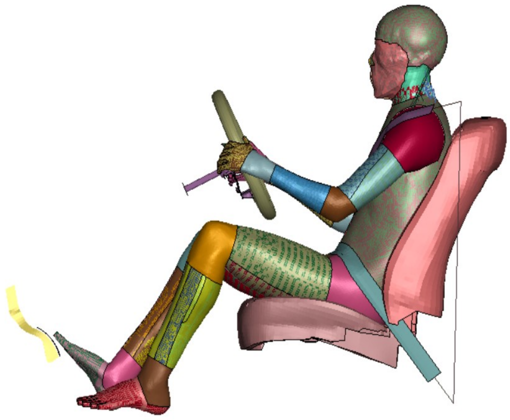

(b) Left side view of THUMS and seat belt.

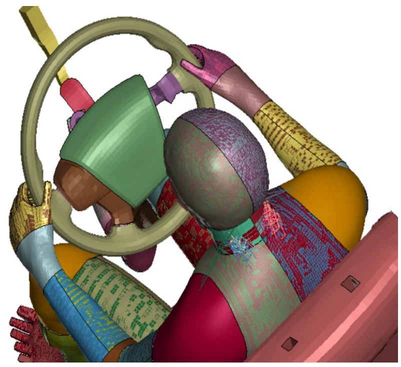

(c) Detail of hands in contact with the steering wheel at a position of quarter to three.

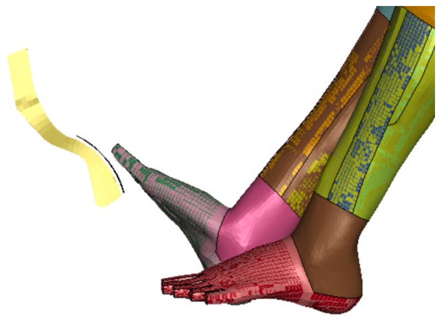

(d) Detail of foots.

Figure 3.9: THUMS inside the vehicle.

3.3 THUMS positioning

The positioning of THUMS inside the vehicle was made following the Euro NCAP standard in a previous work (Garelli 2021). The THUMS with the correct position was kindly granted by the colleague and included in the model by the keyword *INCLUDE.

The THUMS model, with the correct position on the driver seat is presented in figure 3.9. It is visible the torso of the dummy, which is as close as possible to the driver seat and to the H-point; the hands of the dummy are in contact with the steering wheel at the position of quarter to three; the left foot is positioned parallel to the floor in a rest position and the right foot is positioned on the acceleration pedal not pressed, with the heel as far forwards as possible and in contact with the floor.

The NCAP protocol states that the driver should be secured on the seatbelt during the crash test. The seatbelt used in this work is a three-point seatbelt, composed of a B-pillar belt, a shoulder and torso belt, and a lap belt. The seatbelt is positioned on the THUMS, as visible in figure 3.9.

3.4 THUMS sensors

To get biomechanical results, it is necessary to include in the THUMS model a series of sensors that are required by the Euro NCAP protocol. The THUMS model provided by Toyota does

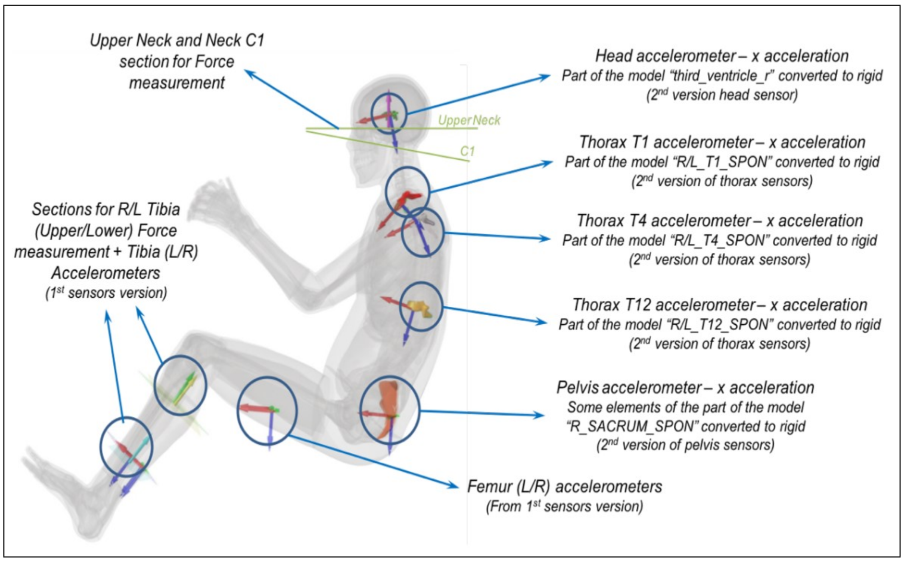

Figure 3.10: Sensor included in THUMS model (Germanetti 2019).

not have pre-installed sensors. However, the THUMS used in this work has been instrumented with sensors in a previous work of Germanetti in 2019 (Germanetti 2019), in which the sensors shown in figure 3.10 were added.

Some modification to the model developed by Germanetti were made in the work of Garelli in 2021 (Garelli 2021), by adding specific sensors to better comply the Euro NCAP requirements. The sensors added were:

- the head accelerometer;
- multiple sensors positioned in the thorax such as accelerometers and load sensors;
- markers on the ribs and vertebrae were added to visualize the deformation of the ribcage;
- specific sensors used to analyze the behavior of internal organs;
- four accelerometers are placed on the lower limbs in order to visualize the data from right and left tibia and femur.

However, the outputs of those added sensors were not used in this work, because the THUMS Injury Visualization tool was not analyzing them. The description of those sensors is however meaningful to describe the HBM used in its entirety.

3.5 Solving

Once the phase of pre-processing was done by defining all the settings, the simulations were launched using LS-Dyna, through the server of HPC@POLITO, an Academic Computing project of the Department of Automatics and Informatics at the Politecnico di Torino `http://www.hpc.polito.it`. The cluster used in this work is the Legion Cluster.

All the six side impact simulations were performed with MPP LS-Dyna, release r9, in single precision. The simulations required around 43 hours each to be completed with 64 cores on 2 nodes. The memory used for each simulation was around 28 GB.

Chapter 4

Results

4.1 Overview

In figures 4.1, 4.3, 4.5, 4.7, 4.9, 4.11 are represented five frames, each every 20 ms of collision, for each crash simulation in isomeric views, while in figures 4.2, 4.4, 4.6, 4.8, 4.10, 4.12 are represented five frames, each every 20 ms of collision, in front view, for each crash simulation in section, to highlight the movement of the THUMS inside the vehicle. In those figures, the parts of the vehicle and of the MDB that could hide the movements of the THUMS have been removed from the visualization, to better highlight the movements of the THUMS.

All the impacts lasted 100 ms, except the right orthogonal one, which has failed after 45 ms of collision.

With the only observation of the figures representing the collisions, it is evident that the side crash which caused the most severe injuries is the left orthogonal one. Those injuries are mainly resulting on the head of THUMS, which collides with the internal parts of the vehicle, on its left side. The head is colliding with the left front door in the part immediately below the window, by doing a movement of approach towards the left shoulder that is resulting also in a distraction of cervical spine, as will be discussed in following sections. In the other five configurations, the space between the THUMS and the MDB incoming is bigger than in the left orthogonal impact: in particular in right configurations, the THUMS is on the other side of the vehicle with respect to the part in which the collision happens, and so the THUMS is performing only a translational movement towards the incoming MDB on its right, but that movement is not resulting in any severe injury. While, in left front and left rear tilted configurations the space of the vehicle between the MDB and the THUMS is bigger than the one in the left orthogonal impact, in which this space consists only in the front door. Hence, the left front and left rear tilted configurations are not resulting in severe injury risks.

Indeed, the left orthogonal configuration is the only one among the six side impacts analyzed in this work, for which the Euro NCAP standard exist, and this can be explained with the extremely severity of the impact.

Before discussing the lesions resulting from the impacts, energy considerations must be done to evaluate the stability of the simulation and, hence, to establish whether the results regarding anatomical lesions can be considered valid or not, from the point of view of numerical simulation.

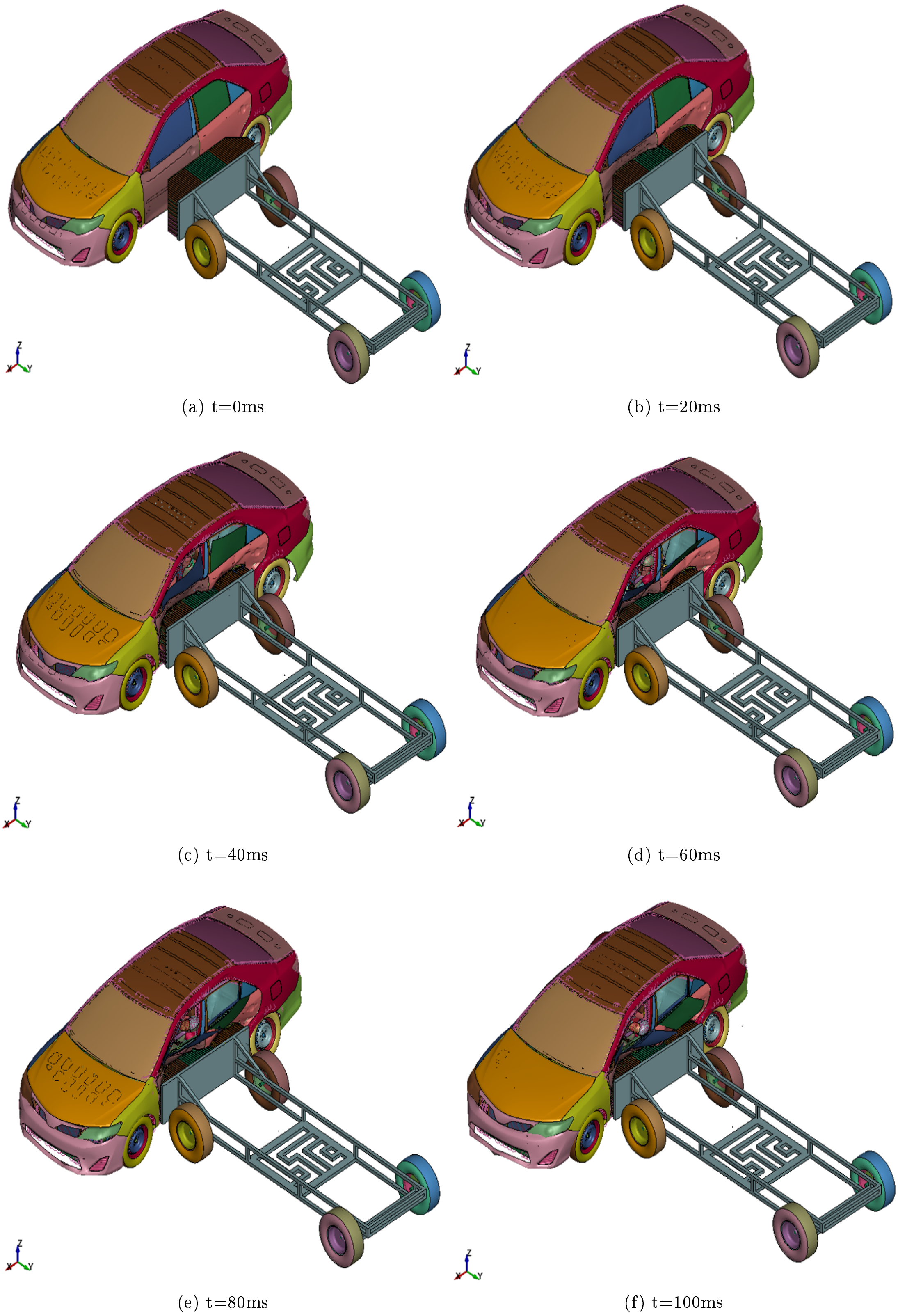

(a) t=0ms

(b) t=20ms

(c) t=40ms

(d) t=60ms

(e) t=80ms

(f) t=100ms

Figure 4.1: Isomeric view of Left Orthogonal Impact.

(a) t=0ms

(b) t=20ms

(c) t=40ms

(d) t=60ms

(e) t=80ms

(f) t=100ms

Figure 4.2: Front view of Left Orthogonal Impact in section.

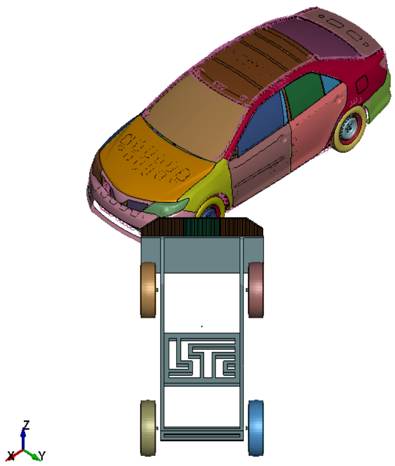

(a) t=0ms

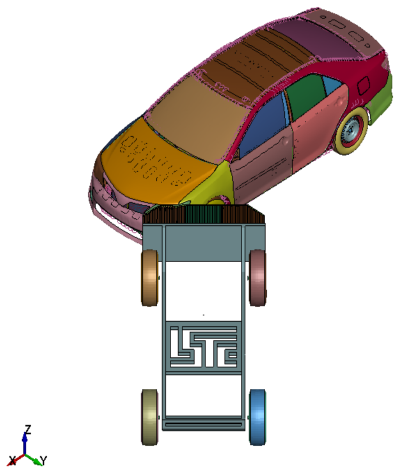

(b) t=20ms

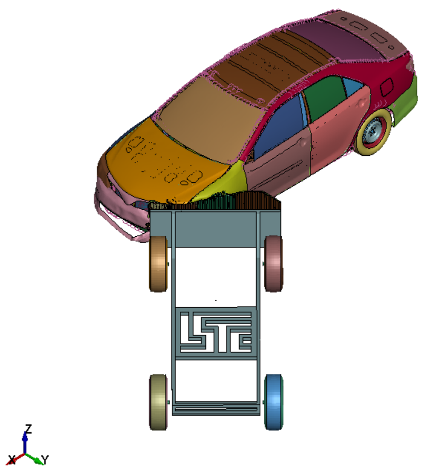

(c) t=40ms

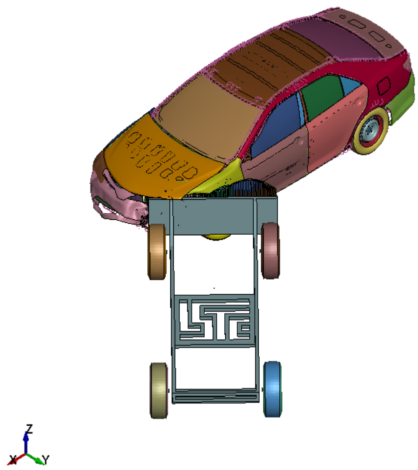

(d) t=60ms

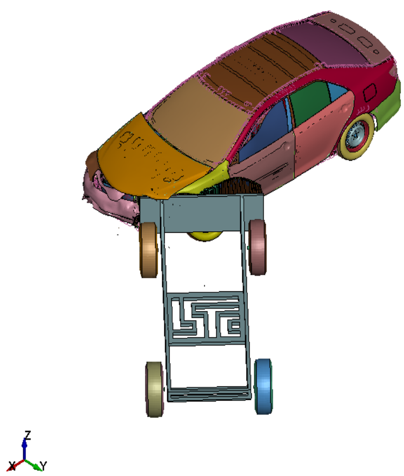

(e) t=80ms

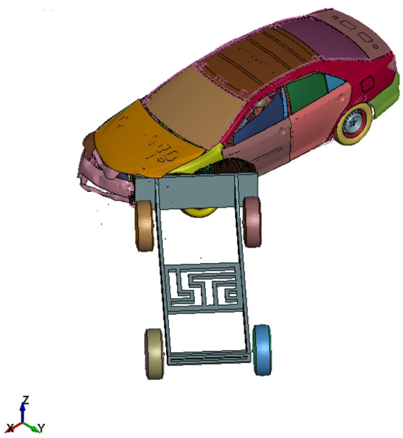

(f) t=100ms

Figure 4.3: Isomeric view of Left Front Tilted 45 Degrees Side Impact.

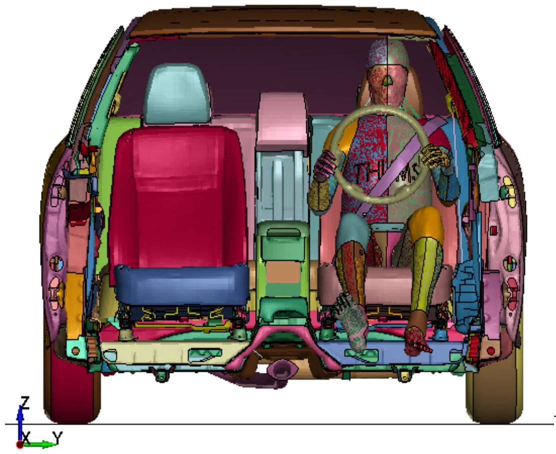

(a) t=0ms

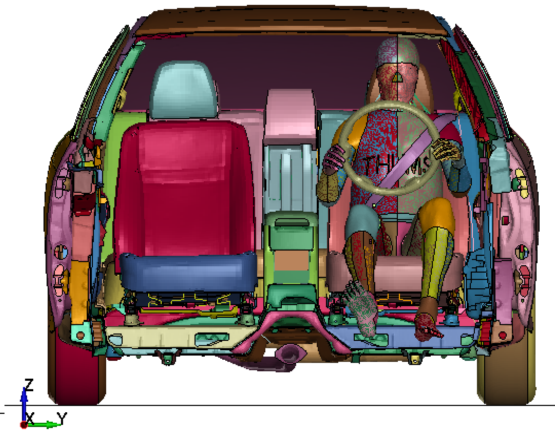

(b) t=20ms

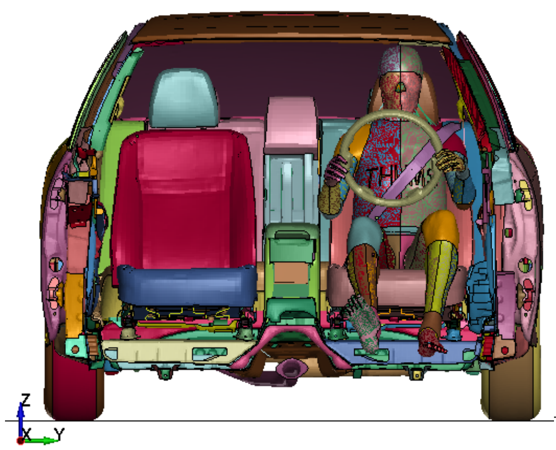

(c) t=40ms

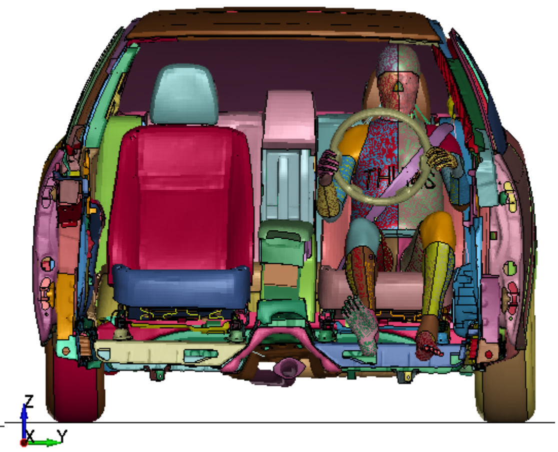

(d) t=60ms

(e) t=80ms

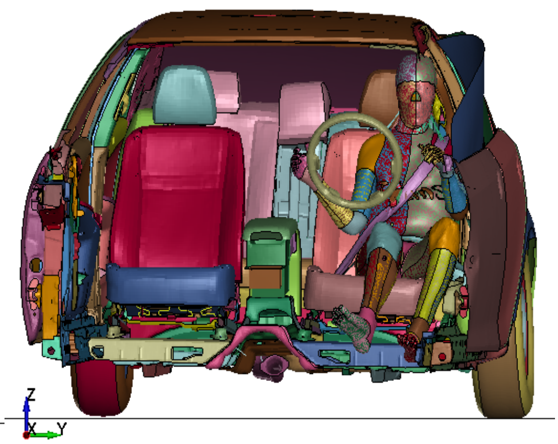

(f) t=100ms

Figure 4.4: Front view of Left Front Tilted 45 Degrees Side Impact in section.

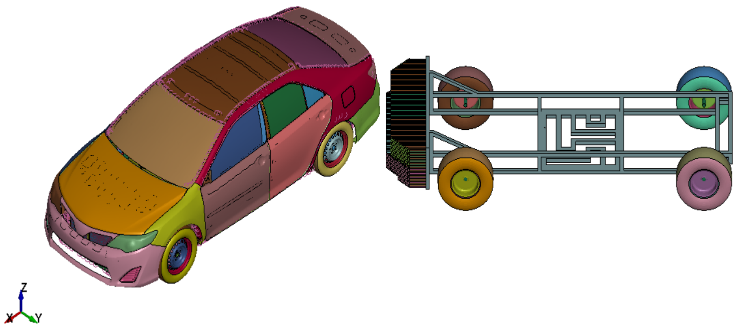

(a) t=0ms

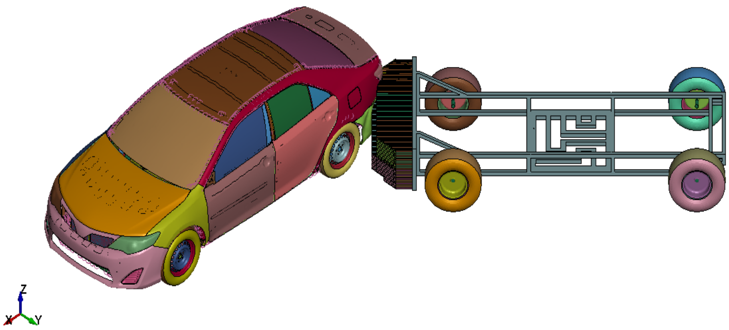

(b) t=20ms

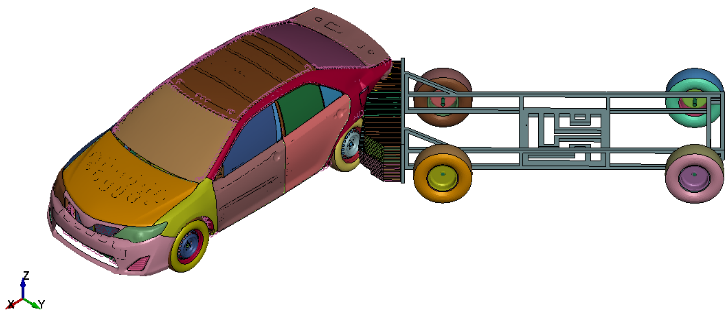

(c) t=40ms

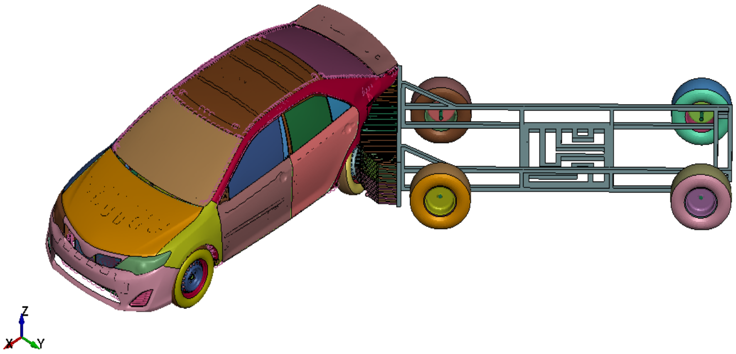

(a) t=60ms

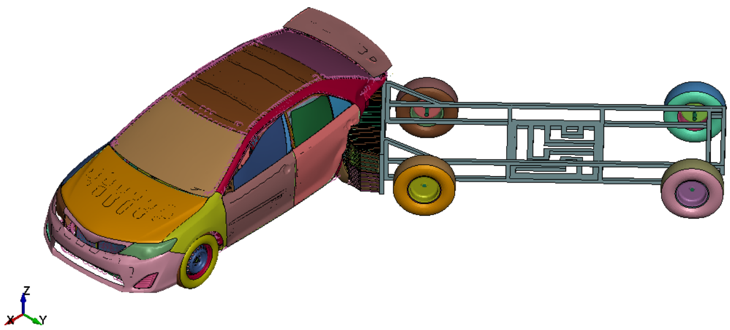

(b) t=80ms

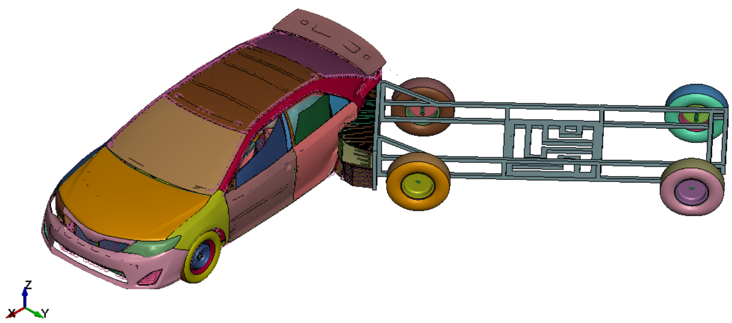

(c) t=100ms

Figure 4.5: Isomeric view of Left Rear Tilted 45 Degrees Side Impact.

(a) t=0ms

(b) t=20ms

(c) t=40ms

(d) t=60ms

(e) t=80ms

(f) t=100ms

Figure 4.6: Front view of Left Rear Tilted 45 Degrees Side Impact in section.

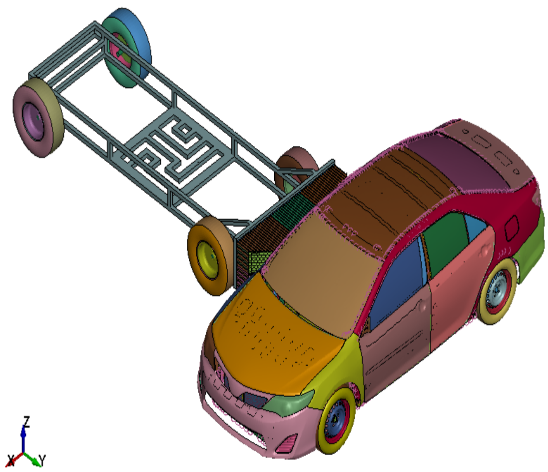

(a) t=0ms

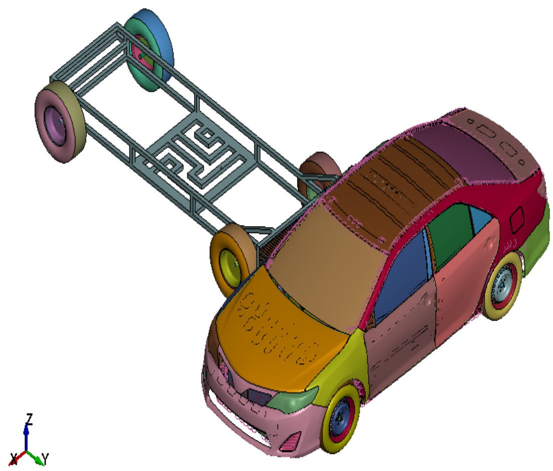

(b) t=20ms

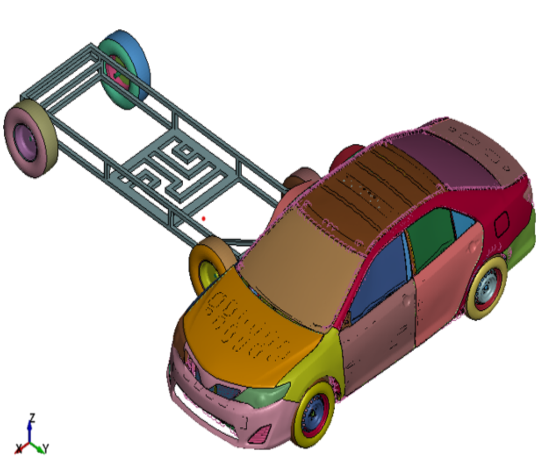

(c) t=35ms

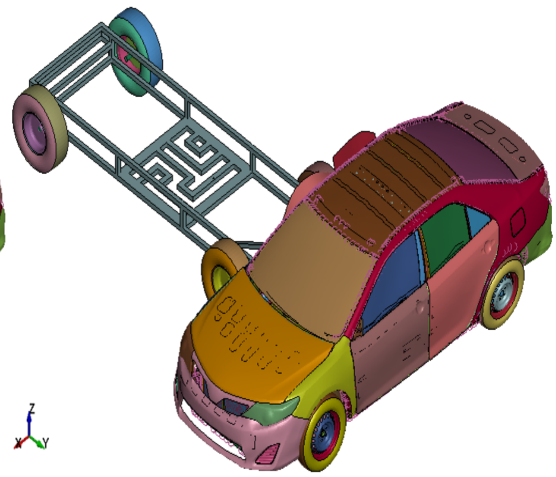

(d) t=45ms

Figure 4.7: Isomeric view of Right Orthogonal Side Impact.

(a) t=0ms

(b) t=20ms

(c) t=35ms

(d) t=45ms

Figure 4.8: Front view of Right Orthogonal Side Impact in section.

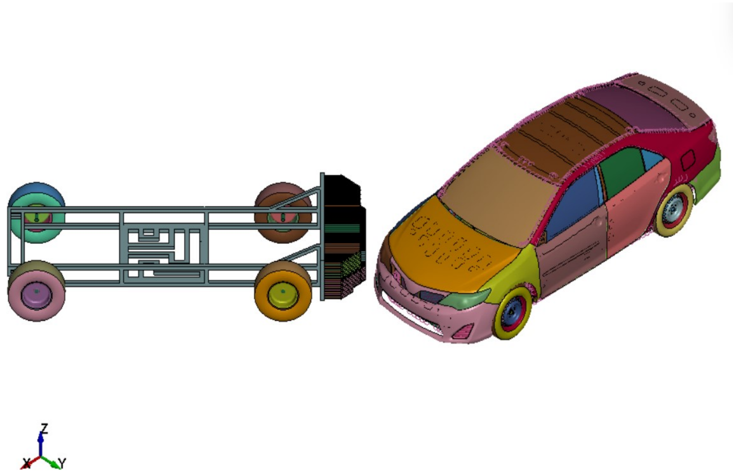

(a) t=0ms

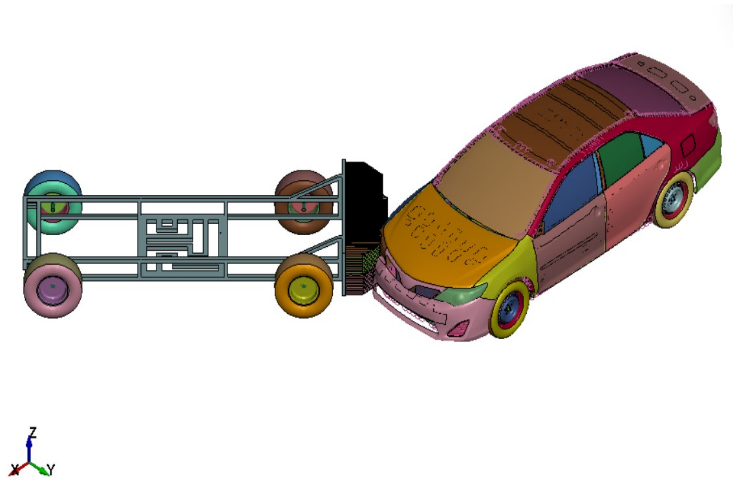

(b) t=20ms

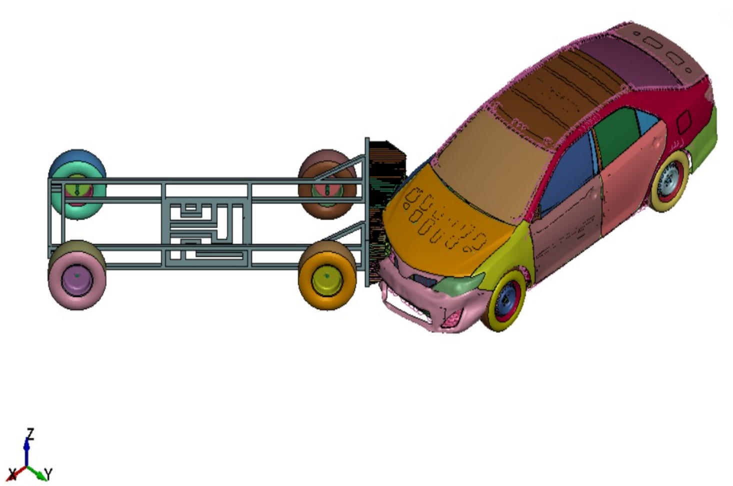

(c) t=40ms

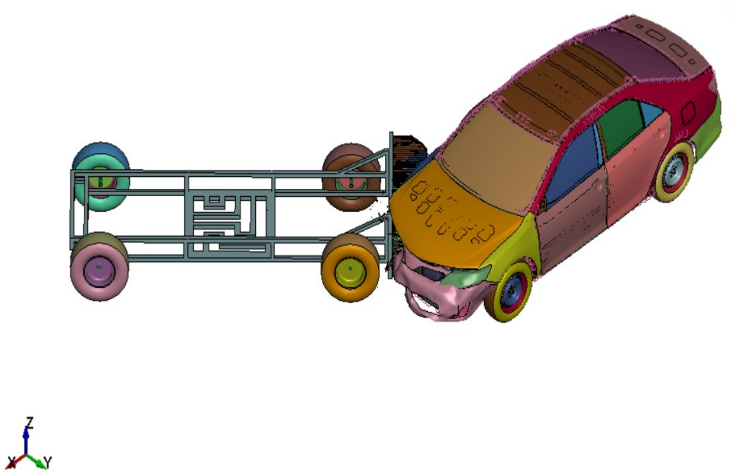

(a) t=60ms

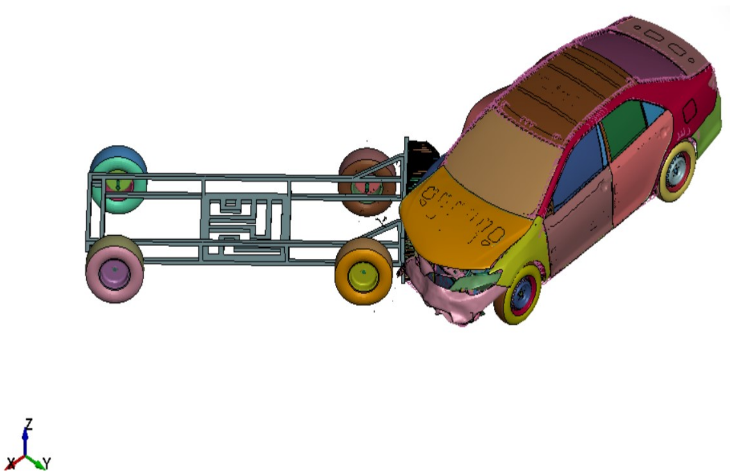

(b) t=80ms

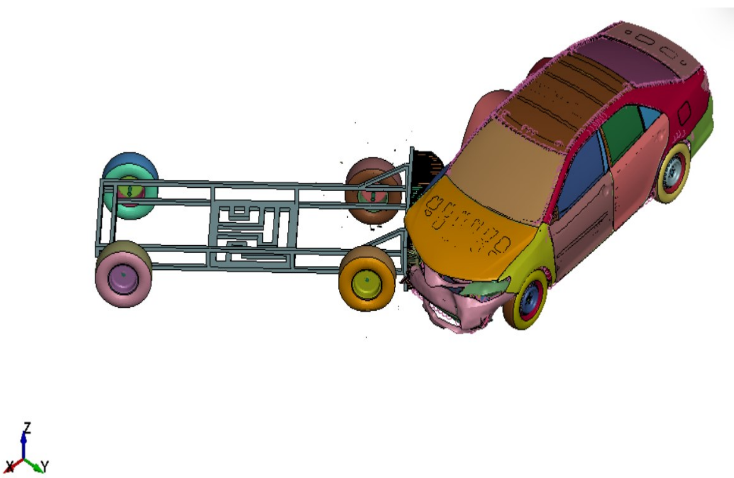

(c) t=100ms

Figure 4.9: Isomeric view of Right Front Tilted 45 Degrees Side Impact.

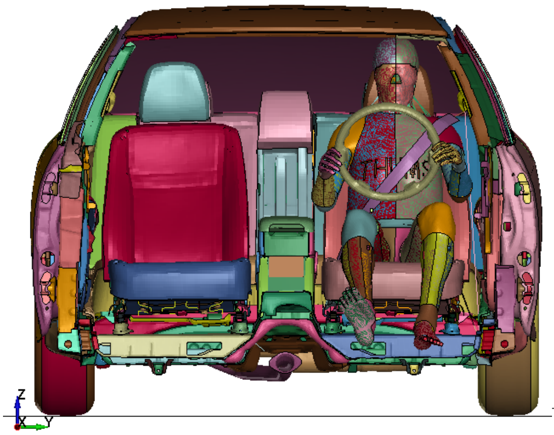

(a) t=0ms

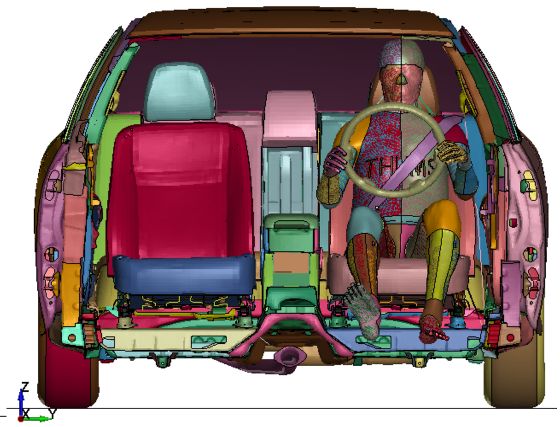

(b) t=20ms

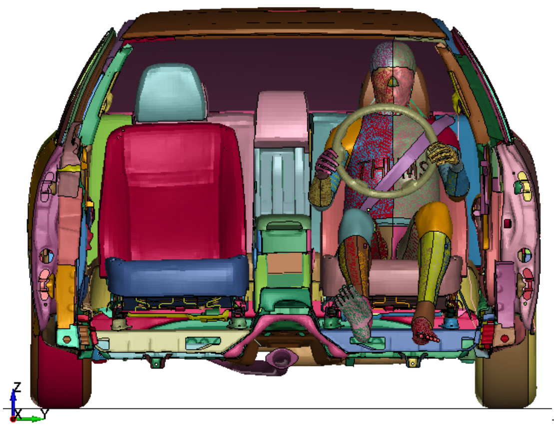

(c) t=40ms

(d) t=60ms

(e) t=80ms

(f) t=100ms

Figure 4.10: Front view of Right Front Tilted 45 Degrees Side Impact in section.

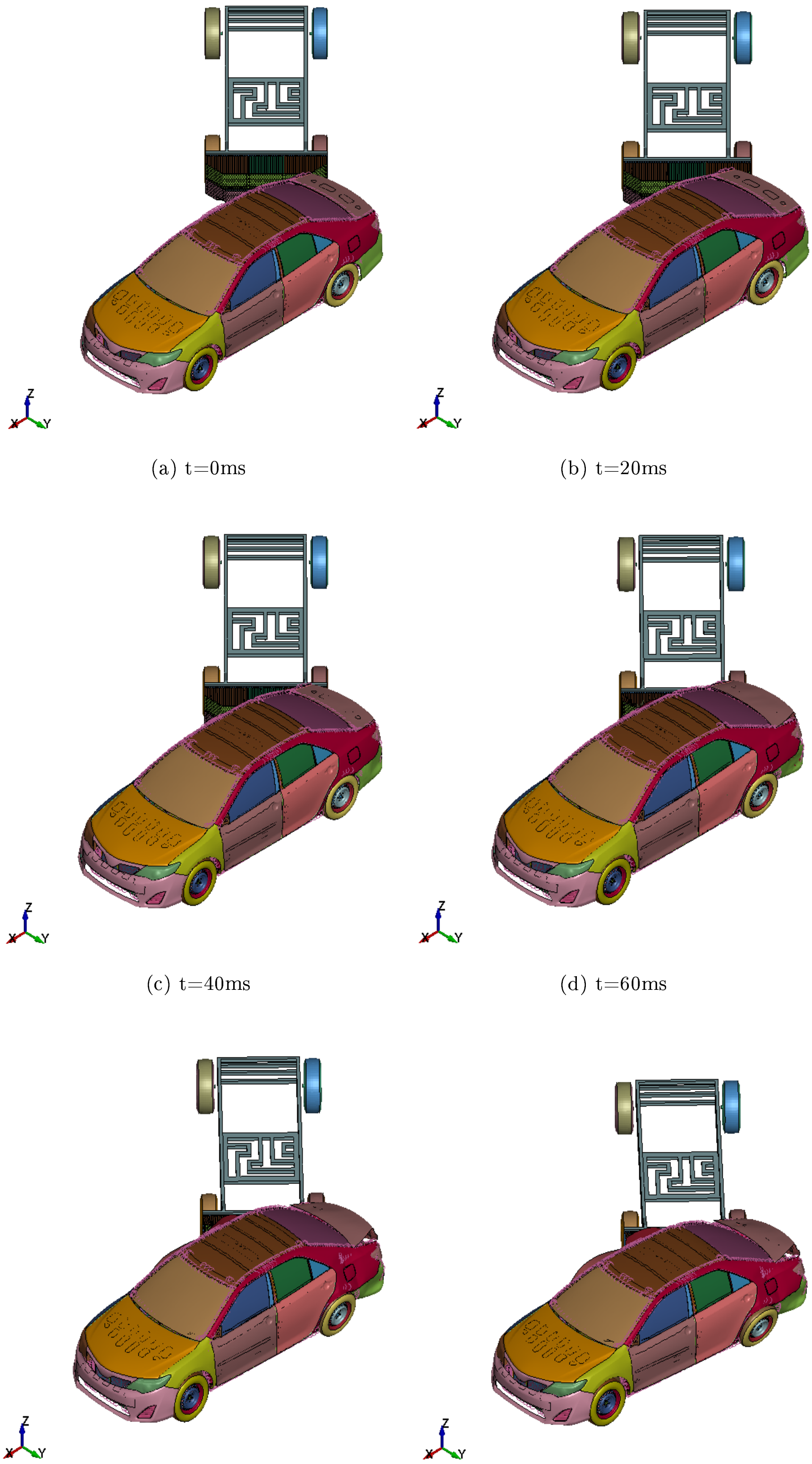

(a) t=0ms

(b) t=20ms

(c) t=40ms

(d) t=60ms

(e) t=80ms

(f) t=100ms

Figure 4.11: Isomeric view of Right Rear Tilted 45 Degrees Side Impact.

(a) t=0ms

(b) t=20ms

(c) t=40ms

(d) t=60ms

(e) t=80ms

(f) t=100ms

Figure 4.12: Front view of Right Rear Tilted 45 Degrees Side Impact in section.

4.2 Energy Considerations

To evaluate the stability of the simulations, some energy considerations must be done. The first evaluation is the one concerning the energy balance, which should be constant over the simulation, and the evaluation of the hourglass energy, which should be as low as possible, as explained in section 2.1.3.

To evaluate the stability of the simulation, the energy balance must be verified through the simulation. It is a good indicator of a simulation without numerical errors. Unexpected trends are symptoms of potential problems or errors.

The energy balance can be written in the following way:

$$E_{kin} + E_{int} + E_{si} + E_{damp} + E_{hg} = E^0_{kin} + E^0_{int} + W_{ext}$$

where contributions are made by:

- E_{kin} is the kinetic energy;
- E_{int} is the internal energy;
- E_{si} is the interface energy;
- E_{damp} is the rigid body energy;
- E_{hg} is the hourglass energy;
- E^0_{kin} is the initial kinetic energy;
- E^0_{int} is the initial internal energy;
- W_{ext} is the external work.

All the contributions together at the left of the equal sign, correspond to the total energy (E_{tot}).

While, in side impact simulations analyzed, there was no external work applied, the total energy must remain constant through the simulation and the value must corresponds to the sum of initial kinetic energy and initial internal energy. If the maximum oscillation of the total energy was less than 5%, the total energy could be considered constant by committing a negligible error.

In figures 4.13, 4.14, 4.15, 4.16, 4.17 and 4.18 are presented, for each impact simulation, the trends of total energy, internal energy, external work, kinetic energy, and hourglass energy

For example, considering the left orthogonal side impact, the total energy must be constant, and the value must be equal to the sum of initial kinetic energy, which value was $E^0_{kin} = 1.8{*}10^5$, and the initial internal energy, which value was zero. Indeed, the value of total energy must be $E^0_{kin} = 1.8 * 10^5 \pm 0.09 * 10^5$.

This requirement was, in fact, respected in the simulation, as evident in the figure 4.13. In that figure, the trend of the total energy is presented in yellow, and it visible that the maximum oscillation of the total energy was less than 5%.

The same observations could be made for all the six simulations, therefore, all of them are energetically stable.

The kinetic energy, in purple in figures, was descending in all the six simulations and that was because the impacts begin with the carriage moving and, because the collision was inelastic, the overall kinetic energy was not conserved but decreases.

While the kinetic energy was decreasing, that should be a contribution of energy that was increasing, to keep the total energy constant. The energy contribution that was increasing is the internal energy, in green in the figures. In fact, the initial internal energy was zero in all the six simulations, hence the total energy was always corresponding to the initial value of the kinetic energy, with a tolerance of $\pm 5\%$.

From the figures it is also visible that there was not any contribution of external work, for all the simulations.

As previously said, the hourglass energy is the energy that is created computationally due to the phenomenon of hourglass. The phenomenon of hourglass should be reduced as much as

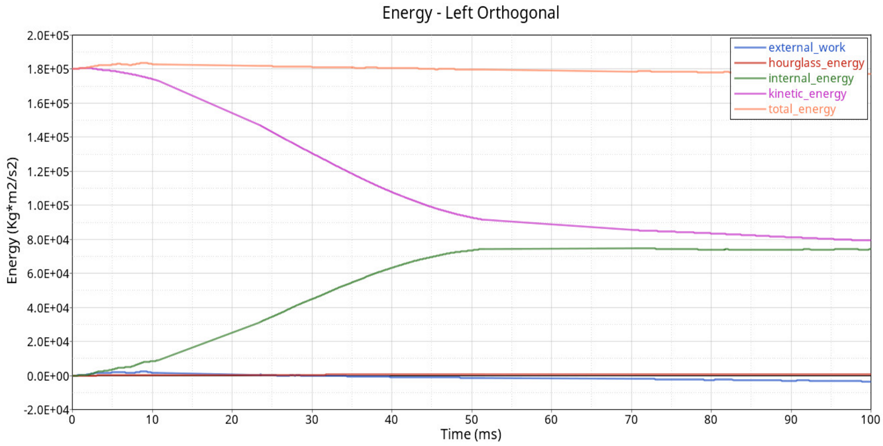

Figure 4.13: Trend of total energy, internal energy, kinetic energy and hourglass energy, in left orthogonal side impact.

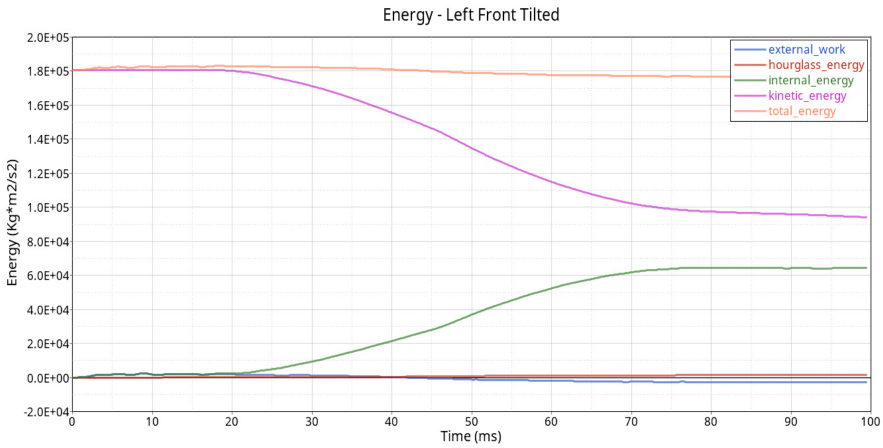

Figure 4.14: Trend of total energy, internal energy, kinetic energy and hourglass energy, in left front tilted side impact.

possible, so the energy associated with it should be low. From figures 4.13, 4.14, 4.15, 4.16, 4.17 and 4.18, it is visible that, in all the six simulations, the contribution of hourglass energy, painted in red, was not exceed the threshold of 5% of the total energy, therefore the error introduced by the hourglass phenomenon could be considered negligible.

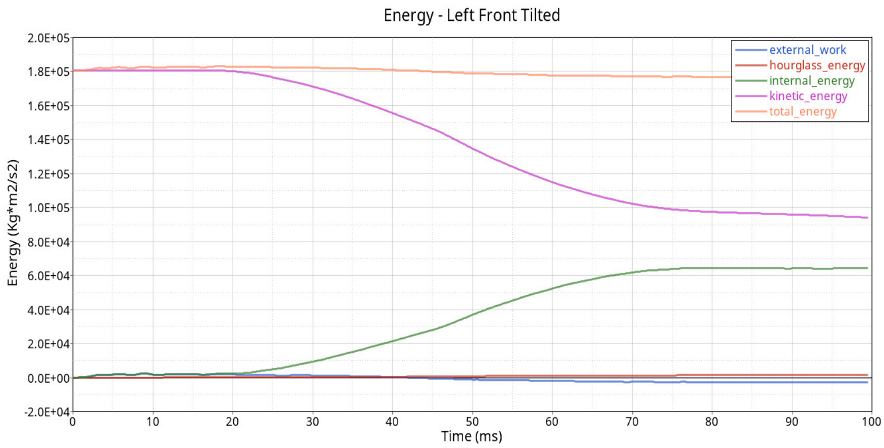

Figure 4.15: Trend of total energy, internal energy, kinetic energy and hourglass energy, in left rear tilted side impact.

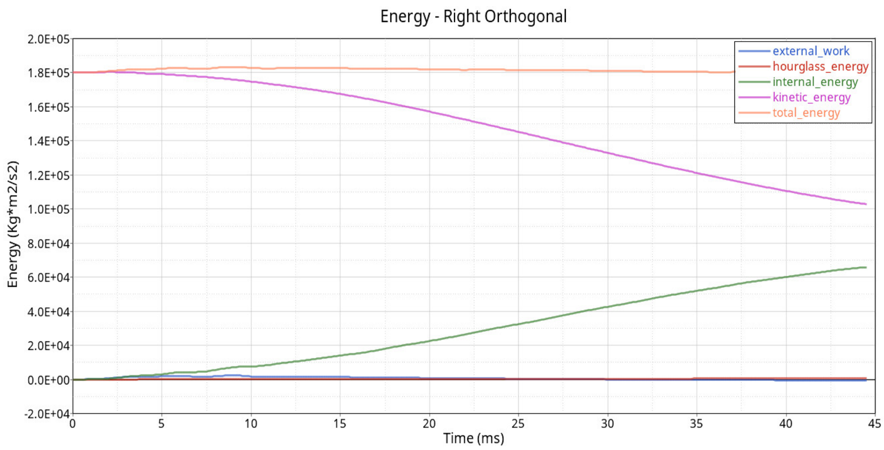

Figure 4.16: Trend of total energy, internal energy, kinetic energy and hourglass energy, in right orthogonal side impact.

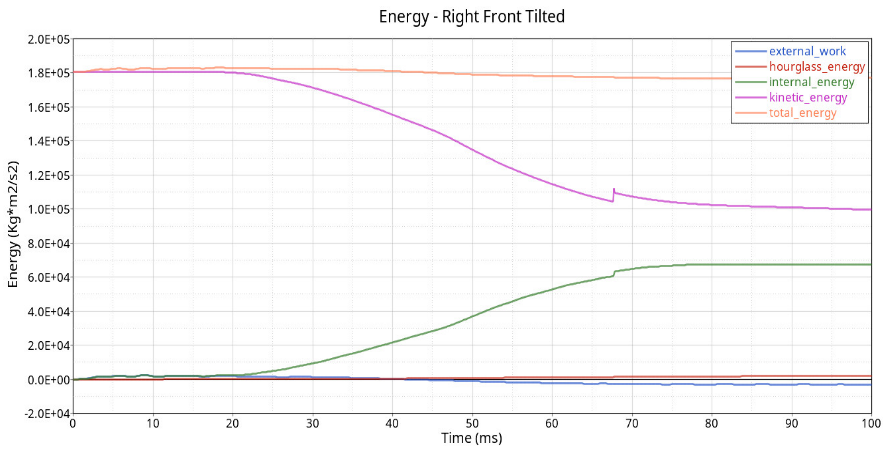

Figure 4.17: Trend of total energy, internal energy, kinetic energy and hourglass energy, in right front tilted side impact.

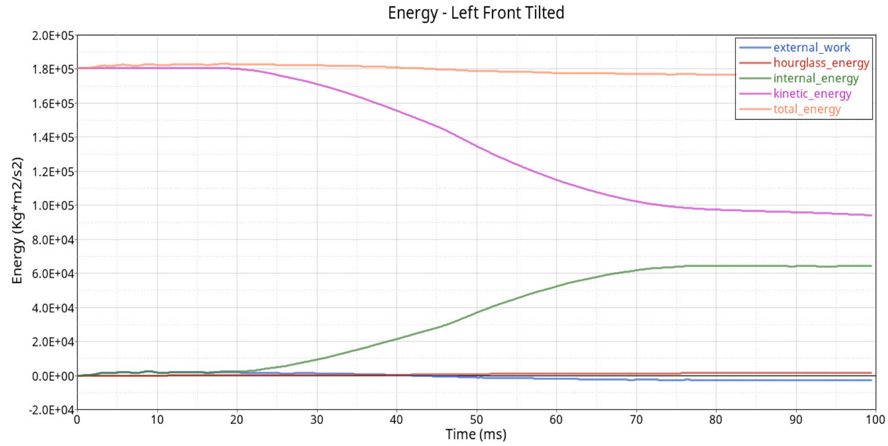

Figure 4.18: Trend of total energy, internal energy, kinetic energy and hourglass energy, in right rear tilted side impact.

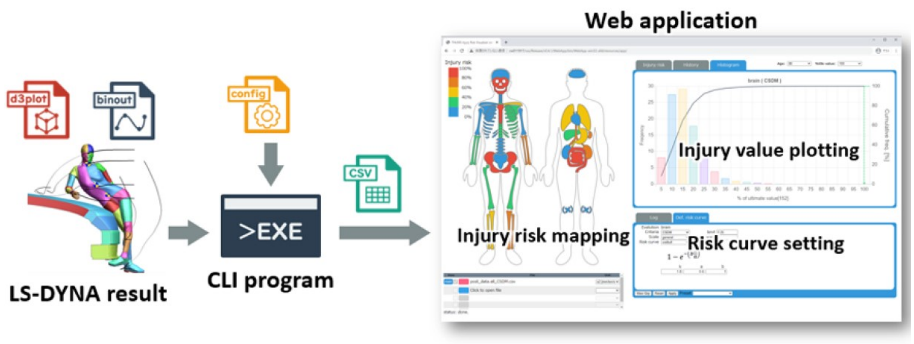

Figure 4.19: Workflow of THUMS Injury Risk Visualization Tool. Source: *jsol-cae.com*

4.3 Analysis of Injuries

4.3.1 THUMS Injury Risk Visualization Tool

The analysis of injuries was performed with the THUMS Injury Risks Visualization tool, made available by JSOL Corporation. THUMS Injury Risk Visualization tool allows the evaluation of injury risks resulting from HBMs, and permits the investigation of injury risk curves, useful to evaluate the actual human body injuries. This tool consists of two programs: the CLI program and the web application.

The CLI (Command Line Interface) program extracts data from LS-Dyna d3plot results file and produces as output a csv file for the web application. It is also possible to use binout files as input for the CLI program.

The web application allows the visualization of injury risks on THUMS skeleton, by using HBM based injury criteria for risk evaluation.

The workflow composing the execution of the tool is presented in figure 4.19.

The web application reads the csv file, which is the output of the CLI program, and produce an injury risk mapping of the human body, by painting with different colors the anatomical parts: the red parts are the ones with the higher injury risk: 80%-100%, the orange ones have injury risks included from 60% to 80%, the yellow ones from 40% to 60%, the green ones from 20% to 40% and finally the blue ones from 0% o 20%.

The risk curve settings can be modified for each anatomical parts, by choosing the evaluation criteria and by defining the type of risk curve and the values of its coefficients. It is also possible to choose if scaling the risk curve to a particular age, which can be set through the web application of the tool.

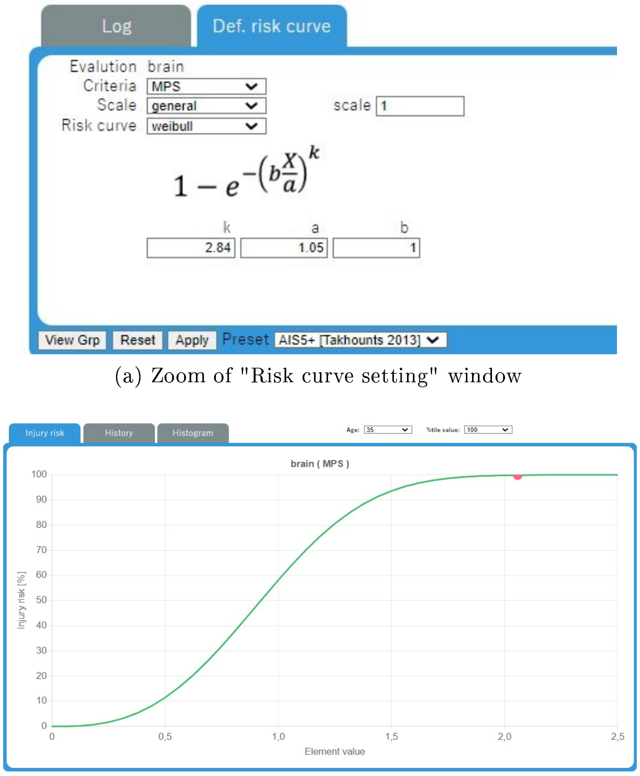

(a) Zoom of "Risk curve setting" window

(b) "Injury value plotting" window

Figure 4.20: Detail of the "Risk curve setting" and "Injury value plotting" windows of the Web Application of the THUMS Injury Visualization tool.

The risk curves can be Weibull distribution, sigmoid function, or normal distribution.

The settings are defined in the "Risk curve setting" window presented in 4.19, highlighted in figure 4.20 (a), and the plot are visible in "Injury value plotting" window presented in 4.19, highlighted in figure 4.20 (b).

For the bones, the only evaluation criterion that can be chosen is the MPS one, while for internal organs both MPS and CSDM criterion can be chosen. However, the risk curves have not been implemented for internal organs by the JSOL application, and so only the values of MPS and CSDM can be read and evaluated, but the risk curves cannot be analyzed. However, as exception for the brain, few evaluation criteria can be chosen from the following, and all of them have risk curve data implemented.

- MPS,
- HIC,
- BrIC,
- CSDM,
- PVP.

Once choose the risk curve settings, the chosen criterion is calculated and plotted over time in the *History* tab of the web application. Whenever the data risk curves have been implemented, is then possible to plot the maximum value of the criterion above the risk curve in tab *Injury Risk*, in order to predict the injury risk. In the end, it is possible to see the risk curve of the chosen criterion and the injury risks in % related to the anatomical part investigated.

The THUMS Injury Visualization tool was used in this work, to predict the injuries resulting from the six side impacts simulated. The age of occupant was set to 35 years old, through the tool. In the following section are presented the injuries resulting for bones and internal organs.

4.3.2 Bones

The THUMS Injury Risks Visualization Tool permit the evaluation of bones injuries only through the MPS criterion. The tool analyzes bone lesions by grouping them into twenty-three parts and by naming them as follows.

- Skull, composed of frontal, parietal, occipital, temporal, sphenoid and ethmoid bones.
- Face, composed of nasal, zygomatic, maxillary, and lacrimal bones, vomer, and mandible.
- Cervical spine, composed of seven cervical vertebrae, from C1 to C7.
- Thoracic spine, composed of twelve thoracic vertebrae, from T1 to T12.
- Lumbar spine, composed of five lumbar vertebrae, from L1 to L5.
- Left clavicle and right clavicle.
- Left scapula and right scapula.
- Left humerus and right humerus.
- Left forearm and right forearm, composed both of left and right radius, ulna, elbow joints and hand bones.
- Sternum.
- Left rib and right rib, composed of the twelve pair of ribs, as discussed right below.
- Sacrum.
- Left pelvis and right pelvis, composed of hip's bones, the ileum, ischium, and pubis, as discussed right below.
- Left femur and right femur.
- Left lower leg and right lower leg, composed both of left and right tibia, fibula, knee joints and foot bones.

Note that both the pelvis and the ribcage anatomically are considered as a unique part. The pelvis is a unique part composed by sacrum, coccyx and two hip's bones: the right one and the left one, both composed of the fusion of the ileum, ischium, and pubis, as shown in 4.21 (a). However, in the Jsol tool the pelvis is divided into three parts: the sacrum, the left part, and the right part of pelvis, as it is visible in 4.21 (b). The right and left part of pelvis are composed of the hip's bones ileum, ischium, and pubis, while the coccyx is not modeled. Indeed, in figure 4.21 there is the comparison between the anatomical pelvis and the modeled one in THUMS Injury Visualization tool.

The pelvis is modeled in such a way in the tool because the strains on one side of the pelvis can be grater the strains in the other side or on the sacrum, hence it is more useful to distinguish the unique anatomical part of the pelvis into these three different parts.

As well, the ribcage is anatomically defined as a unique part composed of twelve pairs ribs, twelve thoracic vertebrae and the sternum. Despite that, the Jsol tool divided the ribcage in four distinct parts: the thoracic spine, in which are considered all the twelve thoracic vertebrae, the sternum, the left twelve ribs and the right twelve ribs. Also in this case the division is useful to distinguish different strains in various parts of the ribcage. In figure 4.22 is presented the comparison between anatomical rib cage and modeled rib cage in THUMS Injury Visualization tool.

It should be noted, also, that for the rib cage, the MPS for each rib is calculated and then the risk of injury of the rib cage is evaluated based on the rib with the highest MPS value. For example, considering the twelve right ribs, it is observed that the rib with the highest value of MPS is the first, with a value of 0.0120 mm/mm and therefore the twelve right ribs are

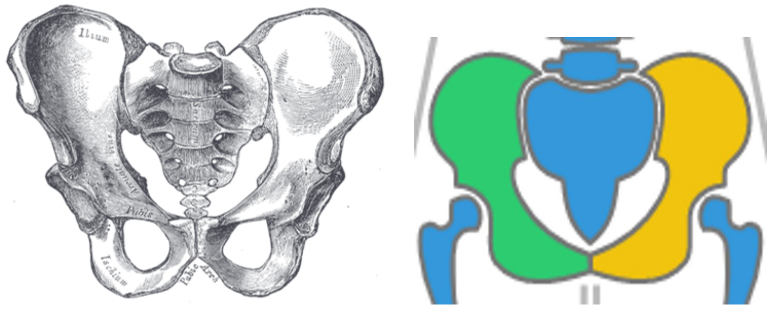

(a) Anatomy of the pelvis of a man. (b) Pelvis in THUMS Injury Visualization tool.

Figure 4.21: Comparison between anatomical pelvis and modeled pelvis in THUMS Injury Visualization tool.

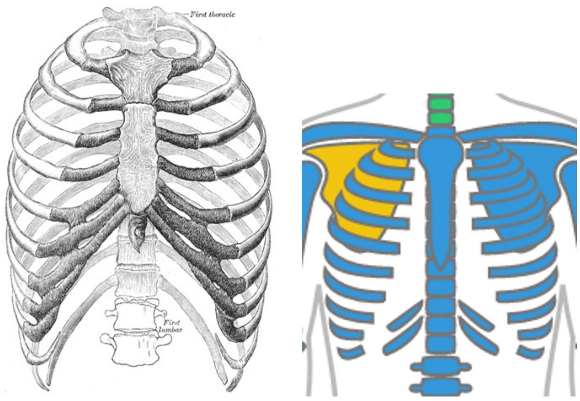

(a) Anatomy of the rib cage of a man. (b) Rib cage in THUMS Injury Visualization tool.

Figure 4.22: Comparison between anatomical rib cage and modeled rib cage in THUMS Injury Visualization tool.

considered as unique part, called right rib by the tool, with a MPS values of 0.0120 mm/mm. The injury risk of the right rib cage is evaluated from that MPS value.

The bones injury risks were calculated scaling with age of 35 years old and using the Weibull distribution. The values of Weibull distribution coefficients used are the ones proposed by the tool. The values are the following:

$$k = 3,013$$

$$a = 0,0275$$

$$b = 1$$

At first glance, the tool provided a graphical visualization of the injuries resulting from the impacts, as visible in figure 4.23. From that figure it is visible that the only configuration resulting in severe injuries was the left orthogonal one, because it was the only case in which few bones resulted in injury risks higher than 20%: the skull presented the higher injury risk, following by gravity cervical vertebrae, right scapula, and pelvis. The others five configurations presented risks of injuries below 20% for all the bones and so are all represented by the skeleton in figure 4.23 (b).

All the MPS values are represented, in a graphical way, in the graph in figure 4.24 and are listed at the top of table 4.1. In first column of the table there are all the bones segments that the THUMS Injury Visualization tool allows to analyze, instead in the columns from two to seven, are listed the MPS values, in mm/mm, for each side impact test: the left orthogonal side impact (*Left*), the left front tilted 45 degrees (*Left F.*), the left rear tilted 45 degrees (*Left*

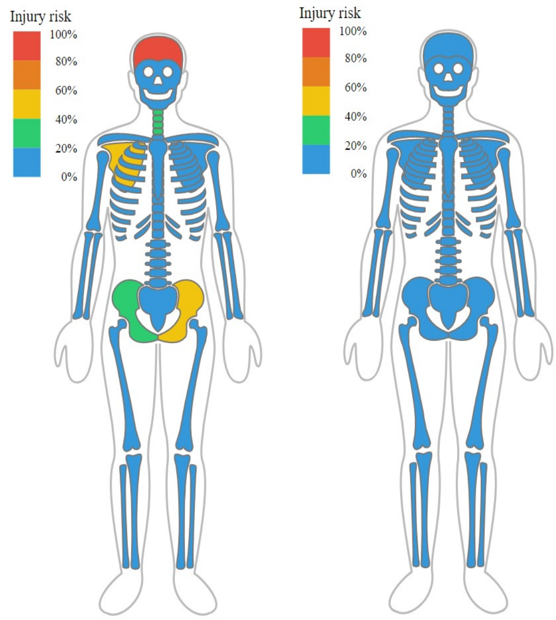

(a) Left Orthogonal Side Impact. (b) Other impact than the left orthogonal one.

Figure 4.23: Graphical visualization of injury risks for all the bones. In (a) is presented the visualization of injuries at bones in left orthogonal impact, while in (b) the one in the other five impacts, that all are resulting in injuries below 20% for all the bones.

R.), the right orthogonal (*Right*), the right front tilted 45 degrees (*Right F.*) and the right rear tilted 45 degrees (*Right R.*).

It is visible from figure 4.24 and table 4.1, that the higher MPS values were reached in the left orthogonal side impact. In this configuration, the skull was the anatomical parts which reached the maximum MPS value. From those values of MPS, the tool allowed the evaluation of the injury risks for all the bones segments, and the skull was the one resulting in the higher MPS injury risk, presenting 100% injury risk. In figure 4.25 are presented the MPS values for all the bones except the skull, to highlight those values, which are all smaller than the MPS at brain. The risks of injuries obtained from MPS values, for all the bones and all the impact configurations, are shown in figure 4.26 and at the bottom of table 4.1. In figure 4.27 are presented the injury risks of all the bones except the skull, to better evaluate the values of injury risk in those parts.

In left orthogonal impact, following the skull by severity, the left pelvis, the right scapula, the right pelvis and the cervical spine were the anatomical parts that presented injury risks higher than 20%. The other anatomical parts of the left orthogonal impact and all the ones in the other configurations have not reached MPS values such as to cause injury risks greater than 20%.

Even if the the results of the right orthogonal impact were not resulting from the same duration of impacts as the other five configurations, they could be compared with the other results, considering that the values were few order of magnitude low with respect to the one from left orthogonal side impact. More, the THUMS in right orthogonal impact was performing only translational movement in the direction of the incoming MDB, and so the injuries resulting may be comparable with the ones from the right tilted impacts.

Body Part	MPS values for each crash [mm/mm]					
	Left	**Left F.**	**Left R.**	**Right**	**Right F.**	**Right R.**
Skull	0,1831	0,0030	0,0095	0,0004	0,0035	0,0033
Face	0,0047	0,0003	0,0031	0,0000	0,0004	0,0002
Cervical Spine	0,0203	0,0023	0,0026	0,0009	0,0034	0,0014
Right Clavicle	0,0019	0,0012	0,0008	0,0001	0,0004	0,0006
Left Clavicle	0,0034	0,0124	0,0052	0,0005	0,0017	0,0015
Right Scapula	0,0246	0,0072	0,0028	0,0002	0,0021	0,0008
Left Scapula	0,0105	0,0047	0,0066	0,0008	0,0033	0,0039
Right Humerus	0,0096	0,0054	0,0029	0,0001	0,0043	0,0003
Left Humerus	0,0062	0,0038	0,0026	0,0019	0,0035	0,0020
Right Forearm	0,0108	0,0026	0,0016	0,0001	0,0020	0,0002
Left Forearm	0,0075	0,0107	0,0014	0,0002	0,0044	0,0030
Right Rib	0,0120	0,0025	0,0037	0,0041	0,0017	0,0015
Left Rib	0,0127	0,0038	0,0052	0,0004	0,0026	0,0013
Sternum	0,0060	0,0063	0,0050	0,0003	0,0035	0,0018
Thoracic Spine	0,0109	0,0049	0,0043	0,0031	0,0085	0,0017
Lumber Spine	0,0029	0,0040	0,0011	0,0005	0,0073	0,0016
Sacrum	0,0025	0,0021	0,0032	0,0018	0,0035	0,0023
Right Pelvis	0,0226	0,0025	0,0048	0,0026	0,0067	0,0025
Left Pelvis	0,0254	0,0050	0,0038	0,0013	0,0018	0,0094
Right Femur	0,0088	0,0014	0,0054	0,0009	0,0048	0,0021
Left Femur	0,0098	0,0032	0,0012	0,0006	0,0014	0,0047
Right Lower Leg	0,0179	0,0063	0,0013	0,0013	0,0064	0,0006
Left Lower Leg	0,0091	0,0085	0,0004	0,0010	0,0023	0,0012
Body Part	MPS Injury Risks for each crash [%]					
	Left	**Left F.**	**Left R.**	**Right**	**Right F.**	**Right R.**
Skull	100,00	0,09	2,83	0,00	0,14	0,11
Face	0,35	0,00	0,10	0,00	0,00	0,00
Cervical Spine	24,76	0,04	0,06	0,00	0,13	0,01
Right Clavicle	0,02	0,01	0,00	0,00	0,00	0,00
Left Clavicle	0,13	6,23	0,47	0,00	0,02	0,01
Right Scapula	40,84	1,23	0,07	0,00	0,03	0,00
Left Scapula	3,90	0,35	0,94	0,00	0,02	0,19
Right Humerus	2,91	0,52	0,08	0,00	0,26	0,00
Left Humerus	0,79	0,18	0,06	0,02	0,14	0,03
Right Forearm	4,19	0,06	0,01	0,00	0,03	0,00
Left Forearm	1,40	4,00	0,01	0,02	0,28	0,09
Right Rib	5,63	0,05	0,16	0,23	0,02	0,01
Left Rib	6,62	0,18	0,47	0,00	0,06	0,01
Sternum	0,72	0,82	0,43	0,00	0,14	0,02
Thoracic Spine	4,30	0,38	0,27	0,10	2,01	0,02
Lumber Spine	0,08	0,21	0,00	0,00	1,32	0,01
Sacrum	0,05	0,03	0,10	0,02	0,14	0,04
Right Pelvis	32,65	0,05	0,37	0,06	1,00	0,05
Left Pelvis	42,80	0,42	0,18	0,01	0,02	2,72
Right Femur	2,24	0,01	0,53	0,00	0,38	0,03
Left Femur	0,98	0,11	0,01	0,00	0,01	0,34
Right Lower Leg	17,74	0,82	0,01	0,01	0,86	0,00
Left Lower Leg	2,51	2,02	0,00	0,00	0,04	0,01

Table 4.1: MPS values and MPS Injury risks for all the bone parts. F. stands for *Front* and R. stands for *Rear*.

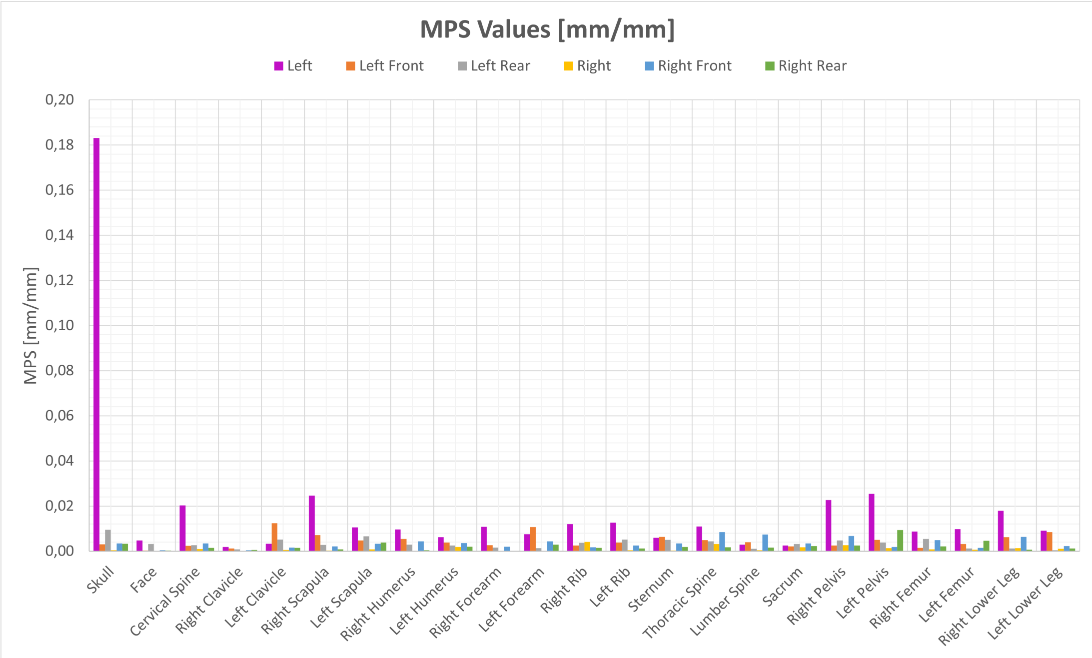

Figure 4.24: MPS values [mm/mm] for each bone part.

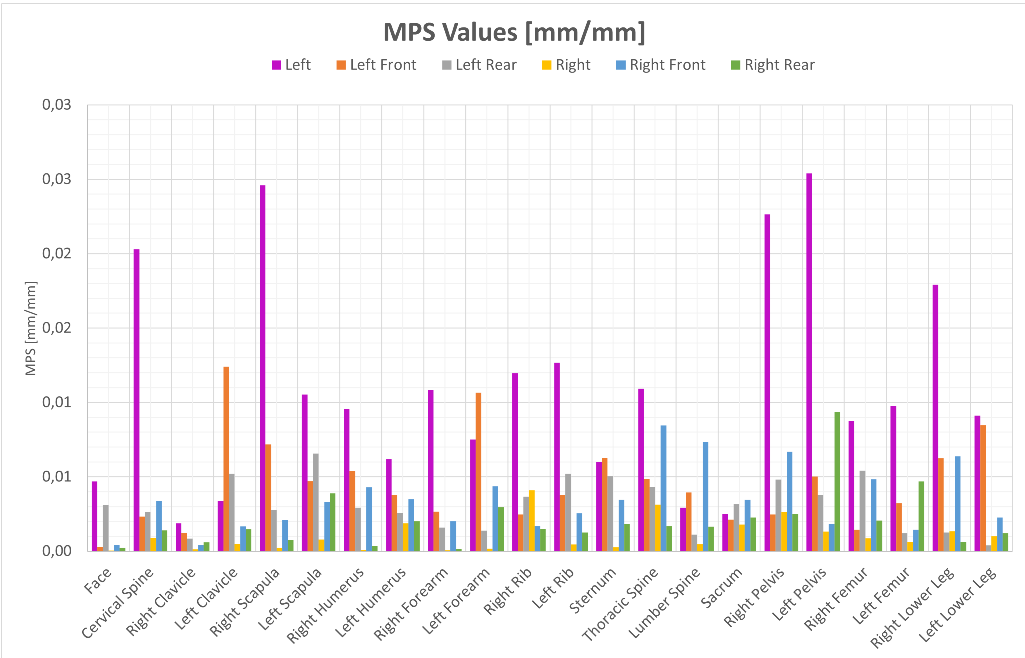

Figure 4.25: MPS values [mm/mm] for each bone part except the skull.

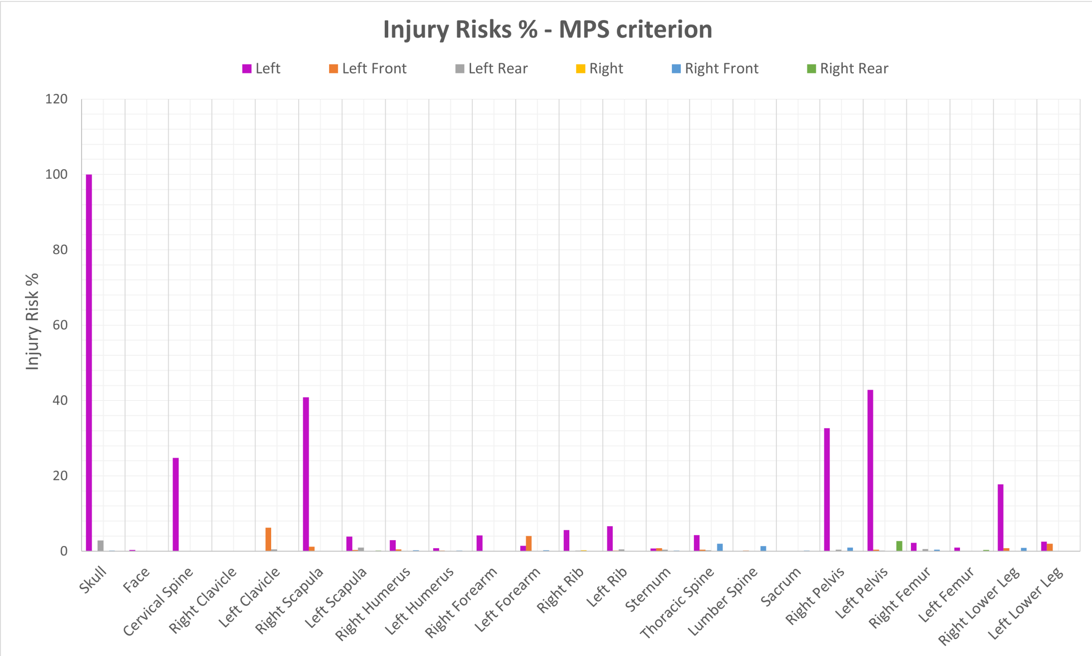

Figure 4.26: MPS Injury risks %.

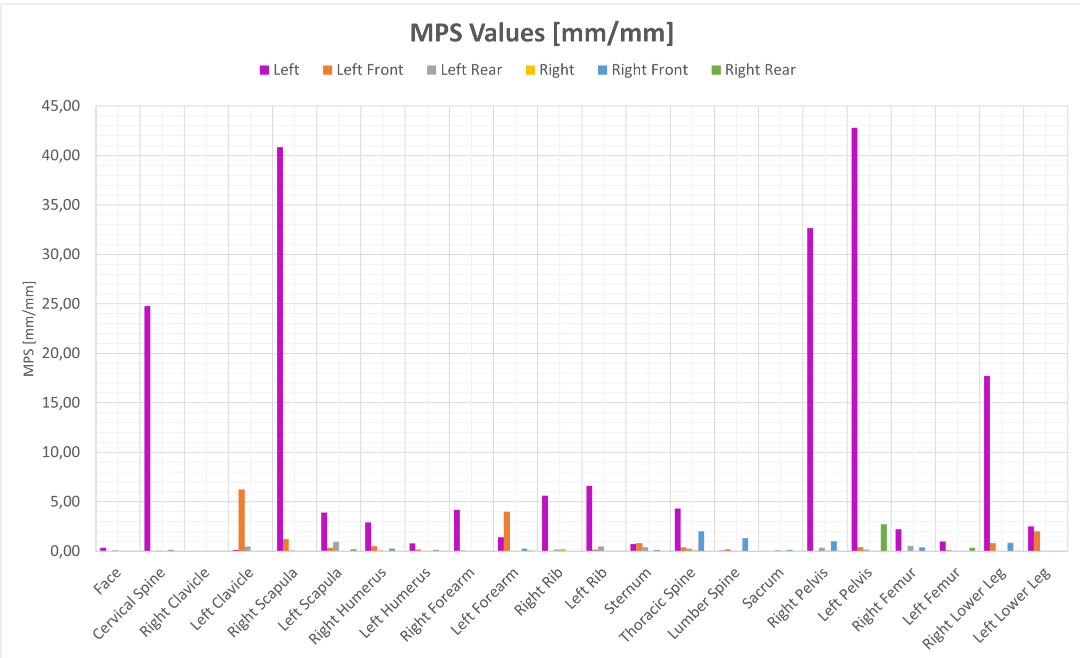

Figure 4.27: MPS Injury risks % for all the bones except the skull.

Skull and Cervical Spine

In left orthogonal collision, the skull has undergone a movement of approaching towards the left shoulder and bumped against the internal part of vehicle for the first time at 54 ms from the beginning of the impact, by touching the left front door in the part right upper the windows, as shown in figure 4.28 (a). Then, the head continued its movements of approaching the left shoulder, but it never contacted the window, as visible in figure 4.28. At the end of the collision, the head slammed into the left front door, on the part immediately below the window, as shown in figure 4.28 (f). The high injury risk at skull was resulting from this movement and it was reached at 81 ms from the beginning of the collision, the maximum MPS was located on the left part of sphenoid bone.

Also the distraction of the cervical spine was due to that movement of the head approaching towards the left shoulder, in particular the injury to the cervical spine was due to the seat belt that held back the shoulders and the neck. As discussed in section 1.1.2, this event is typical of side crashes at left side of vehicle. The distraction of spinal cord in vehicle collision is often resulting in vertebral fractures. The maximum MPS was reached in the cancellous bones of C3 vertebrae at 66 ms from the beginning of the impact. In figure 4.29 is represented the configuration of the spine when the maximum MPS was reached (66 ms) and at the end of the collision. The image shows the movement of cervical spine which was the result of its distraction.

In the other two left configurations of impact, the head has not undergone to such a movement of approaching the left shoulder: the dummy made a translational movement towards the incoming carriage, and only in the rear configuration the head came into contact with the higher part of the vehicle door, as shown in 4.30. Despite that, the MPS resulted from that touch is small (0,0095 mm/mm) related to the one resulted from the collision of the head in the left orthogonal impact (0,1831 mm/mm). Therefore, the injury risk at head resulted from the left rear side impact is 2,83%, that is minor compared to the 100% injury risk resulted in the left side orthogonal crash.

The distraction movement of cervical spine was present also in the other two left configurations, but it was not as marked as in the case of the orthogonal impact, as visible from the comparison between figures 4.31 and 4.29. Indeed, the MPS values resulting were two orders of magnitude lower than the one resulting in left orthogonal impact, as shown in table 4.1.

In right configurations of the impact, the THUMS has undergone to a translational movement toward the carriage, that, in those cases, was coming from the right side. The head was not presenting any collisions or any movement towards the right shoulder, hence the risks resulted in skull and, also, in cervical spine were extremely low, compared to the ones resulted in left orthogonal side impact. To see the movements of the head in those cases, see figures 4.8, 4.10, 4.12. While, the movements of the cervical spine in right configurations of impact are highlighted in figure 4.32.

Trunk and Upper Extremity

Generically, the trunk and upper extremities were not resulting in severe injuries in all the six configurations, as visible from figure 4.23. Only the right scapula in left orthogonal impact presented an injury risk higher than 20%, correspondents to 40,84%. Even if the left side part of THUMS was colliding with the left door, in left orthogonal and left front tilted impacts, the right scapula and right humerus presented higher injury risks, with respect to the left ones. This can be explained by analyzing the forward twisting motion that THUMS performed at the end of the collisions. In figure 4.33 there is the top view of THUMS in left orthogonal impact, sitting on the driver seat, at the moment in which the greater MPS value on right scapula was reached. It is visible from that figure the forward movement of the right scapula and right humerus.

The higher MPS in the right scapula was located in the glenoid cavity, while the MPS in right humerus was located on the coronoid fossa.

While in right configurations the THUMS is performing only a translational movement, it was not hitting any part of the vehicle and that is why the injury risks resulted from those im-

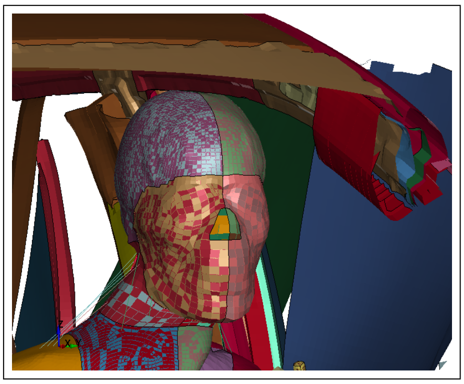

(a) 54 ms.

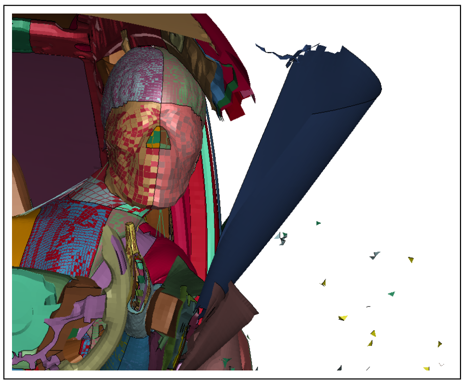

(b) 57 ms.

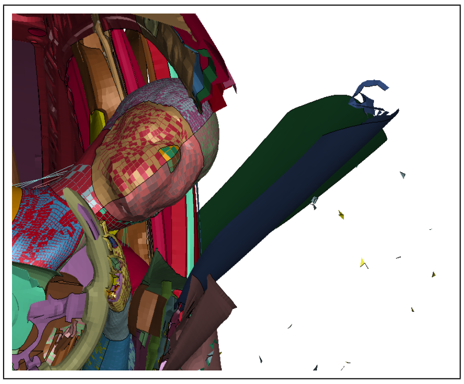

(c) 75 ms.

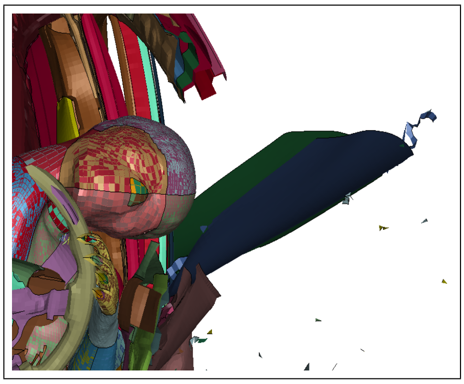

(d) 87 ms.

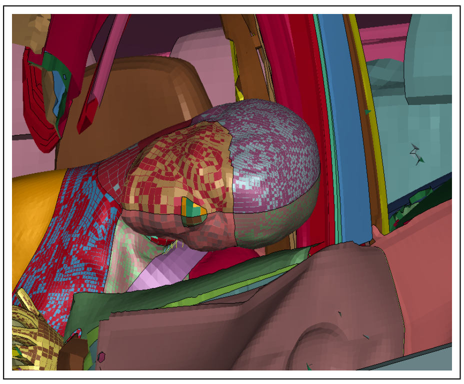

(e) 93 ms.

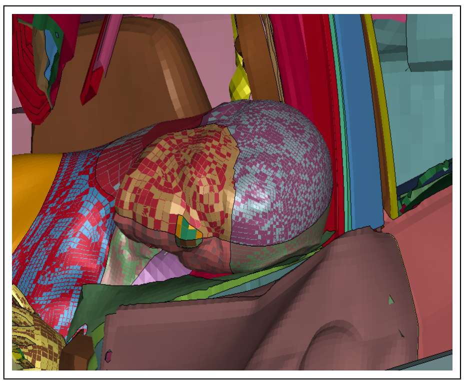

(f) 100 ms.

Figure 4.28: Particular of the head of the THUMS approaching the left shoulder in Left Orthogonal Impact at different times from the beginning of the collision.

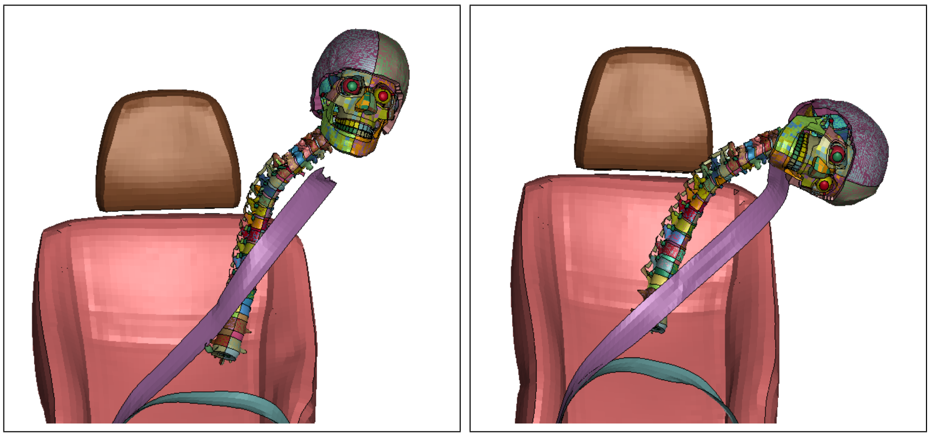

(a) 67 ms.

(b) 100 ms.

Figure 4.29: Front view of the configuration of the upper part of the spine, together with the left front seat and seat belt, at different time of the collision, in left orthogonal impact.

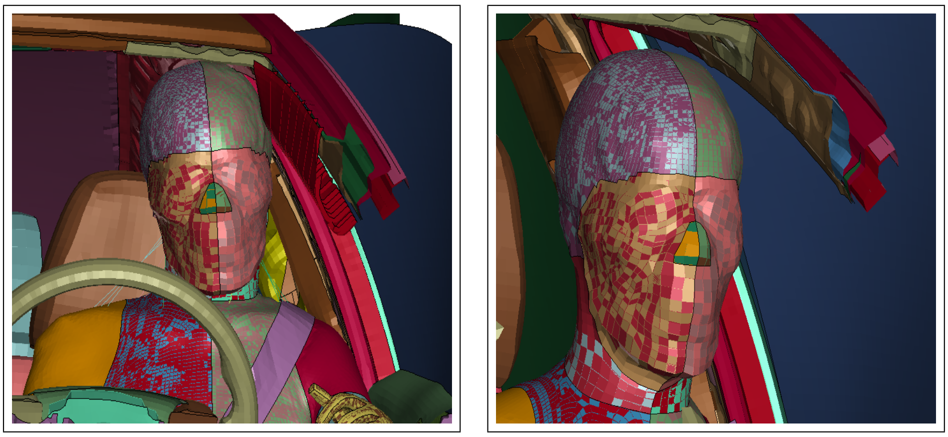

(a) Left rear tilted impact, at 88 ms from the beginning of the impact.

(b) Left front tilted impact, at 96 ms from the beginning of the impact.

Figure 4.30: Particular of the head of the THUMS in its closest position to the left door, in both left rear and left front tilted impacts.

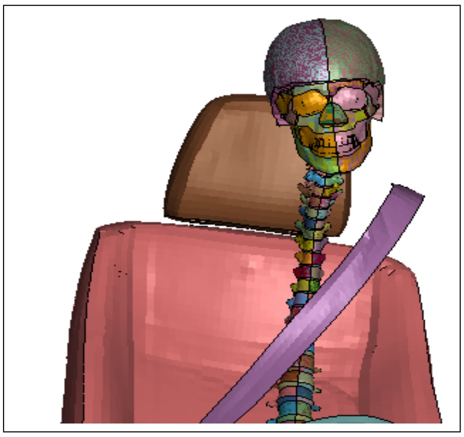

(a) Left rear tilted impact.

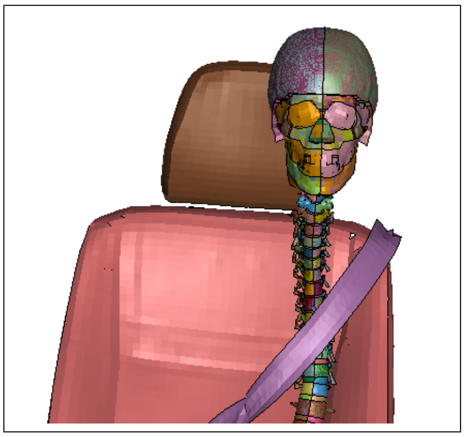

(b) Left front tilted impact.

Figure 4.31: Front view of the upper part of the spine, together with the left front seat and seat belt, at 100 ms from the beginning of the collision, in different impacts.

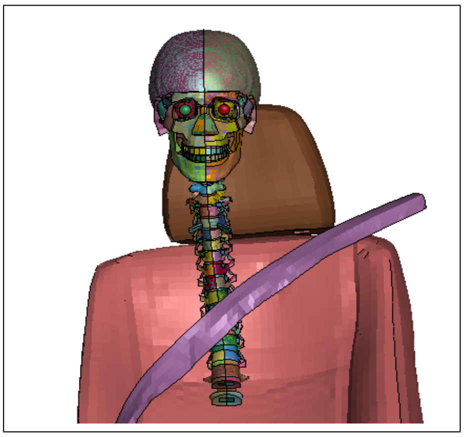

(a) Right rear tilted impact.

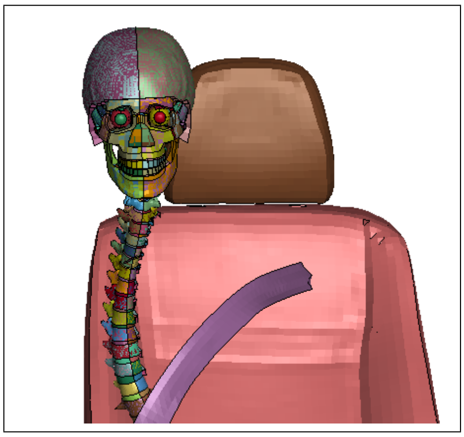

(b) Right front tilted impact.

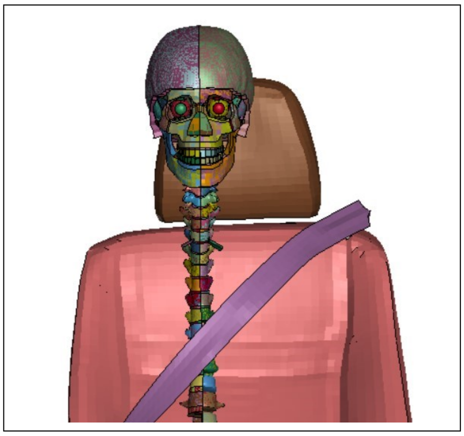

(c) Right orthogonal impact.

Figure 4.32: Front view of the of the upper part of the spine, together with the left front seat and seat belt, at the end of the collision, in different configurations of impact.

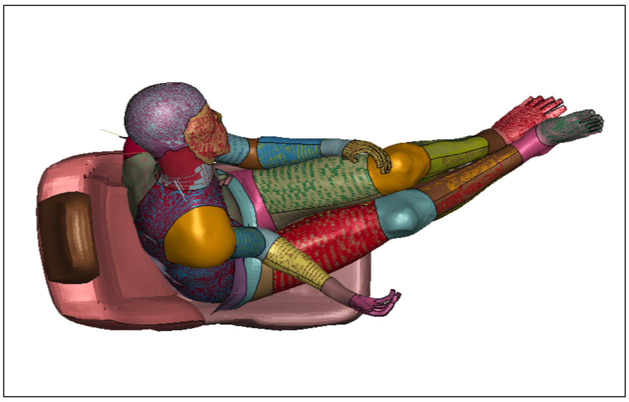

Figure 4.33: Top view of THUMS at 81 ms from the beginning of the impact, which is the moment in which the greater MPS value on right scapula is reached.

pacts are extremely low in trunk's bones, compared to the ones resulting from left side impacts. Indeed, the injury risks in trunk and upper extremity were below one order of magnitude low than the ones in left orthogonal impact.

The left part of trunk and the left arm in all the configurations were not resulting in severe injury risks: the values were below one order of magnitude low than the ones in right scapula and right humerus in left orthogonal impact. However, the left clavicle and left forearm were the only exception for which the maximum MPS was reached not in the left orthogonal side impact, but in left front and left rear tiled ones. In particular, in left front tilted impact, the left clavicle reached the maximum injury risks, equal to 6,23% and the left forearm equal to 4,00%. Those values were not meaning of severe injury, but they were greater than the injury risk at left clavicle and left forearm in left orthogonal side impact, which was the most critical impact for all the others body parts. In figure 4.34 are presented the particulars of the clavicle at the moment in which it was reaching the maximum MPS, in left configurations of crashes.

Another exception was performed by the lumber spine, which reached its maximum MPS in right front tilted side impact, by presenting 1,32% injury risks, in left front tilted side impact presented 0,21%, while in left orthogonal side impact 0,08% injury risks. In the other configurations the injury risks were near zero. In all of the six impact the injury risk of the lumber spine is not critical, but it is meaningful to highlight that, for lumber spine, the left orthogonal side impact is not the most severe one.

Pelvis and Lower Extremity

Also the pelvis was presenting critical injury risks only in the left orthogonal side impact, with 32.65% for right part of pelvis and 42.80% for left part. The injury risks resulted from the other configurations, both left and right ones, were equal or below 1%. This is due to the severity of the left orthogonal impact, compared to the other ones, in which the pelvis was compressed downwards by the seatbelt. This compression is visible in figure 4.35 in which only the THUMS, the seat belts, and the carriage are represented in the two configurations: at beginning of the simulation and after 50ms, which is the moment when the pelvis was in its lowest position.

The higher MPS for the pelvis was resulting in the pubic symphisis, in both its left and right parts.

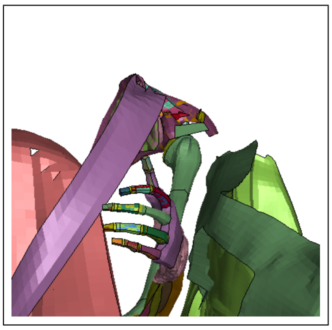

(a) Left orthogonal side impact, at 60ms from the beginning of the impact.

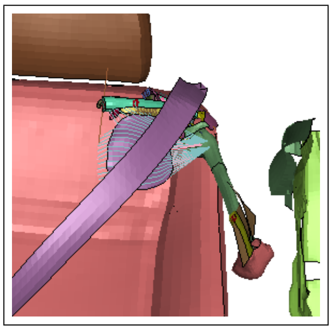

(b) Left front tilted side impact, at 76ms from the beginning of the impact.

(c) Left front tilted side impact, at 80ms from the beginning of the impact.

Figure 4.34: Comparison between the clavicle when reaching its maximum MPS value, in different side impact at different time.

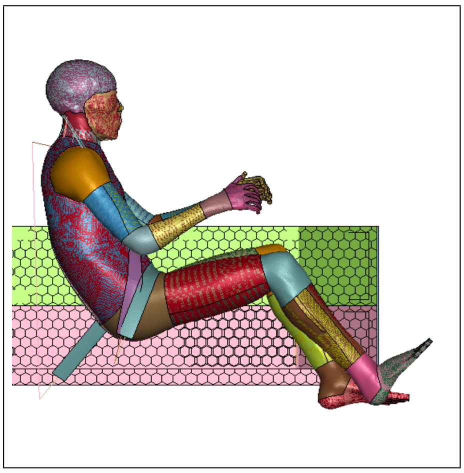

(a) THUMS and carriage at the beginning of the impact.

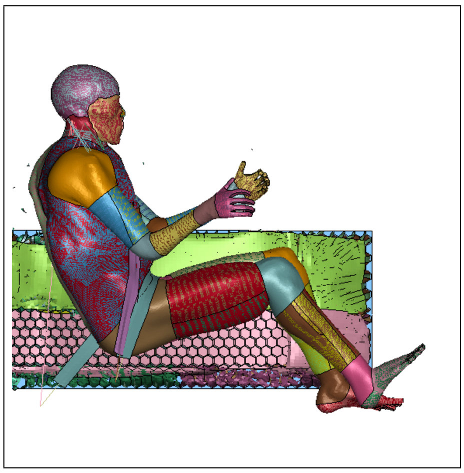

(b) THUMS and carriage at 50 ms from the beginning of the impact.

Figure 4.35: Comparison between THUMS and carriage at beginning and at the end of the impact.

4.3.3 Internal Organs

The THUMS Injury Risks Visualization Tool provides the MPS and CSDM values for the following internal organs.

- Brain.
- Lungs.
- Heart.
- Liver.
- Stomach.
- Spleen.
- Aorta.
- Kidneys.
- Intestine.
- Knee ligaments.

The MPS values provided by the tool are listed in table 4.2 and presented graphically in figure 4.36, while the CSDM values are listed in table 4.3 and presented graphically in figure 4.37. However, for the organs, it is not possible to evaluate the injury risk in % with the tool, because risk curve data have not been implemented in the tool, for both MPS and CSDM criterion.

Body Part	MPS values for each crash [mm/mm]					
	Left	**Left F.**	**Left R.**	**Right**	**Right F.**	**Right R.**
Brain	2,0578	0,0952	0,5872	0,01473	0,1420	0,0904
Right Lung	0,3357	0,1648	0,1265	0,0820	0,1303	0,1603
Left Lung	0,3407	0,2323	0,2411	0,0723	0,1463	0,1276
Heart	0,7064	0,4652	0,5302	0,2204	0,3947	0,5186
Liver	1,0778	0,4224	0,3741	0,5115	0,7111	0,5891
Stomach	1,1066	0,7733	0,5202	0,1991	0,7807	0,4497
Spleen	1,0734	0,5370	0,4937	0,1320	0,9932	0,2398
Aorta	0,3600	0,2811	0,1713	0,0855	0,3737	0,1277
Right Kidney	0,9450	0,4057	0,4316	0,4999	0,5661	0,5222
Left Kidney	0,6862	0,3366	0,6222	0,1651	0,6073	0,4679
Intestine	2,2625	1,0744	1,0514	0,2349	0,9922	0,3403
Right Knee Ligament	0,2138	0,1458	0,0647	0,0343	0,1345	0,0511
Left Knee Ligament	0,1351	0,1065	0,0376	0,0129	0,0895	0,0486

Table 4.2: MPS values for all the internal organs. F. stands for *Front* and R. stands for *Rear*.

In general, the MPS values reached by the internal organs were higher than the MPS values reached for the bones, for all the six configurations of impacts. It means that the lesions resulting from the six side impact crashes were mainly located inside the body, in the internal organs, rather than in the bones, which are supposed to act as a barrier to these organs.

From data in table 4.2, it is visible that the higher values of MPS were reached in left orthogonal impact, by the intestine and brain following by severity: stomach, liver, spleen, heart, and kidneys. Aorta, lungs, and knee ligaments presented low MPS values, than the organs above.

Also the CSDM criterion provides the same results: the higher values were reached in left orthogonal impact. While the CSDM can not be implemented for the bones, in this case the

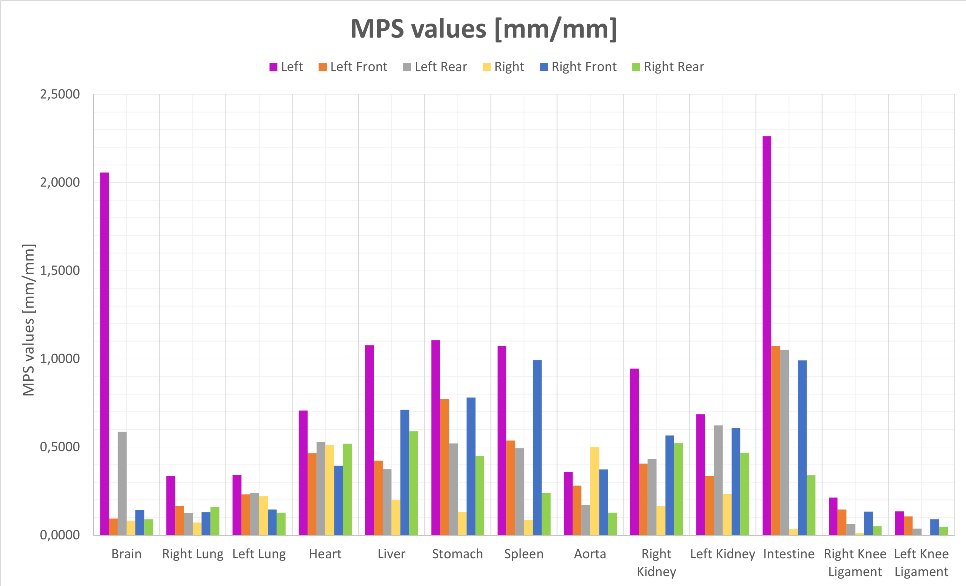

Figure 4.36: MPS values [mm/mm] for each organs.

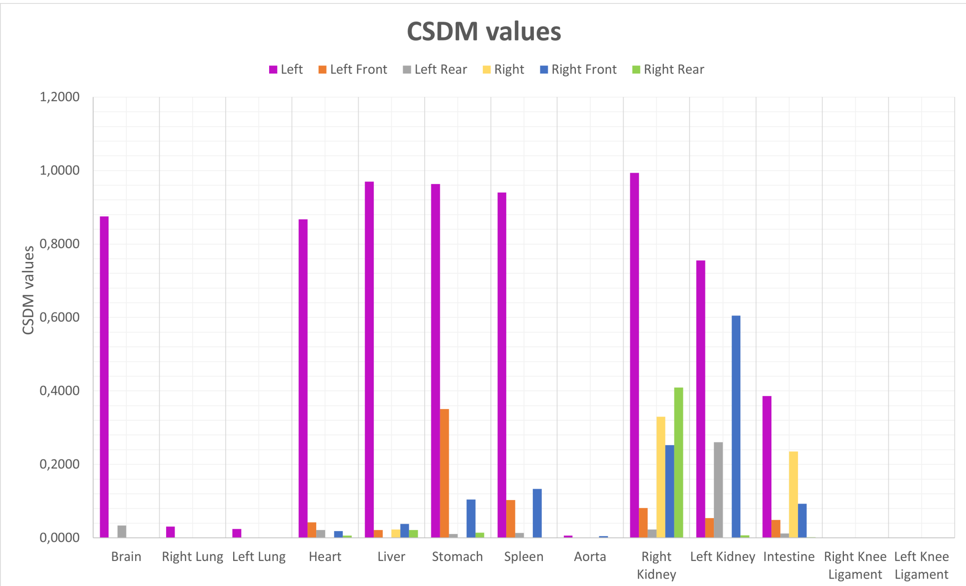

Figure 4.37: CSDM values for each organs.

Body Part	CSDM values for each crash					
	Left	**Left F.**	**Left R.**	**Right**	**Right F.**	**Right R.**
Brain	0,8750	0,0000	0,0337	0,0000	0,0000	0,0000
Right Lung	0,0306	0,0000	0,0000	0,0000	0,0000	0,0000
Left Lung	0,0244	0,0000	0,0000	0,0000	0,0000	0,0000
Heart	0,8673	0,0423	0,0213	0,0000	0,0187	0,0065
Liver	0,9695	0,0217	0,0014	0,0229	0,0381	0,0215
Stomach	0,9634	0,3506	0,0103	0,0000	0,1042	0,0139
Spleen	0,9398	0,1032	0,0135	0,0000	0,1336	0,0000
Aorta	0,0063	0,0002	0,0000	0,0000	0,0047	0,0000
Right Kidney	0,9938	0,0815	0,0226	0,3298	0,2522	0,4095
Left Kidney	0,7556	0,0541	0,2607	0,0000	0,6051	0,0071
Intestine	0,3860	0,0487	0,0122	0,2349	0,0926	0,0020
Right Knee Ligament	0,0000	0,0000	0,0000	0,0000	0,0000	0,0000
Left Knee Ligament	0,0000	0,0000	0,0000	0,0000	0,0000	0,0000

Table 4.3: CSDM values for all the internal organs. F. stands for *Front* and R. stands for *Rear*.

comparison between lesions in bones and organs is not possible. Anyway, the organs that were experiencing the higher values of CSDM are the brain, the heart, the liver, the stomach, the spleen, the kidneys, and the intestine.

In following paragraphs, the most injured internal organs will be taken into analysis. However, the lesion resulting in the brain, will be discussed more specifically in 4.3.4 section below, because of their criticality.

Intestine

The intestine was experiencing the higher MPS and CSDM values in left orthogonal side impact, at 50 ms from the beginning of the collision. In fact, at that time, in left orthogonal impact the intestine reached its state of greatest deformation, appearing very compressed, as evident from the comparison between figure 4.38 (a) and (b).

The instant in which the intestine presented its greatest deformation corresponds to the instant in which the pelvis presented the maximum MPS. Hence, the lesions resulting in the intestine can be attribute to the same compression downwards of the pelvis by the seatbelt, which was causing the injuries at pelvis.

In left front and rear tilted configurations, the intestine was the internal organs which was presenting the higher MPS value, while was not the internal organ presenting the higher CSDM value. From comparison between figures 4.38 (a) and (c) and the comparison between figures 4.38 (a) and (d), the deformations of the intestine in both the two impact configurations are shown. Note that the maximum MPS, in those cases, were reached at the end of simulation, while the pelvis was not experiencing the compression downwards, instead presented in left orthogonal configuration, indeed the injury risks at pelvis were extremely low, as discussed above.

In right configurations the intestine was experiencing low MPS values, compared to the ones of the other impact discussed above. In fact, from comparisons between figures 4.38 (a) and (e), figures 4.38 (a) and (f), and figures 4.38 (a) and (g), is evident the minor compression in intestine than the ones in the left impact collisions. To note that in right orthogonal impact the analysis of the intestine is at 50 ms because it corresponded to the end of the simulation.

Heart, Liver, Stomach, Spleen and Kidneys

Heart, liver, stomach, spleen and kidneys were presenting critical MPS and CSDM values in left orthogonal side impact, even if for the MPS criterion those values were minor than the one of the intestine and brain, while for CSDM criterion were greater than the one of intestine

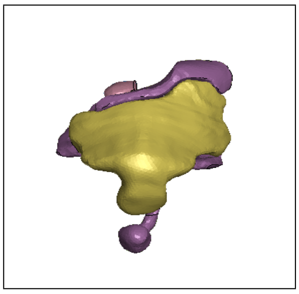

(a) At beginning of impact.

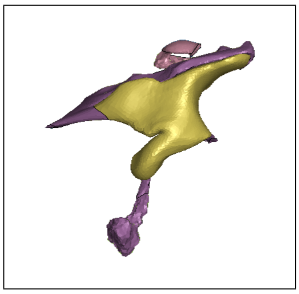

(b) Left orthogonal side impact, at 50 ms from the beginning of impact.

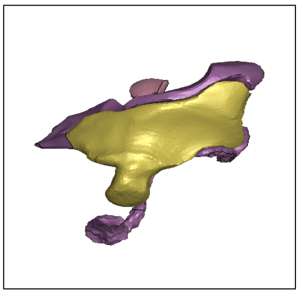

(c) Left front tilted side impact, at the end of the impact.

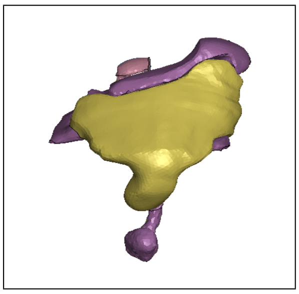

(d) Left rear tilted side impact, at the end of the impact.

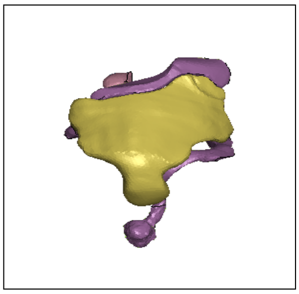

(e) Right front tilted side impact, at the end of the impact.

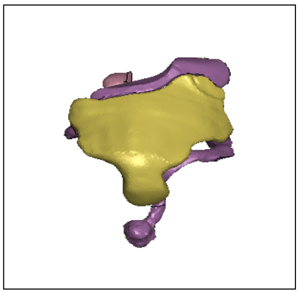

(f) Right rear tilted side impact, at the end of the impact.

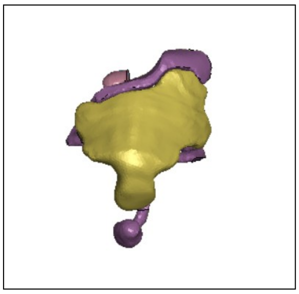

(g) Right orthogonal side impact, at 50 ms from the beginning of impact.

Figure 4.38: Comparison of intestine in different times of different simulations.

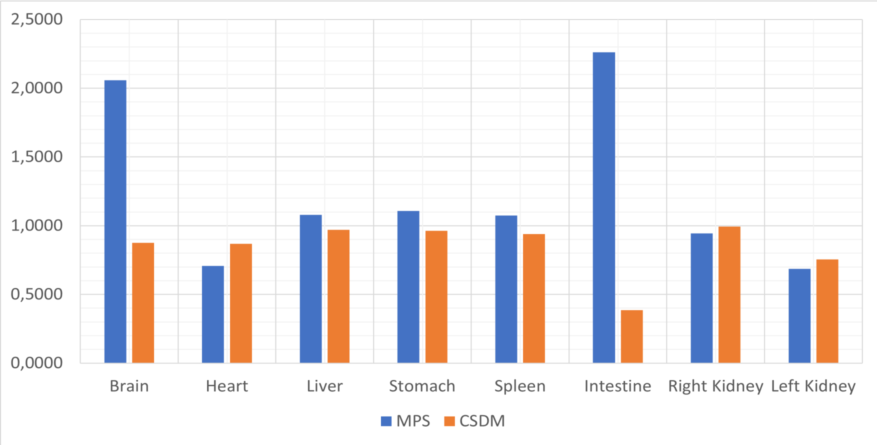

Figure 4.39: Comparison between MPS and CSDM values for brain, heart, liver, stomach, spleen, intestine and kidneys in left orthogonal side impact.

and comparable to the CSDM value at brain, as shown in tables 4.36 and 4.37. It means that, in left orthogonal side impact, the CSDM criterion was indicating a situation of which heart, liver, stomach, spleen and kidneys were subjected to lesions comparable or greater to the one at brain and intestine, while the MPS criterion was indicating a situation in which heart, liver, stomach, spleen and kidneys were subjected to lesions less critical to the ones in brain and intestine. These two criteria contradict each other in those cases, whereby one of the two was underestimating or overestimating the lesions in the organs.

The comparison between those values has been highlighted in the figure 4.39.

This trend is present also in the other side impacts, but the value of CSDM and MPS are lower, and so less critical.

Lungs and Knee Ligaments

Both lungs and knee ligaments were presenting very low values of MPS and CSDM in all the six configurations. The MPS criterion was providing small but non-zero values, while the CSDM was providing zero values for both lungs and knee ligaments, in all cases except for lungs in left orthogonal impact. It means that or the CSDM was underestimating the lesions in lungs and knee ligaments, or the MPS was overestimating them. In table 4.4 there is an extract of data from tables 4.36 and 4.37, to give a simple comparison of them.

Body Part	MPS values for each crash [mm/mm]					
	Left	**Left F.**	**Left R.**	**Right**	**Right F.**	**Right R.**
Right Lung	0,3357	0,1648	0,1265	0,0820	0,1303	0,1603
Left Lung	0,3407	0,2323	0,2411	0,0723	0,1463	0,1276
Right Knee Ligament	0,2138	0,1458	0,0647	0,0343	0,1345	0,0511
Left Knee Ligament	0,1351	0,1065	0,0376	0,0129	0,0895	0,0486
Body Part	CSDM values for each crash					
	Left	**Left F.**	**Left R.**	**Right**	**Right F.**	**Right R.**
Right Lung	0,0306	0,0000	0,0000	0,0000	0,0000	0,0000
Left Lung	0,0244	0,0000	0,0000	0,0000	0,0000	0,0000
Right Knee Ligament	0,0000	0,0000	0,0000	0,0000	0,0000	0,0000
Left Knee Ligament	0,0000	0,0000	0,0000	0,0000	0,0000	0,0000

Table 4.4: MPS and CSDM values comparison for lungs and knee ligaments in all the impact configurations. F. stands for *Front* and R. stands for *Rear*.

MPS brain values for each crash [mm/mm]					
Left	**Left F.**	**Left R.**	**Right**	**Right F.**	**Right R.**
2,0578	0,0952	0,5872	0,0147	0,1420	0,0904
MPS Injury Risks for each crash [%]					
Left	**Left F.**	**Left R.**	**Right**	**Right F.**	**Right R.**
99,8839	0,1092	17,4672	0,0005	0,3403	0,0945

Table 4.5: MPS values and MPS injury risks for the brain. F. stands for *Front* and R. stands for *Rear.*

CSDM values for each crash					
Left	**Left F.**	**Left R.**	**Right**	**Right F.**	**Right R.**
0,87450	0,0000	0,0337	0,0000	0,0000	0,0000
CSDM Injury Risks for each crash [%]					
Left	**Left F.**	**Left R.**	**Right**	**Right F.**	**Right R.**
86,0833	0,0000	0,5581	0,0000	0,0000	0,0000

Table 4.6: CSDM values and CSDM injury risks for the brain. F. stands for *Front* and R. stands for *Rear.*

4.3.4 Brain

The brain, as exception from the other internal organs, has risk curve data implemented, hence it was possible to evaluate not only the MPS values, but also the injury risks in % related to them.

For both CSDM and MPS, the injury risks were calculated scaling with age of 35 years old and using the Weibull distribution. The values of Weibull distribution coefficients used are the ones proposed by the tool. The values used for MPS were the following:

$$k = 2.84$$

$$a = 1.05$$

$$b = 1$$

While the values used for CSDM were the following:

$$k = 1.8$$

$$a = 0.6$$

$$b = 1$$

In table 4.5 are presented the MPS values and the MPS injury risks for the brain for the six configurations of impact, while the CSDM values and CSDM injury risks provided by the tool are presented in table 4.6.

Both the MPS and the CSDM criterion showed that the greatest injury risks are resulting in the left orthogonal impact.In this configuration, an injury risk of 99,88% was resulting in the brain from MPS criterion and an injury risk of 86,08% from CSDM criterion. Despite the MPS has not correlation with the AIS scale, there are thresholds values for brain currently used by scientific community when using HBMs: when reaching 26% of MPS injury risk for gray matter, the AIS 3 level is reached, and when reaching 21% of MPS injury risk for white matter, the AIS 4 level is reached. Anyway, the tool was not providing the possibility to evaluate the distinct MPS values on gray and white matter of the brain, but, considering that the MPS injury risk returned for all the brain is 99.88%, at least AIS 3 level and AIS 4 level were reached, respectively, by the gray and white matter. Hence, considering the Maximum AIS principle, the brain was presenting at least AIS 4 score as result of left orthogonal side impact. It means that the resulting injuries were severe, with respect to the AIS scale definition, presented in section 1.1.1.

The CSDM criterion, instead, as it was constructed in the tool, returned the injury risks % related to the AIS 4 level: is means that, while the CSDM injury risks at brain in left orthogonal side impact was equal to 86,08%, there was a probability of 86,08% that the injuries resulted in the brain got AIS 4 score.

The brain in the other configurations was not resulting in such severe injuries: both MPS and CSDM injury risks for brain were extremely low, the CSDM ones even near zero. In fact, in those impacts, the head has not undergone to such a movement of approach the left or right shoulders: the dummy made a translational movement towards the incoming carriage, and only in the left rear tilted configuration the head came into contact with the higher part of the vehicle door. Despite that, the MPS injury risk resulted to be equal to 17,45% and the CSDM injury risks to 0,56%. Those values of injury risk are very small compared with ones resulted from the collision of the head in the left orthogonal impact. However, all the configurations other than the left orthogonal one, were resulting in injury risk at brain minor than 26% or 21%, as shown in table 4.5, therefore the AIS score for brain in those impact were at least minor than AIS 3 score, and so the injuries could be minor, such as bruises of hematomas, or, in worst case, moderate.

Comparing the injuries resulting from the MPS and CSDM criterion, it is visible that the injuries resulting from the MPS criterion are more critical than the ones resulting from the CSDM criterion. A comparison between MPS and CSDM values for the brain is presented in figure 4.40.

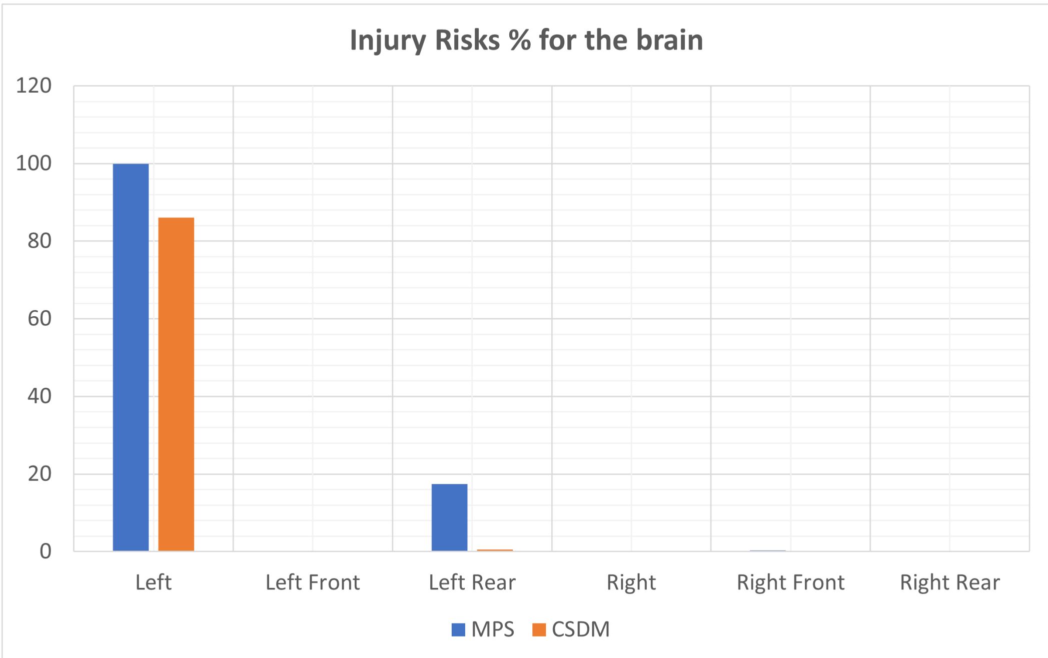

Figure 4.40: Injury Risks % for each crash simulations, resulting from MPS and CSDM values.

In particular, in left orthogonal side impact, the CSDM criterion provided an injury risks 13,8006% lower than the one provided by MPS criterion, while in left rear tilted side impact, the CSDM criterion provided an injury risks 16,9091% lower than the one provided by MPS criterion. In left front tiled side impact and in all the impacts at right of vehicle, the CSDM provided zero values of injury risks, hence the brain was not experiencing any stress. However, the MPS criterion for those impacts provided non-zero values, but extremely low, with respect to the values provided by left orthogonal and left rear tilted impact. It means that, for MPS criterion, the brain in those impacts was experiencing some stresses, but the values were very low compared to the left orthogonal and left rear tilted impact.

Also in this case, or the CSDM was underestimating the injuries or the MPS was overestimating them. A better understanding of the injuries could be possible by using the PVP (Peak Virtual Power) criterion, which is is a particularly useful criterion, which also permit the estimation of the injury's AIS score. Unfortunately, the PVP has not already been correctly implemented by the THUMS Injury Visualization tool for what concern the models in kg-mm-ms. The tool is currently under development.

Chapter 5

Conclusions

In this thesis six different side impact crash tests were reproduced in a FE environment; the collisions were set between a Moving Deformable Barrier (MDB) and a mid-size sedan. The main goal was to investigate and compare the possible injuries that the car occupant at driver seat may suffer in those type of impacts, using a Human Body Model (HBM).

The simulations analyzed were left and right orthogonal side impact at right angle and the front and rear tilted of 45 degrees side impact, both at left and right side of vehicle.Among the six configuration analyzed, only the left orthogonal one was regulated by Euro NCAP, while the other impacts were not regulated by Euro NCAP or by some other world's safety protocols. The trolley was translated and rotated to simulate the different configurations, and the trolley's velocity was set by considering the direction of carriage's movement, in each impact.

The biomechanical results were analyzed with the THUMS Injury Visualization tool, by using HBMs based injury criteria. The results showed that the most critical impact is the left orthogonal one. In this impact, the main body parts involved in severe lesions were the head, the cervical spine, the pelvis and the right scapula and humerus.

The head resulted to by critically injured: the AIS 4 level was reached at brain with both MPS and CSDM criterion. It means that the resulting injuries were severe, with respect to the AIS scale definition. The configurations other than the left orthogonal one, were resulting in injury risk with AIS score for brain at least minor than AIS 3 score, and so the injuries could be minor, such as bruises of hematomas, or, in worst case, moderate.

The movement of the head approaching towards the left shoulder was also resulting in a distraction of the cervical spine, in particular the injuries were due to the seat belt that held back the shoulders and the neck.

Also by analyzing the injuries at trunk, internal organs and extremity, the most severe impact was the left orthogonal one. The THUMS was experiencing both forward twisting movement with right shoulder and arm, and a downwards compression of the pelvis. Those movements were resulting in injuries in bones, such as in right scapula, right humerus, and pelvis, but also in internal organs such as intestine, heart, liver, stomach, spleen, and kidneys. In the other five configurations of impact, those movement were not present in such critical way.

However, while there is not direct correlation between MPS and AIS scale, for the bones and for the internal organs, rather than the brain, it was not possible to establish the AIS score reached in the impacts. It could be only highlighted that the injury risk resulted in right scapula, right humerus, and right pelvis were less than half the value of the risk at the skull, hence they could be considered severe but not as critical as the injuries resulted in the skull. However, the tool, at the moment of this work, is not providing the opportunity to evaluate the injury risk deriving in internal organs, hence it was not possible to compare the injury risk at brain for which the AIS score could be derived, and the injury risks at the other internal organs.

Since the values of MPS and CSDM resulting in the organs are greater than the values of MPS resulting in the bones, it could be interesting to evaluate the injury risks resulting from them in the future, once the tool has received the necessary implementation regarding the risk curve data.

It must be noted that, overall, the MPS and CSDM values provided by the tool, for the internal organs, were in contrast each other. The CSDM was presenting lower values than the MPS ones, which, in the only case in which was possible to evaluate the injury risk, that was the brain, were resulting in lower injury risk. It means that or the MPS was overestimating the in injuries, or the CSDM was underestimating them. This can be lead to the construction of those criteria: the MPS returned only the maximum strain reached in the anatomical part, while the CSDM is providing also a functional analysis. For example, the intestine is reaching an higher MPS value than the right kidney, because the intestine is presenting the higher deformation and so the higher MPS values, but its tissue is more elastic than the one of the kidneys, and so a minor deformation at kidneys could be responsible of higher injuries. That means that the volume of nerve fibers which exceeds the functionality threshold is higher than the ones in the intestine, and that is why the CSDM injury risks in right kidney is higher than the one in intestine.

In conclusion, the use of an HBM allows the evaluations of the behavior of human body during several types of impact by giving the chance of analyzing more data, compared to the real dummies, such as the evaluation of internal organs in an accurate way. The use of HBM makes also cheaper the passive safety evaluation, than the traditional ones with physical dummies.

In this context, the THUMS Injury Visualization tool, developed by Jsol company, provide the possibility of estimation and comparison between different injury criteria and the graphical visualization of injuries. However, at the moment of this thesis work, it is not using all its potential and some implementations have to be done.

Appendix A

This Appendix contains road deaths data across the world, to highlight the severity of the safety conditions on worldwide roads. Consequently, the importance of vehicle safety studies and analysis becomes even more evident.

All the data are taken from World Health Organization (WHO).

Country/Region	**Deaths in last available year**	**Last available year**
Afghanistan	4,734	2013
Albania	478	2016
Algeria	9,337	2013
Andorra	6	2013
Angola	5,769	2013
Antigua and Barbuda	6	2013
Argentina	5,619	2013
Armenia	546	2016
Australia	1,131	2018
Austria	455	2016
Azerbaijan	943	2016
Bahamas	52	2013
Bahrain	78	2017
Bangladesh	21,316	2013
Barbados	19	2013
Belarus	1282	2016
Belgium	657	2019
Belize	81	2013
Benin	2,986	2016
Bhutan	114	2013
Bolivia	3,476	2013
Bosnia and Herzegovina	676	2016
Botswana	477	2013
Brazil	46,935	2013
Bulgaria	601	2019
Burkina Faso	5,072	2013
Cambodia	2,635	2013
Cameroon	6,136	2013
Canada	2,118	2016
Cape Verde	130	2013
Central African Republic	1,546	2016
Chad	3,089	2013
Chile	2,179	2013
China	261,367	2016

Table 1: Road death data in countries from Afghanistan to China

Country/Region	Deaths in last available year	Last available year
Colombia	8,107	2013
Congo	1,174	2013
Cook Islands	5	2013
Costa Rica	676	2013
Croatia	340	2019
Cuba	840	2013
Cyprus	60	2019
Czech Republic	630	2019
Democratic Republic of Congo	26,529	2016
Denmark	227	2019
Djibouti	216	2013
Dominica	11	2013
Dominican Republic	3,052	2013
Ecuador	3,164	2013
Egypt	10,466	2013
El Salvador	1,339	2013
Eritrea	1,527	2013
Estonia	90	2016
Ethiopia	27,326	2016
Fiji	51	2013
Finland	260	2019
France	3,585	2019
Gabon	383	2013
Gambia	544	2013
Georgia	449	2021
Germany	3,327	2019
Ghana	6,789	2013
Greece	699	2019
Guatemala	2,939	2013
Guinea	3,490	2016
Guinea-Bissau	468	2013
Guyana	138	2013
Honduras	1,408	2013
Hong Kong	97	2020
Hungary	756	2019
Iceland	8	5-y avg. 2016–2021
India	207,551	2016
Indonesia	38,279	2016
Iran	16,426	2016
Iraq	6,826	2013
Ireland	194	2019
Israel	345	2016
Italy	3,333	2019
Ivory Coast	4,924	2013
Jamaica	320	2013

Table 2: Road death data in countries from Colombia to Jamaica

Country/Region	**Deaths in last available year**	**Last available year**
Japan	5,224	2016
Jordan	750	2016
Kazakhstan	3,983	2016
Kenya	12,891	2013
Kiribati	3	2013
Kuwait	629	2013
Kyrgyzstan	1220	2016
Laos	971	2013
Latvia	205	2019
Lebanon	1088	2016
Lesotho	584	2013
Liberia	1,657	2016
Libya	1,645	2016
Lithuania	234	2019
Luxembourg	46	2016
North Macedonia	198	2016
Madagascar	6,506	2013
Malawi	5,601	2016
Malaysia	7,374	2016
Maldives	12	2013
Mali	3,920	2013
Malta	22	2016
Marshall Islands	3	2013
Mauritania	952	2013
Mauritius	158	2013
Mexico	15,062	2013
Federated States of Micronesia	2	2013
Monaco	0	2013
Mongolia	597	2016
Montenegro	67	2016
Morocco	6,870	2013
Mozambique	8,173	2013
Myanmar	10,809	2013
Namibia	551	2013
Nepal	4,713	2013
Netherlands	648	2019
New Zealand	364	2016
Nicaragua	931	2013
Niger	4,706	2013
Nigeria	35,621	2013
Norway	110	2019
Oman	924	2013
Pakistan	25,781	2013
Palau	1	2013
Panama	386	2013
Papua New Guinea	1,232	2013

Table 3: Road death data in countries from Japan to Papua New Guinea

Country/Region	Deaths in last available year	Last available year
Paraguay	1,408	2013
Peru	4,234	2013
Philippines	10,379	2013
Poland	3,698	2019
Portugal	768	2019
Qatar	161	2021
Republic of Moldova	437	2016
Romania	1,881	2019
Russia	16,981	2019
Rwanda	3,782	2013
Saint Lucia	33	2013
S. Vincent and the Grenadines	9	2013
Samoa	30	2013
San Marino	1	2013
São Tomé and Príncipe	55	2016
Saudi Arabia	7,898	2013
Senegal	3,844	2013
Serbia	649	2019
Seychelles	8	2013
Sierra Leone	1,661	2013
Singapore	197	2013
Slovakia	330	2019
Slovenia	134	2019
Solomon Islands	108	2013
Somalia	3,884	2016
South Africa	13,273	2013
South Korea	3,349	2019
Spain	1,922	2019
Sri Lanka	3,691	2013
Sudan	9,221	2013
Suriname	103	2013
Swaziland	303	2013
Sweden	223	2019
Switzerland	223	2019
Taiwan	2,865	2019
Tajikistan	1,543	2016
Tanzania	16,211	2013
Thailand	22,491	2016
Timor-Leste	188	2013
Togo	2,123	2013
Tonga	8	2013
Trinidad and Tobago	189	2013
Tunisia	2,679	2013
Turkey	9,782	2016
Turkmenistan	914	2016
Uganda	10,280	2013
Ukraine	6,089	2016
United Arab Emirates	1,678	2013
United Kingdom	2,026	2019
United States	39,888	2018
Uruguay	460	2016
Uzbekistan	3,617	2016

Table 4: Road death data in countries from Paraguay to Uzbekistan

Country/Region	**Deaths in last available year**	**Last available year**
Vanuatu	42	2013
Vietnam	22,419	2013
Yemen	5,248	2013
Zambia	3,586	2013
Zimbabwe	3,985	2013

Table 5: Road death data in countries from Vanuatu to Zimbabwe

Appendix B

In this appendix are presented all the injury risk curves provided by the THUMS Injury Visualization tool for all the bones and for the brain. For the bones, two curves are plotted: the red one is the curve adjusted at age of 35 years old, while the green one is the not-scaled curve, which corresponds to an age of 55 years old. Indeed, the green curve is growing faster than the red one: it means that the same MPS value at 35 years old is resulting in a minor injury risk, rather than at 55 years old.

The injury risks resulting from the right orthogonal side impact are not presented here, because the simulation did not reach the 100 ms of simulations as the other five did. For that reason, the results of this simulation were not meaningful to insert in those graphs.

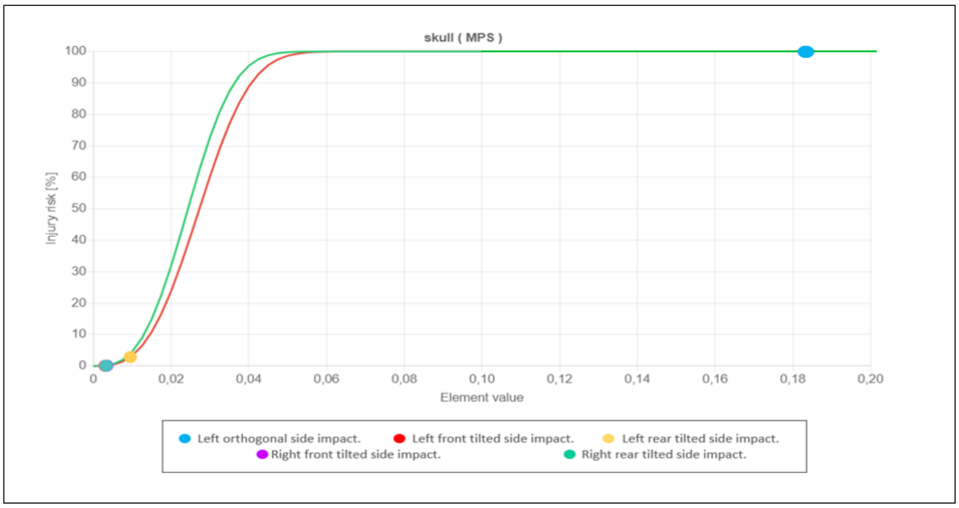

Figure 1: Injury risk curve for the skull.

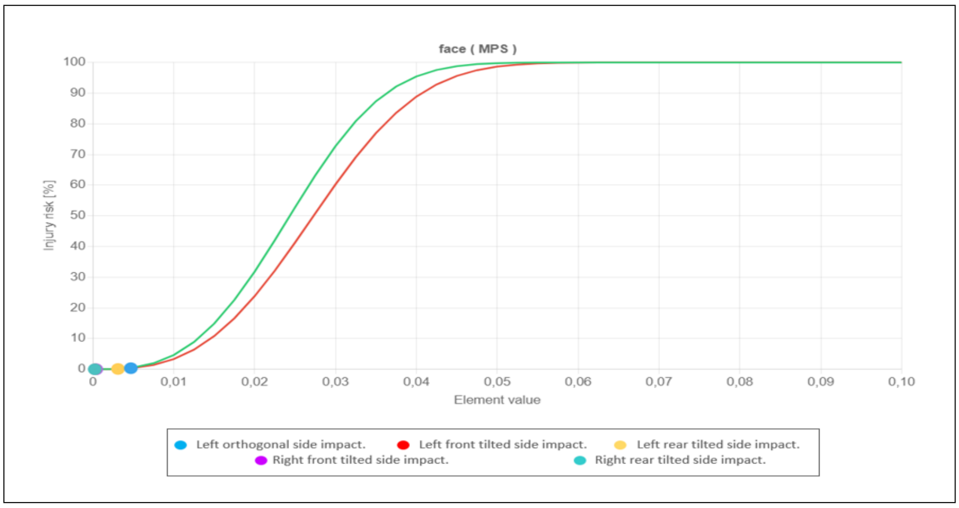

Figure 2: Injury risk curve for the face.

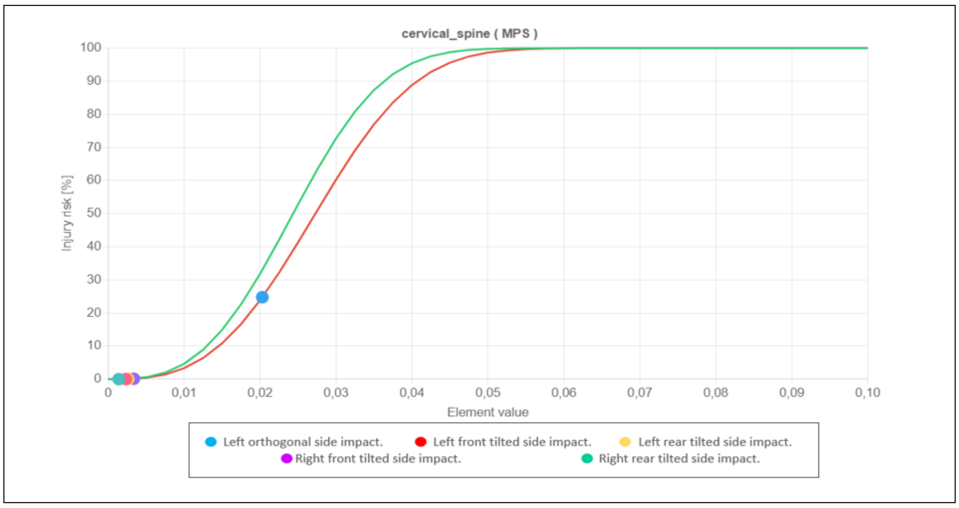

Figure 3: Injury risk curve for the cervical spine.

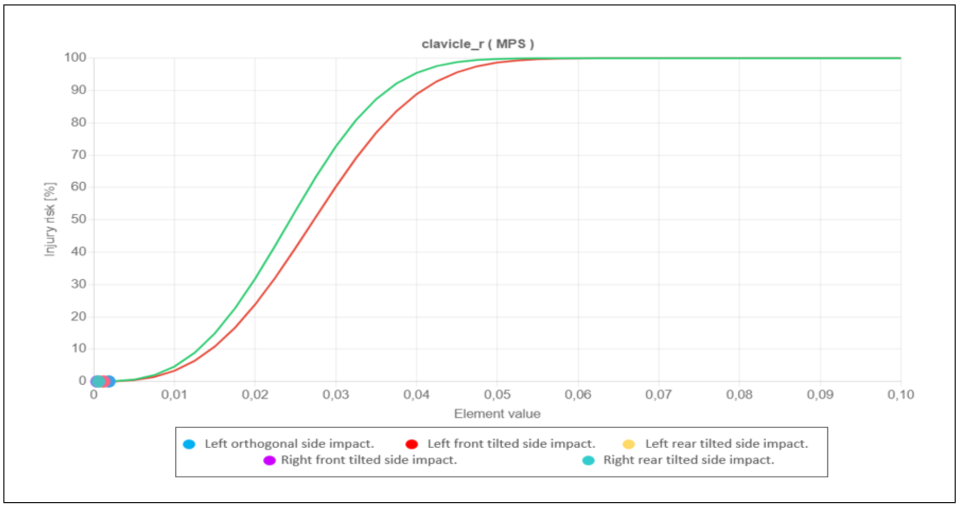

Figure 4: Injury risk curve for the right clavicle.

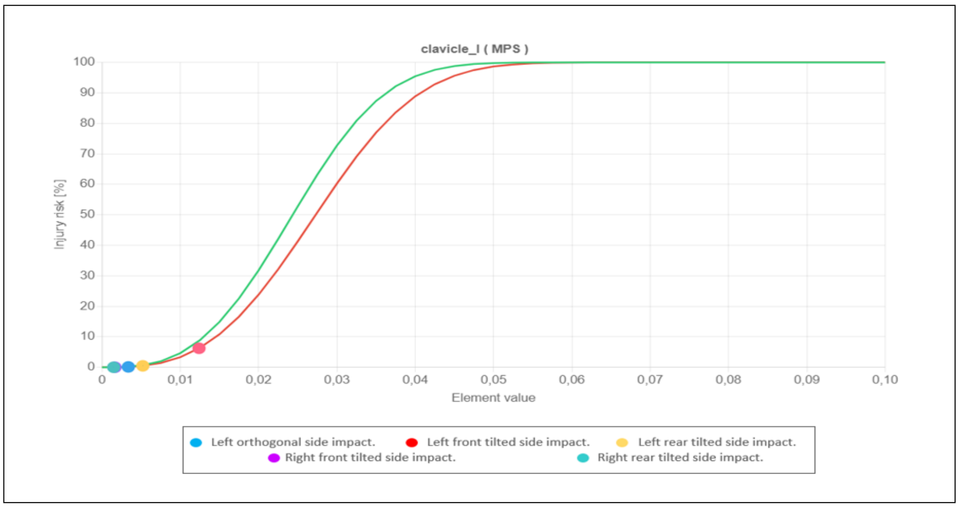

Figure 5: Injury risk curve for the left clavicle.

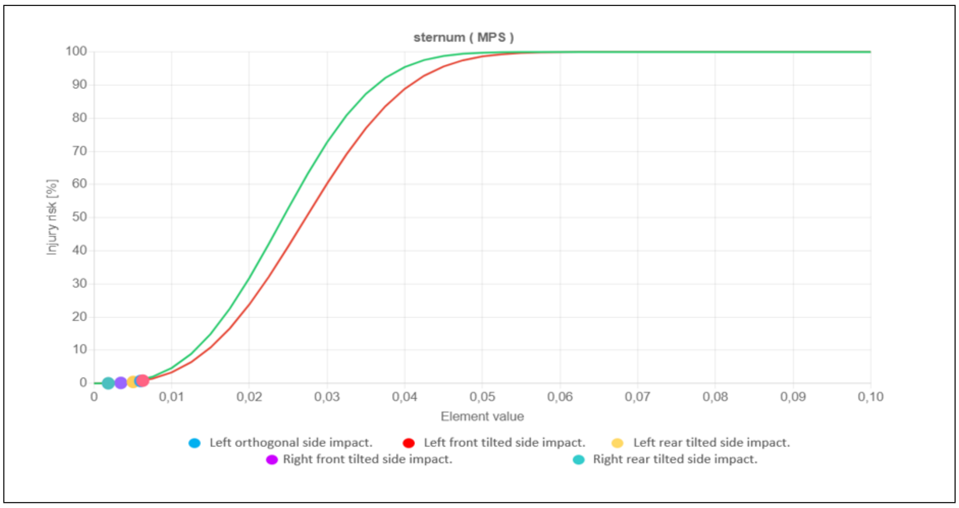

Figure 6: Injury risk curve for the sternum.

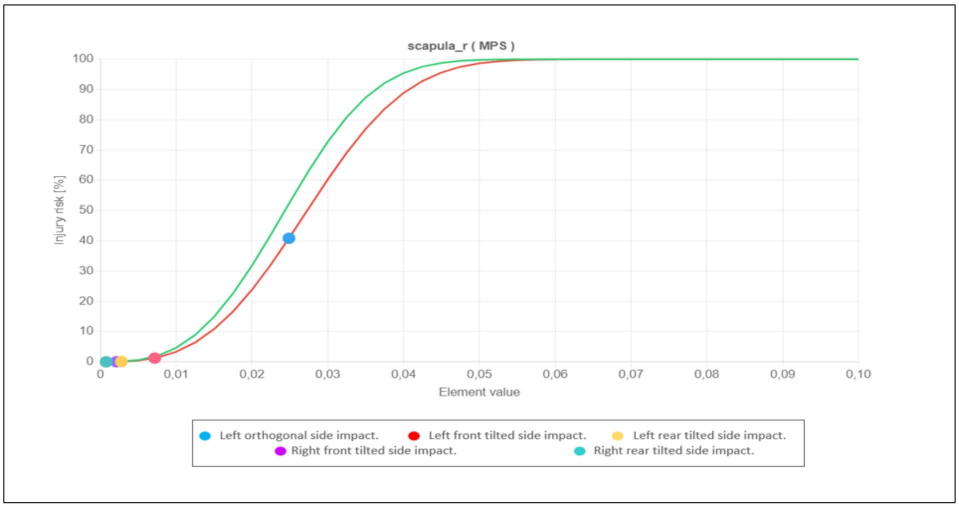

Figure 7: Injury risk curve for the right scapula.

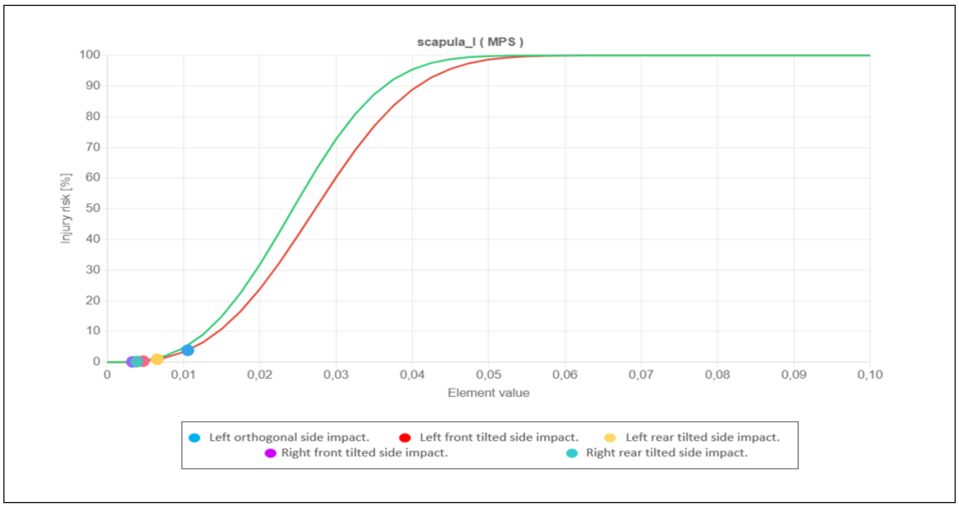

Figure 8: Injury risk curve for the left scapula.

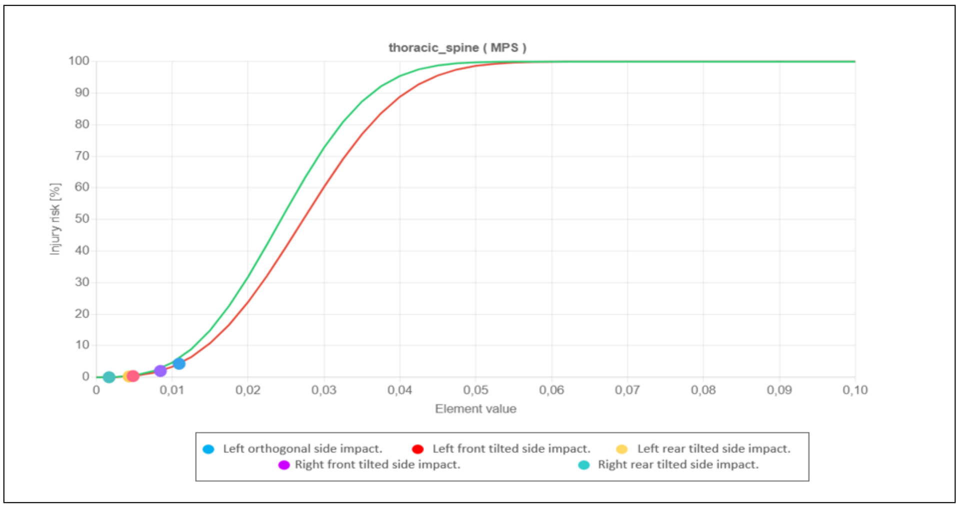

Figure 9: Injury risk curve for the toracic spine.

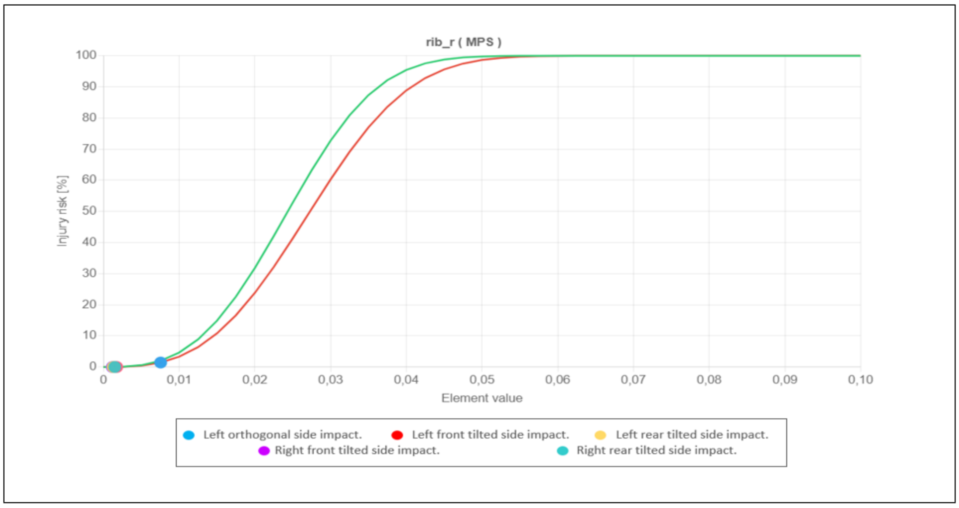

Figure 10: Injury risk curve for the right rib.

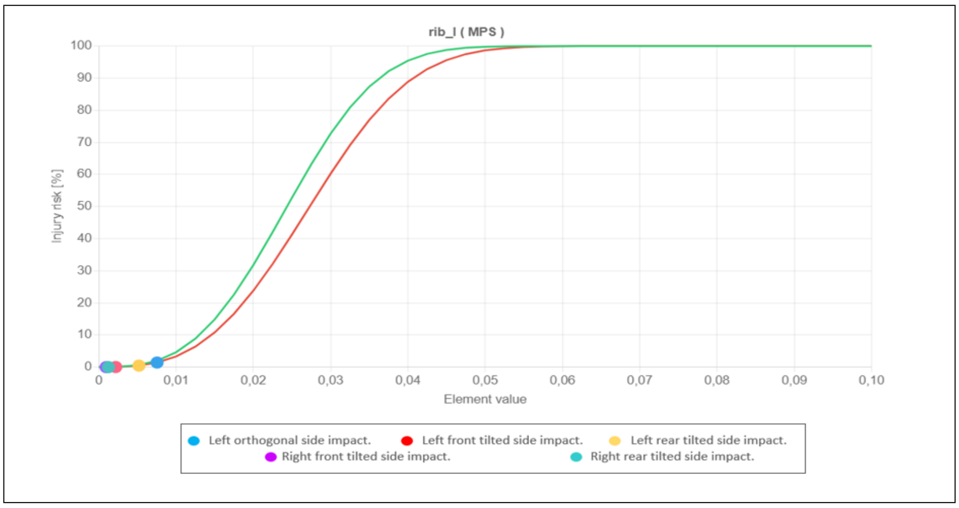

Figure 11: Injury risk curve for the left rib.

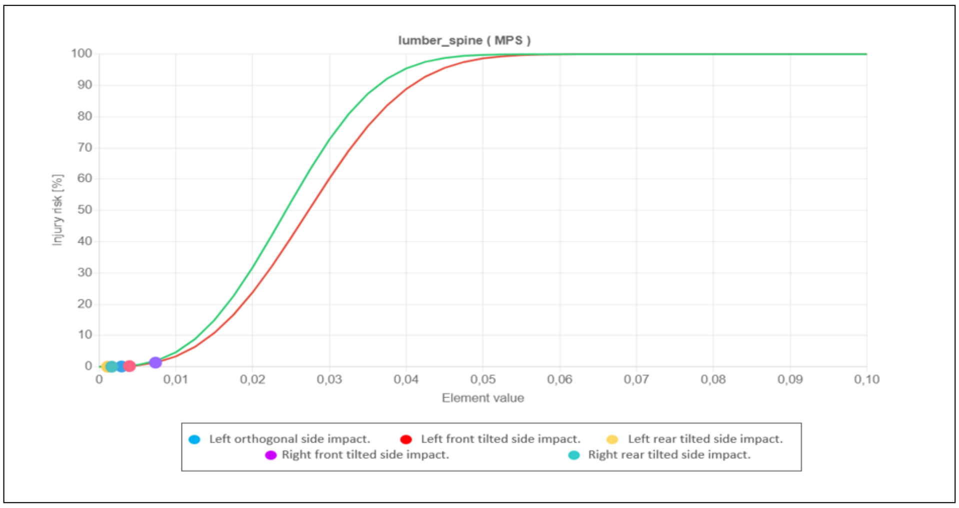

Figure 12: Injury risk curve for the lumber spine.

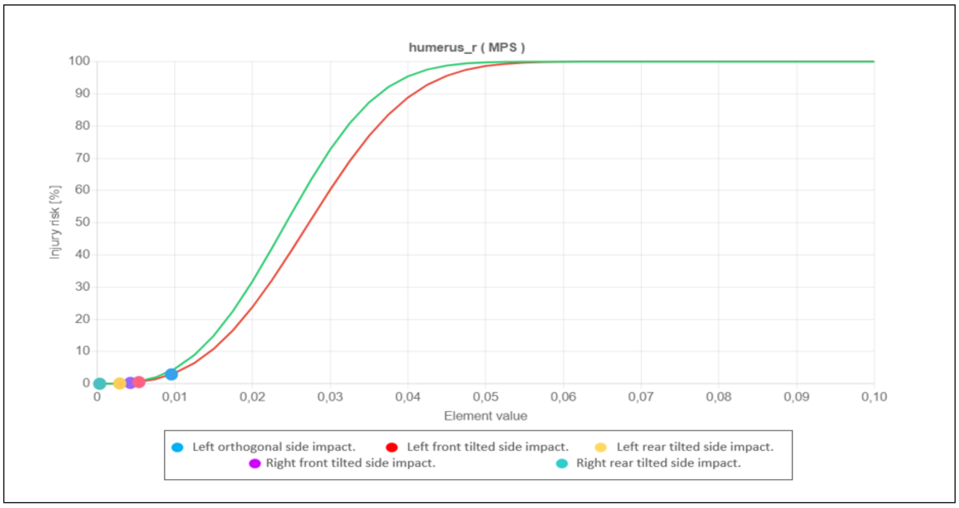

Figure 13: Injury risk curve for the right humerus.

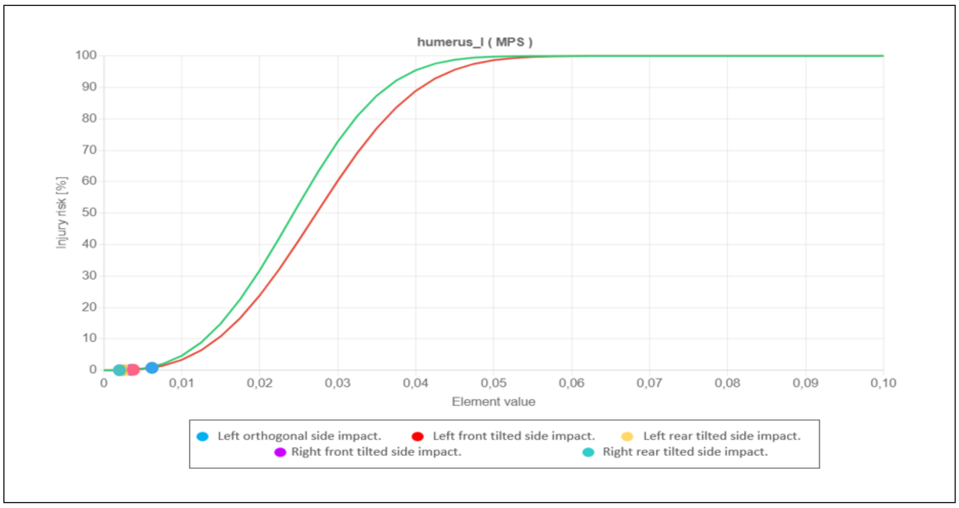

Figure 14: Injury risk curve for the left humerus.

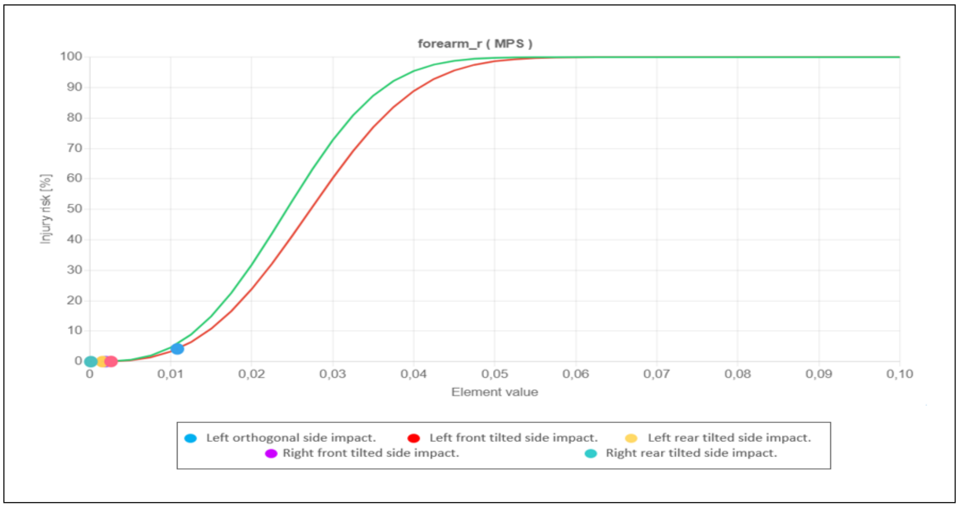

Figure 15: Injury risk curve for the right forearm.

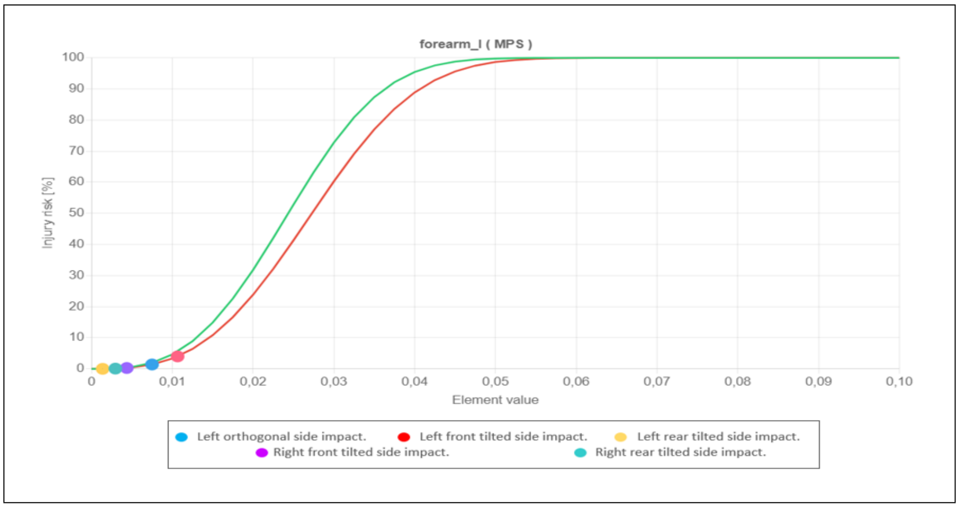

Figure 16: Injury risk curve for the left forearm.

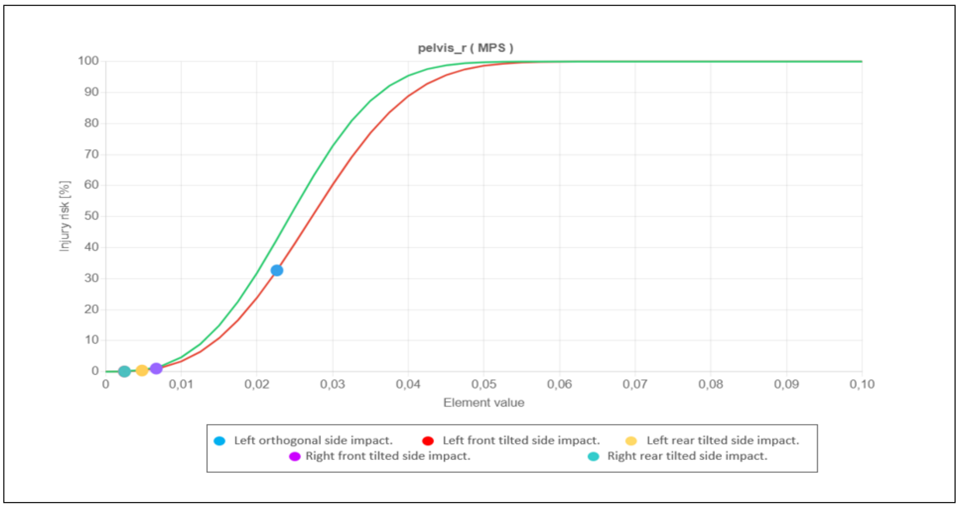

Figure 17: Injury risk curve for the right pelvis.

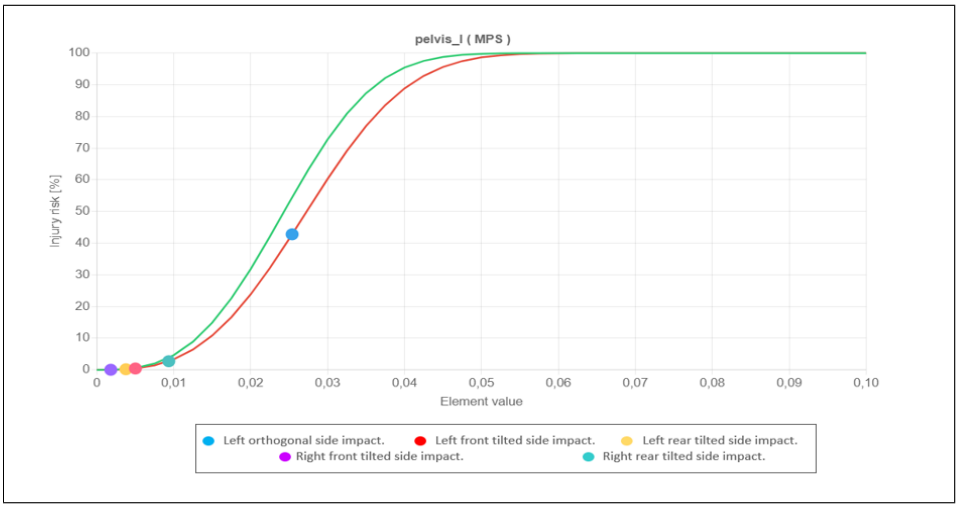

Figure 18: Injury risk curve for the left pelvis.

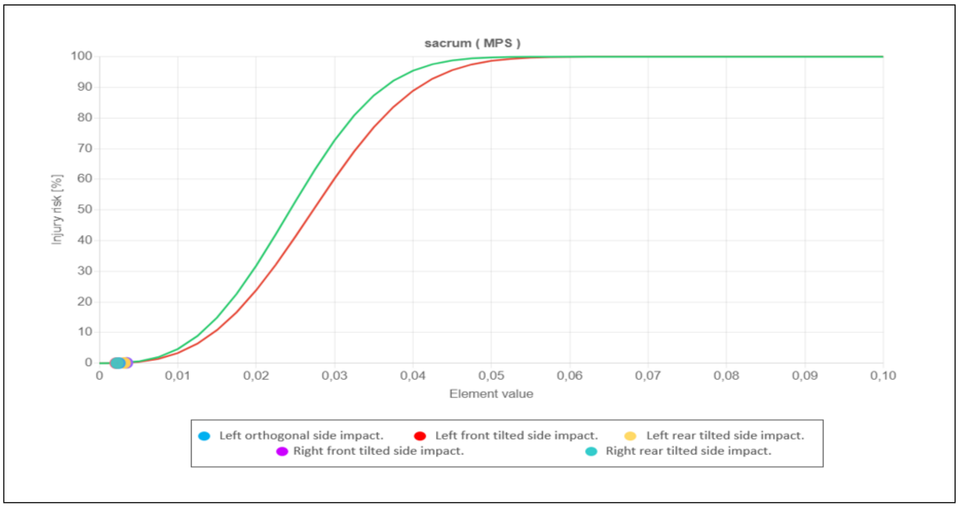

Figure 19: Injury risk curve for the sacrum.

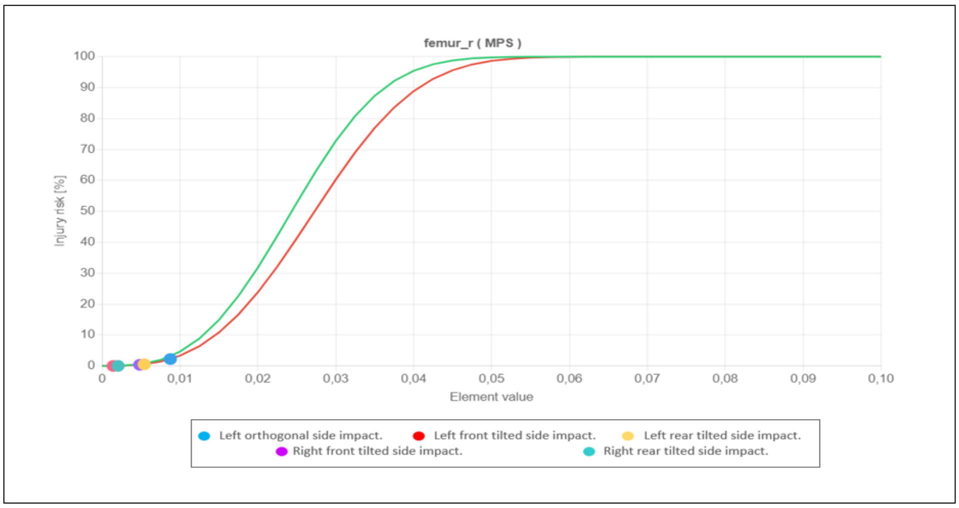

Figure 20: Injury risk curve for the right femur.

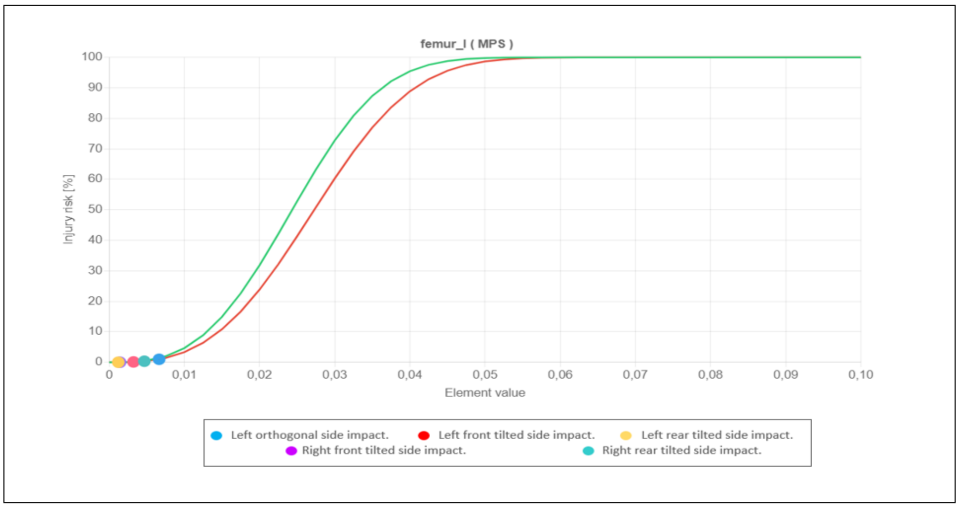

Figure 21: Injury risk curve for the left femur.

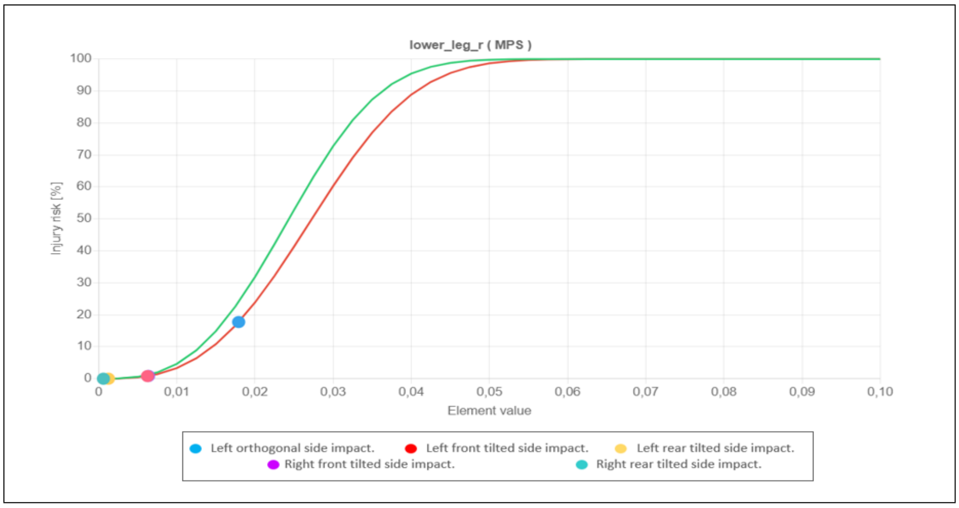

Figure 22: Injury risk curve for the right lower leg.

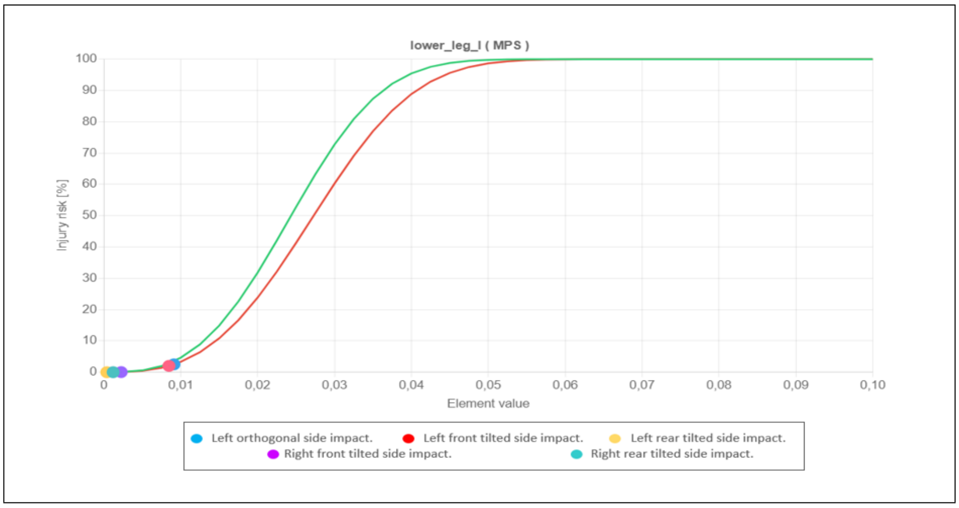

Figure 23: Injury risk curve for the left lower leg.

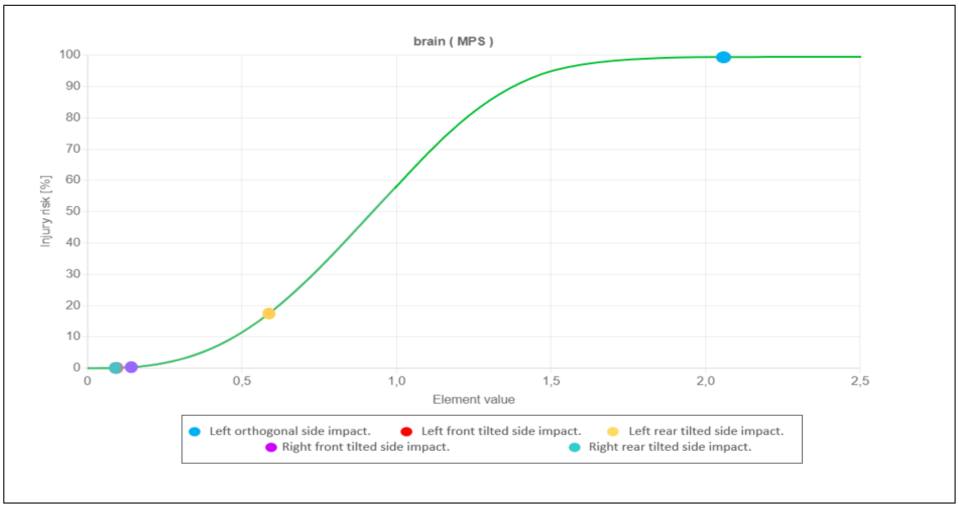

Figure 24: Injury risk curve for the brain.

Appendix C

In this appendix are presented the MPS values and MPS injury risks for the ribs. As explain in section 4.3.2 of this work, the MPS of left and right rib parts were obtained by taking the higher MPS value, resulting from the rib with the maximum MPS. Are here presented the numbers of the ribs which were experiencing the maximum MPS, value from which the tool has calculated the injury risks presented in this work. Then all the MPS values and injury risks were presented, for each rib in all the six impacts.

	Left	**Left F.**	**Left R.**	**Right**	**Right F.**	**Right R.**
Right Rib	6	5	5	11	1	8
Left Rib	11	8	4	5	8	4

Table 6: Number of the rib which was experiencing the maximum MPS above all ribs, for each simulation. F stands for *Front* and R. stands for *Rear*.

Rib	**MPS[mm/mm]**	**Injury Risk[%]**
1	0,0101	3,4589
2	0,0046	0,3201
3	0,0043	0,2650
4	0,0052	0,4611
5	0,0099	3,2428
6	0,0120	5,6331
7	0,0094	2,7316
8	0,0076	1,4400
9	0,0040	0,2085
10	0,0046	0,3277
11	0,0020	0,0273
12	0,0011	0,0040

(a) Right Ribs

Rib	**MPS[mm/mm]**	**Injury Risk[%]**
1	0,0050	0,4220
2	0,0035	0,1383
3	0,0095	2,8163
4	0,0075	1,4303
5	0,0079	1,6523
6	0,0059	0,6696
7	0,0098	3,1556
8	0,0081	1,7577
9	0,0078	1,6010
10	0,0112	4,6802
11	0,0127	6,6241
12	0,0045	0,3063

(b) Left Ribs

Table 7: MPS values [mm/mm] and injury risks % for all the ribs in left orthogonal impact.

Rib	MPS[mm/mm]	Injury Risk[%]
1	0,0021	0,0315
2	0,0011	0,0040
3	0,0015	0,0118
4	0,0014	0,0093
5	0,0025	0,0502
6	0,0024	0,0430
7	0,0020	0,0269
8	0,0018	0,0178
9	0,0014	0,0085
10	0,0012	0,0061
11	0,0007	0,0012
12	0,0005	0,0005

(a) Right Ribs

Rib	MPS[mm/mm]	Injury Risk[%]
1	0,0014	0,0097
2	0,0026	0,0580
3	0,0024	0,0452
4	0,0022	0,0347
5	0,0025	0,0534
6	0,0029	0,0811
7	0,0032	0,1131
8	0,0038	0,1812
9	0,0015	0,0116
10	0,0028	0,0755
11	0,0004	0,0002
12	0,0003	0,0001

(b) Left Ribs

Table 8: MPS values [mm/mm] and injury risks % for all the ribs in left front tilted side impact.

Rib	MPS[mm/mm]	Injury Risk[%]
1	0,0031	0,0961
2	0,0009	0,0023
3	0,0013	0,0080
4	0,0015	0,0117
5	0,0037	0,1624
6	0,0031	0,0944
7	0,0024	0,0458
8	0,0013	0,0073
9	0,0003	0,0001
10	0,0007	0,0010
11	0,0005	0,0003
12	0,0004	0,0003

(a) Right Ribs

Rib	MPS[mm/mm]	Injury Risk[%]
1	0,0015	0,0111
2	0,0018	0,0197
3	0,0046	0,3334
4	0,0052	0,4683
5	0,0049	0,3887
6	0,0033	0,1195
7	0,0028	0,0697
8	0,0031	0,0969
9	0,0021	0,0305
10	0,0031	0,0972
11	0,0026	0,0586
12	0,0022	0,0350

(b) Left Ribs

Table 9: MPS values [mm/mm] and injury risks % for all the ribs in left rear tilted side impact.

Rib	MPS[mm/mm]	Injury Risk[%]
1	0,0004	0,0001
2	0,0002	0,0000
3	0,0003	0,0001
4	0,0002	0,0000
5	0,0004	0,0002
6	0,0004	0,0001
7	0,0004	0,0002
8	0,0007	0,0010
9	0,0009	0,0021
10	0,0024	0,0470
11	0,0041	0,2294
12	0,0019	0,0227

(a) Right Ribs

Rib	MPS[mm/mm]	Injury Risk[%]
1	0,0003	0,0001
2	0,0003	0,0001
3	0,0003	0,0001
4	0,0004	0,0002
5	0,0004	0,0003
6	0,0003	0,0001
7	0,0003	0,0001
8	0,0004	0,0002
9	0,0002	0,0000
10	0,0004	0,0003
11	0,0002	0,0000
12	0,0002	0,0000

(b) Left Ribs

Table 10: MPS values [mm/mm] and injury risks % for all the ribs in right orthogonal side impact.

Rib	MPS[mm/mm]	Injury Risk[%]
1	0,0007	0,0013
2	0,0006	0,0009
3	0,0006	0,0007
4	0,0008	0,0015
5	0,0008	0,0015
6	0,0007	0,0009
7	0,0008	0,0017
8	0,0015	0,0110
9	0,0013	0,0065
10	0,0014	0,0098
11	0,0013	0,0077
12	0,0007	0,0011

(a) Right Ribs

Rib	MPS[mm/mm]	Injury Risk[%]
1	0,0008	0,0017
2	0,0010	0,0036
3	0,0009	0,0023
4	0,0013	0,0065
5	0,0007	0,0014
6	0,0008	0,0020
7	0,0009	0,0024
8	0,0007	0,0012
9	0,0009	0,0021
10	0,0008	0,0017
11	0,0007	0,0012
12	0,0006	0,0006

(b) Left Ribs

Table 11: MPS values [mm/mm] and injury risks % for all the ribs in right rear tilted side impact.

Rib	**MPS[mm/mm]**	**Injury Risk[%]**
1	0,0017	0,0160
2	0,0011	0,0044
3	0,0008	0,0014
4	0,0006	0,0007
5	0,0017	0,0155
6	0,0014	0,0097
7	0,0008	0,0017
8	0,0012	0,0053
9	0,0011	0,0049
10	0,0009	0,0020
11	0,0005	0,0005
12	0,0015	0,0110

(a) Right Ribs

Rib	**MPS[mm/mm]**	**Injury Risk[%]**
1	0,0011	0,0040
2	0,0012	0,0057
3	0,0013	0,0073
4	0,0009	0,0028
5	0,0018	0,0184
6	0,0024	0,0449
7	0,0016	0,0124
8	0,0026	0,0554
9	0,0020	0,0244
10	0,0023	0,0377
11	0,0022	0,0351
12	0,0009	0,0021

(b) Left Ribs

Table 12: MPS values [mm/mm] and injury risks % for all the ribs in right front tilted side impact.

Bibliography

Arthur J., Hallinan Jr. (1993). 'A Review of the Weibull Distribution'. In: *Journal of Quality Technology* 25.2, pp. 85–93.

Bandak, Faris A and Rolf H Eppinger (1994). 'A three-dimensional finite element analysis of the human brain under combined rotational and translational accelerations'. In: *SAE transactions*, pp. 1708–1726.

Bastien, Christophe, Clive Neal-Sturgess et al. (2020). 'Computing brain white and grey matter injury severity in a traumatic fall'. In: *Mathematical and Computational Applications* 25.3, p. 61.

Bastien, Christophe, Clive Neal Sturgess et al. (2021). 'Definition of Peak Virtual Power Brain Trauma Variables for the use in the JSOL THUMS injury post-processor web-based estimator'. In: *3th European LS-DYNA Conference 2021 (online and onsite)*.

Carson, Jenny, Graziella Jost and Maria Meiner (2022). 'RANKING EU PROGRESS ON ROAD SAFETY, 16th Road Safety Performance Index Report'. In: *European Transport Safety Council*.

Carter, Dennis R and Dan M Spengler (1978). 'Mechanical properties and composition of cortical bone'. In: *Clinical Orthopaedics and Related Research®* 135, pp. 192–217.

Collision Safety, Center for and Analysis (CCSA) (2016). 'Development and Validation of a Finite Element Model for the 2012 Toyota Camry Passenger Sedan'. In: DOI: https://doi.org/10.13021/G8N889.

Couturier, Stéphane et al. (2007). 'Procedure to assess submarining in frontal impact'. In: *20th International Conference on the Enhanced Safety of Vehicles*, pp. 18–21.

Farmer, Charles M, Elisa R Braver and Eric L Mitter (1997). 'Two-vehicle side impact crashes: the relationship of vehicle and crash characteristics to injury severity'. In: *Accident Analysis & Prevention* 29.3, pp. 399–406.

Forman, Jason L et al. (2012). 'Predicting rib fracture risk with whole-body finite element models: development and preliminary evaluation of a probabilistic analytical framework'. In: *Annals of Advances in Automotive Medicine/Annual Scientific Conference*. Vol. 56. Association for the Advancement of Automotive Medicine, p. 109.

Garelli, Federico (2021). 'Side impact crash studied with FE simulation and Human Body Model.' In.

Gennarelli, Thomas A. and Elaine Wodzin (2006). 'AIS 2005: A contemporary injury scale'. In: *Injury* 37.12. Special Issue: Trauma Outcomes, pp. 1083–1091. ISSN: 0020-1383. DOI: https://doi.org/10.1016/j.injury.2006.07.009. URL: https://www.sciencedirect.com/science/article/pii/S0020138306004190.

Germanetti, Filippo (2019). 'Finite Element Simulation of Impact of Autonomous Vehicle with Human Body Model in Out-of-Position Configuration'. In.

Gierczycka, Donata, Brock Watson and Duane Cronin (2015). 'Investigation of occupant arm position and door properties on thorax kinematics in side impact crash scenarios–comparison of ATD and human models'. In: *International journal of crashworthiness* 20.3, pp. 242–269.

Golman, Adam J. et al. (2014). 'Injury prediction in a side impact crash using human body model simulation'. In: *Accident Analysis & Prevention* 64, pp. 1–8. ISSN: 0001-4575. DOI: https://doi.org/10.1016/j.aap.2013.10.026. URL: https://www.sciencedirect.com/science/article/pii/S0001457513004363.

Huston, RL and CE Passerello (1971). 'On the dynamics of a human body model'. In: *Journal of Biomechanics* 4.5, pp. 369–378.

Kumaresan, Srirangam et al. (2006). 'Biomechanics of side impact injuries: evaluation of seat belt restraint system, occupant kinematics and injury potential'. In: *2006 International Conference of the IEEE Engineering in Medicine and Biology Society*. IEEE, pp. 87–90.

Lau, Ian V and David C Viano (1986). 'The viscous criterion—bases and applications of an injury severity index for soft tissues'. In: *SAE transactions*, pp. 672–691.

NCAP, Euro (2022). URL: `%5Curl%7Bhttps://www.euroncap.com/en%7D`.

— (2013). *AE-MDB specification version 1.0.* (Visited on 2013).

— (2021). *Side Impact Mobile Deformable Barrier Testing Protocol.* (Visited on 2021).

Takhounts, Erik G, Matthew J Craig et al. (2013). 'Development of brain injury criteria (BrIC)'. In: *Stapp car crash journal* 57, p. 243.

Takhounts, Erik G, Vikas Hasija et al. (2011). 'Kinematic rotational brain injury criterion (BRIC)'. In: *Proceedings of the 22nd enhanced safety of vehicles conference. Paper*. 11-0263. Citeseer, pp. 1–10.

Toyota Offers Free Access to THUMS Virtual Human Body Model Software. (2020). URL: `%5Curl%7Bhttps://global.toyota/en/newsroom/corporate/32665896.html#%7D` (visited on 2020).

Toyota Unveils Virtual Human Body for Simulated Crashes. (2000). URL: `%5Curl%7Bhttps://global.toyota/en/detail/7935083%7D` (visited on 2000).

Viano, David C and Ian V Lau (1988). 'A viscous tolerance criterion for soft tissue injury assessment'. In: *Journal of Biomechanics* 21.5, pp. 387–399.

Yoganandan, Narayan et al. (2007). 'Biomechanics of side impact: injury criteria, aging occupants, and airbag technology'. In: *Journal of biomechanics* 40.2, pp. 227–243.

Zhang, Liying, King H Yang and Albert I King (2004). 'A proposed injury threshold for mild traumatic brain injury'. In: *J. Biomech. Eng.* 126.2, pp. 226–236.

Acknowledgements

Vorrei ringraziare innanzi tutto il mio relatore, Professor Alessandro Scattina, per avermi seguita in questo percorso e per avermi dato la possibilità di svolgere questo lavoro: scrivere la tesi con il libro di anatomia da una parte e il metodo agli elementi finiti dall'altra era un po' il mio sogno quando mi sono iscritta all'università.

In maniera un po' più generale, vorrei ringraziare i professori che ho incontrato nella mia carriera universitaria al Politecnico di Torino, che mi hanno insegnato l'arte della perseveranza e della dedizione, armi che mi sono state preziosissime in diversi momenti.

Ringrazio Valerio, per il grande supporto durante questo lavoro.

Ringrazio inoltre la mia famiglia, mamma e papà in particolar modo, per avermi dato l'opportunità di studiare e la serenità per poterlo fare bene. Il mio voler rendervi orgogliosi è stato un motore fortissimo in tanti momenti difficili.

Rigrazio Vittorio, per avermi supportato ed aiutato in qualsiasi momento di bisogno.

Infine, un particolare ringraziamento va a Stefania, con le parole è difficile spiegare la forza che mi dà averti sempre accanto.